INVESTIGATING THE INTERFACE BETWEEN THE CALVIN-BENSON CYCLE AND PLANT METABOLISM: THE GLUCOSE-6-PHOSPHATE SHUNT

By

Alyssa L. Preiser

A DISSERTATION

Submitted to
Michigan State University
in partial fulfillment of the requirements
for the degree of

Biochemistry and Molecular Biology – Doctor of Philosophy

2020

PUBLIC ABSTRACT

INVESTIGATING THE INTERFACE BETWEEN THE CALVIN-BENSON CYCLE AND PLANT METABOLISM: THE GLUCOSE-6-PHOSPHATE SHUNT

By

Alyssa L. Preiser

During the day, leaves collect energy from sunlight. They use this energy to make their food in a process called photosynthesis. During photosynthesis, plants combine carbon dioxide (CO_2) with other ingredients to make their own food and building materials. This process is called the Calvin-Benson cycle. While they are taking in CO_2, leaves also give off CO_2, similar to how we breathe out CO_2 from our lungs. This is called light respiration. Unlike our breathing, we don't know yet how plants give off CO_2. Our lab proposed an assembly line of chemical reactions called the glucose-6-phosphate shunt that might contribute to this. I studied two of the enzymes, or assembly line workstations. This helped us learn when they were active and when the assembly line might be running. From this, we learned that the G6P shunt is active and responsible for a majority of the CO_2 plants 'breathe out'. The Calvin-Benson cycle is essential to life on Earth. It provides carbon that becomes our food and fuel. Knowing how leaves use carbon can help us increase yields of crops or sources of fuels.

ABSTRACT

INVESTIGATING THE INTERFACE BETWEEN THE CALVIN-BENSON CYCLE AND PLANT METABOLISM: THE GLUCOSE-6-PHOSPHATE SHUNT

By

Alyssa L. Preiser

Recently, the Sharkey lab proposed an alternative pathway around the Calvin-Benson cycle, called the glucose-6-phosphate shunt. This is a futile cycle, consuming ATP and releasing CO_2. However, it may address unexplained observations about the Calvin-Benson cycle. To understand the regulation and flux through the glucose-6-phosphate shunt, we have characterized two key enzymes. Phosphoglucoisomerase (PGI) provides the substrate for the pathway and glucose-6-phosphate dehydrogenase (G6PDH) is the first committed step. We found that PGI has a higher K_m for glucose 6-phosphate (G6P) compared to fructose 6-phosphate (F6P). This, in combination with maintaining a disequilibrium between F6P and G6P, allows it to act as a one-way valve to partition carbon out of the Calvin-Benson cycle. PGI also acts as a key regulatory enzyme in starch synthesis and degradation. We found that plastidic G6PDH is redox regulated. Reduction catalyzed by thioredoxin causes a decrease in substrate affinity but the enzyme maintains activity in the light. This regulation can be overcome by oxidation by hydrogen peroxide or by an increase in substrate concentration. We also found that the midpoint potential of G6PDH is in a range to allow dynamic regulation in the light. In addition to characterization of key enzymes, we investigated whether the G6P shunt is responsible for respiration in the light (R_L). We found that all loss-of-function G6PDH isoform mutants decreased R_L. This also allowed us to explain respiration phenotypes in a variety of mutant lines. Overall, we have shown that the G6P shunt is the source of R_L and have used biochemical characteristics of key enzymes to understand and predict changes in flux through the shunt.

ACKNOWLEDGEMENTS

There are so many people without whom I would not have made it through these last five years. I have been exceptionally fortunate to have you all supporting and encouraging me throughout my time in graduate school. I would like to express my most heartfelt thanks to the following people:

First, to my advisor, Dr. Tom Sharkey, who took me into his lab as an undergraduate and encouraged me to apply to graduate school. His patience, advice, and encouragement have been invaluable, and I would not have been able to accomplish this research without him. He has always supported both my academic and my extra-curricular endeavors and I am extremely grateful for his guidance over the years.

To the rest of my committee—Dr. Dan Jones, Dr. Dave Kramer, Dr. Beronda Montgomery, and Dr. Yair Shachar-Hill—for their valuable suggestions and feedback. I am especially grateful for their support, patience, and counsel during my preliminary exams. I also want to give special thanks to Dr. Jones who taught me mass spectrometry, which was essential to complete this work.

To the Sharkey lab, current and past—Dr. Sean Weise, Dr. Sarathi Weraduwage, Dr. James Santiago, Dr. Thomas Wieloch, Alan McClain, Dr. Aparajita Banerjee, Dr. Linus Gog, Dr. Alexandra Lantz, and the many undergraduates who have been in the lab. I am thankful for the time I have gotten to spend with them sharing bench space, discussing ideas during lab meeting, and celebrating with pie. I am extremely thankful to Dr. Sean Weise. He hired me as an inexperience undergraduate and has answered countless questions over the years. He has been an excellent mentor, co-worker, and friend over all these years, and I would not be here without him.

To Lijun Chen, Linda Danhof, Igor Houwat, Dr. Jyothi Kumar, Jessica Lawrence, Dr. Tony Schilmiller, Heather Sharick, Eunice Van Ells, and the countless others who have kept programs and facilities running. I'm grateful for the time and effort they have put in behind the scenes to keep my research running smoothly. A special thanks to Dr. Rachel Morris who has helped me pursue my love of teaching and communication, has provided so many opportunities and support, and has been a wonderful podcast co-host.

To my family—Merle, Dawn, Brandon, Andrew, Valerie, Karissa, Breezy, and Tory—who have supported me and provided continuous and loving encouragement. I am exceedingly grateful to my husband, Ben Preiser. He has supported me mentally and emotionally through my doctoral work. He has listened to many practice talks, read many rough drafts, and helped me through the most difficult days. I would not have completed this without his encouragement. And thank you to our son, Calvin, who, although he has provided many challenges in completing my dissertation, he has also provided more motivation than he knows.

Finally, to my friends, in and outside MSU, and my church family at University Reformed Church, who rejoiced in the best of moments with me and also walked with me in the hardest ones.

"And whatever you do, whether in word or deed, do it all in the name of the Lord Jesus, giving thanks to God the Father through him." - Colossians 3:17

TABLE OF CONTENTS

LIST OF TABLES

LIST OF FIGURES

KEY TO ABBREVIATIONS

a	measured absorptivity of a leaf
β	partitioning of light between PSI and PS II, assumed to be 0.5
γ	McCree corrected value for ($f_{red} + f_{blue}$)
Γ^*	CO_2 compensation point
ΦII	efficiency of photosystem II
6PG	6-phosphogluconate
6PGD	6-phosphogluconate dehydrogenase
6PGL	6-phosphogluconolactone
6PGLase	6-phosphogluconolactonase
A	assimilation
ADP	adenosine diphosphate
ADPG	adenosine diphosphate glucose
AGPase	ADP-glucose pyrophosphorylase
At	*Arabidopsis thaliana*
ATP	adenosine triphosphate
BEH	ethylene bridged hybrid
BSA	bovine serum albumin
C_c	CO_2 concentration at the site of carboxylation
C_i	internal CO_2 concentration
Cl^-	chloride ion
CO_2	carbon dioxide
Col-0	Columbia-0 ecotype

cPGI	cytosolic PGI
DHAP	dihydroxyacetone phosphate
DIRKs	dark interval relaxation kinetic transients
DMADP	dimethylallyl diphosphate
DTT	dithiothreitol
DNA	deoxyribonucleic acid
DXP	1-deoxy-D-xylulose 5-phosphate
E4P	erythrose 4-phosphate
EDTA	ethylenediaminetetraacetic acid
ESI	electrospray ionization
F6P	fructose 6-phosphate
f_{blue}	fraction of blue light
FBP	fructose 1,6-bisphosphate
FBPase	fructose-1,6-bisphosphatase
f_{red}	fraction of red light
GAP	glyceraldehyde 3-phosphate
G1P	glucose 1-phosphate
G6P	glucose 6-phosphate
G6PDH	glucose-6-phosphate dehydrogenase
GLBRC	Great Lakes Bioenergy Research Center
GPT2	glucose 6-phosphate/phosphate translocator 2
g_m	stomatal conductance
H	Hill coefficient
H^+	hydrogen ion

H_2O_2	hydrogen peroxide
HEPES	4-(2-hydroxyethyl)-1-piperazineethanesulfonic acid
HMBDP	4-hydroxy-3- methylbut-2-enyl diphosphate
HWS	high working standard
I	absorbed light based on steady state fluorescence
IDP	isopentenyl diphosphate
IPTG	isopropyl β-D-1 thiogalactopyranoside
IRGA	infra-red gas analyzer
ISO	isoprene
J_f	electron transport from fluorescence
k_{cat}	turnover number
K_i	inhibition constant
K_m	Michaelis constant
KOH	potassium hyroxide
LB	lysogeny broth
LC	liquid chromatography
LEF	linear electron flow
LWS	low working standard
MDH	malate dehydrogenase
MES	2-(N-morpholino)ethanesulfonic acid
MEP	methyl-D-erythritol 4-phosphate
$MgCl_2$	magnesium chloride
$MnCl_2$	manganese chloride
MS/MS	tandem mass spectrometry

N_2	nitrogen
NaCl	sodium chloride
$NADP^+$	nicotinamide adenine dinucleotide phosphate (oxidized)
NADPH	nicotinamide adenine dinucleotide phosphate (reduced)
Ni-NTA	nickle-nitrilotriacetic acid
O_2	oxygen
OD	optical density
PAR	photosynthetic active radiation
PCR	polymerase chain reaction
PGA	3-phosphoglycerate
PGI	phosphoglucoisomerase
PGM	phosphoglucomutase
P_i	inorganic phosphate
pPGI	plastidic PGI
PRK	phosphoribulokinase
PS I	photosystem I
PS II	photosystem II
QCL	quantum cascade laser
qPCR	quantitative polymerase chain reaction
TCA	tricarboxylic acid
${}^{12}_{O}R$	respiration of $^{12}CO_2$ from other sources
${}^{12}_{S}R$	respiration of $^{12}CO_2$ from the G6P shunt
${}^{12}_{T}R$	total respiration of $^{12}CO_2$
${}^{13}_{O}R$	respiration of $^{13}CO_2$ from other sources

${}^{13}_{S}R$	respiration of $^{13}CO_2$ from the G6P shunt
${}^{13}_{T}R$	total respiration of $^{13}CO_2$
R_D	day respiration
R_L	light respiration
R_T	total non-photorespiratory respiration
R5P	ribose 5-phosphate
RMSE	root mean squared error
ROS	reactive oxygen species
RuBP	ribulose-1,5-bisphosphate
Ru5P	ribulose 5-phosphate
S	substrate concentration
$S_{0.5}$	half-saturation concentration from the maximum velocity
S.D.	standard deviation
SDS-PAGE	sodium dodecyl sulfate polyacrylamide gel electrophoresis
S.E.	standard error
So	*Spinacia oleracea*
TCA	tricarboxylic acid
TPT	triose phosphate translocator
SPME	solid phase microextraction
Ru5P	ribulose 5-phosphate
UDP	uridine diphosphate
UDPG	uridine diphosphate glucose
UPLC	ultra performance liquid chromatography
v	velocity of enzymatic reaction

v_{H+}	velocity of hydrogen ions across the thylakoid membrane
VPDB	Vienna Pee Dee Belemnite
V_{max}	maximum velocity
WT	wild type
XPT	xylulose-5-phosphate/phosphate translocator
Xu5P	xylulose 5-phosphate
YFP	yellow fluorescent protein

CHAPTER 1

The glucose-6-phosphate shunt in the plastid and cytosol

1.1 INTRODUCTION

The Calvin-Benson cycle is the predominant mechanism for fixing carbon in plants (Figure 1.1). Carbon dioxide is added to ribulose bisphosphate to produce two molecules of 3-phosphoglyceric acid (PGA). Energy from the light reactions converts PGA into various intermediates that can be partitioned toward starch, sucrose, fatty acids, amino acids, or recycled to regenerate ribulose bisphosphate (Miziorko and Lorimer, 1983). The flow of carbon through the cycle was documented in the 1950's (Bassham *et al.*, 1954; Bassham and Calvin, 1957), but characterization of specific reactions and regulation is still being undertaken and unexplained observations still remain to be addressed.

Previous work from the Sharkey lab proposed the presence of an alternative pathway around a portion of the Calvin-Benson cycle, the glucose-6-phosphate (G6P) shunt (Sharkey and Weise, 2016). The shunt utilizes a portion of the oxidative pentose phosphate pathway and operates in parallel with the Calvin-Benson cycle. Presence of the oxidative portion of the pentose phosphate pathway in plastids has been shown to be essential (Schnarrenberger *et al.*, 1995; Schnarrenberger *et al.*, 1973; Weise *et al.*, 2006; Xiong *et al.*, 2009). It can interact with the Calvin-Benson cycle due to the use and production of overlapping metabolites. Metabolic interaction of the G6P shunt with other cellular processes has not been previously considered since glucose-6-phosphate dehydrogenase (G6PDH), the first committed step of the shunt, is thought to be inactive during the day (Kruger and von Schaewen, 2003; Scheibe, 1990).

The shunt converts G6P to ribulose 5-phosphate (Ru5P), releasing one molecule of carbon dioxide. While this is a futile cycle resulting in no net gain of carbon, it may regulate photosynthetic carbon metabolism. Our understanding of the enzymes that control flux into the shunt is limited and current photosynthetic models do not take the shunt into account. Better characterization of key enzymes and metabolites of the glucose 6-phosphate shunt will provide

better models of photosynthesis and carbon flux in central metabolism. This may be applied to challenges in creating sustainable food and energy crops.

1.2 OVERVIEW OF THE GLUCOSE-6-PHOSPHATE SHUNT

1.2.1 Enzymatic steps of the glucose-6-phosphate shunt

The G6P shunt is composed of three enzymatic steps (Figure 1.2) (Sharkey and Weise, 2016). G6P is synthesized either in the cytosol or plastid as an intermediate in sucrose or starch synthesis. In the first committed step, G6PDH produces 6-phosphogluconolactone (6PGL) from G6P. The lactone is then either spontaneously hydrolyzed or converted by 6-phosphogluconolactonase (6PGLase) to 6-phosphogluconate (6PG). Finally, 6PG is oxidized by 6-phosphogluconate dehydrogenase (6PGD) to Ru5P and CO_2. Ribulose 5-phosphate can then enter the Calvin-Benson cycle, nucleotide synthesis, or other pentose phosphate metabolism.

1.2.1.1 Phosphoglucoisomerase

Although phosphoglucoisomerase (PGI) is not part of the G6P shunt, this step produces the substrate for the pathway. PGI catalyzes the reversible isomerization of fructose 6-phosphate (F6P) and G6P. The K_{eq} for G6P → F6P is 3.31-3.7 (Backhausen *et al.*, 1997; Dyson and Noltmann, 1968). Previous studies have shown that PGI is inhibited by erythrose 4-phosphate (E4P), PGA, dihydroxyacetone phosphate (DHAP), 6PG, and P_i with K_i*'s* of 2 μM, 2.1-5 mM, 0.3 mM, 0.8 mM, and 8 mM, respectively (Backhausen *et al.*, 1997; Dietz, 1985; Grazi *et al.*, 1960; Mathur *et al.*, 2005; Salas *et al.*, 1964). In higher order plants there are at least two isoforms of PGI: one in the plastid and one in the cytosol (Schnarrenberger *et al.*, 1973).

The cytosolic PGI reaction is at equilibrium (Gerhardt *et al.*, 1987; Sharkey and Vassey, 1989; Szecowka *et al.*, 2013). However, PGI in the plastid is displaced from equilibrium (Backhausen *et al.*, 1997; Gerhardt *et al.*, 1987; Schnarrenberger and Oeser, 1974; Sharkey and Vassey, 1989; Szecowka *et al.*, 2013). Hydrogen isotope measurements using natural abudance

of deuterium support this conclusion (Schleucher *et al.*, 1999). It is also known that the plastidic isoform has a higher K_m for G6P compared to F6P (Dyson and Noltmann, 1968; Schnarrenberger and Oeser, 1974). In the light plastidic PGI becomes inhibited by metabolites in central carbon metabolism and its activity becomes limiting (Backhausen *et al.*, 1997). These observations support the hypothesis that plastidic PGI plays a role in regulating production of G6P (Noltmann, 1964; Sharkey and Vassey, 1989).

1.2.1.2 Glucose-6-phosphate dehydrogenase

After PGI isomerizes F6P to G6P, G6PDH oxidizes G6P to 6-phosphogluonolactone. In addition to producing 6PGL, G6PDH reduces $NADP^+$ to NADPH. Plants have varying numbers of genes for this enzyme both in the plastid and the cytosol (Esposito *et al.*, 2001; Hauschild, 2003; Knight *et al.*, 2001; Schnarrenberger *et al.*, 1973; Semenikhina *et al.*, 1999; Wakao and Benning, 2005; Wendt *et al.*, 2000). However, due to multiple isoforms in the same compartment, biochemical separation methods have not been effective in characterizing each isoform. Modern recombinant technology allows each enzyme to be separately synthesized and characterized.

In Arabidopsis, there are four plastidic isoforms (Meyer *et al.*, 2011; Wakao and Benning, 2005). One of these isoforms is non-functional and is involved in alternative targeting of another plastidic isoform to the peroxisome (Meyer *et al.*, 2011). Plastidic isoforms are redox regulated; reduced G6PDH has a much higher K_m for G6P than does the oxidized form (Née *et al.*, 2014; Preiser *et al.*, 2019; Scheibe *et al.*, 1989). G6PDH can also be regulated by phosphorylation. Plastidic isoforms are quickly deactivated by phosphorylation (Hauschild and von Schaewen, 2003), while one of the cytosolic G6PDH isoforms has been shown to increase activity when phosphorylated (Dal Santo *et al.*, 2012).

G6PDH across different plant species have K_m's for G6P of 0.3-7 mM, for $NADP^+$ of 4.3-17 μM, and K_i's for NADPH of 2.5-70 μM (Esposito *et al.*, 2003; Née *et al.*, 2014; Schnarrenberger *et al.*, 1973; Wakao and Benning, 2005; Wenderoth *et al.*, 1997). G6P protects G6PDH from redox deactivation and inhibition by NAPDH (Née *et al.*, 2014; Olavarría *et al.*, 2012; Shreve and Levy, 1980). There are conflicting reports of other effectors (e.g. F6P has been shown to have both neutral and inhibitory effects) (Semenikhina *et al.*, 1999; Wendt *et al.*, 2000). Despite the presence of plastidic isoforms in leaf tissue, this reaction is generally thought to not occur in the light due to the redox regulation (Anderson *et al.*, 1974; Buchanan, 1980; Buchanan *et al.*, 2015; Heldt and Piechulla, 2005; Née *et al.*, 2014; Scheibe *et al.*, 1989; Wakao and Benning, 2005). However, in conditions such as high CO_2 or increases in light intensity, the enzyme may become oxidized and active (Dyson *et al.*, 2015; Leakey *et al.*, 2009) and in the presence of a high concentration of G6P even the reduced form could have activity.

There are two cytosolic isoforms in Arabidopsis that are highly prevalent in leaf tissue. In contrast to plastidic isoforms, cytosolic isoforms are redox insensitive (Hauschild, 2003; Wakao and Benning, 2005). They have K_m's for G6P of 0.8-1 mM and for $NADP^+$ of 19-6500 μM (Hauschild, 2003; Wakao and Benning, 2005). Only one is inhibited by NAPDH (Wakao and Benning, 2005). Cytosolic G6PDH can quickly respond to changes in G6P. First, it has been shown that export of sugars from the plastid to the cytosol can stimulate cytosolic G6PDH activity (Hauschild, 2003). Second, one of the G6PDH isoforms is sub-saturated and activity will quickly increase with increases in substrate concentration. The other isoform has maximum activity during the day to maintain the redox balance of the cell (Wakao and Benning, 2005).

1.2.1.3 6-phosphogluconolactonase and 6-phosphogluconate dehydrogenase

The final two steps of the G6P shunt are the formation of 6PG and its subsequent oxidative decarboxylation to Ru5P. These steps are found in both the plastid and the cytosol and are practically irreversible (Debnam and Emes, 1999; Herbert *et al.*, 1979).

There are four cytosolic isoforms of 6PGLase and one isoform targeted to both the plastid and peroxisome (Kruger and von Schaewen, 2003; Reumann *et al.*, 2004). Kinetic constants of 6PGLase from plants are not known, but analysis from other organisms show that 6PGL has a K_m of 0.02 – 0.7 mM (Bauer *et al.*, 1983; Medina-Puerta *et al.*, 1988; Schofield and Sols, 1976; Scopes, 1985). It is competitively inhibited by G6P with a K_i of 0.3 mM (Scopes, 1985). While this hydrolysis reaction can occur spontaneously, 6PGLase increases the efficiency of this reaction to avoid production of the dead-end product, γ-6-phosphogluconolactone. Loss-of-function of plastidic 6PGLase is lethal (Miclet *et al.*, 2001; Xiong *et al.*, 2009). This is not observed with cytosolic isoforms due to redundant isoenzymes (Xiong *et al.*, 2009).

In Arabidopsis, there are three isoforms of 6PGD. They are localized in the cytosol, plastid, and transiently in peroxisomes (Hölscher *et al.*, 2016; Hölscher *et al.*, 2014; Meyer *et al.*, 2011). The K_m for the plastidic enzyme is 9.6-100 µM for 6PG and 5.4-6 µM for $NADP^+$ (Krepinsky *et al.*, 2001; Schnarrenberger *et al.*, 1973; Simcox and Dennis, 1978). The K_m of the cytosolic isoenzyme is 12 µM-0.32 mM for 6PG and 4.1-42.2 µM for $NADP^+$ (Bailey-Serres and Nguyen, 1992; Schnarrenberger *et al.*, 1973; Simcox and Dennis, 1978). Similar to G6PDH, 6PGD is inhibited by NADPH with a K_i of 10 µM and E4P (Bailey-Serres and Nguyen, 1992; Signorini *et al.*, 1995). The K_i for E4P has not been determined. 6GPD is also inhibited by fructose 2,6-bisphosphate with a K_i of ~9 µM (Miernyk *et al.*, 1984).

1.2.2 The cytosolic and plastidic glucose-6-phosphate shunts

The G6P shunt can occur in both the plastid and the cytosol (Figure 1.3). In the light, triose phosphates are exported from the Calvin-Benson cycle to the cytosol. G6PDH isoenzymes in the cytosol are not redox regulated and are active during the day, and G6P, which is an intermediate in sucrose synthesis, can also act as a substrate for the cytosolic glucose-6-phosphate shunt (Anderson *et al.*, 1974; Buchanan, 1980; Buchanan *et al.*, 2015; Heldt and Piechulla, 2005; Née *et al.*, 2014; Scheibe *et al.*, 1989; Wakao and Benning, 2005). After Ru5P is produced in the shunt, it can be imported into the plastid to re-enter the Calvin-Benson cycle or can be used in the cytosol for nucleotide synthesis.

The plastidic shunt, which may occur during the day, is regulated by G6PDH kinetics to minimize flux and loss of CO_2. However, this regulation is dynamic and increased flux through the plastidic shunt can occur when G6PDH is oxidized by hydrogen peroxide or thioredoxin (Brennan and Anderson, 1980; Née *et al.*, 2009; Preiser *et al.*, 2019) or when plastidic G6P concentrations increase to overcome the high K_m of reduced G6PDH (Preiser *et al.*, 2019; Scheibe *et al.*, 1989). Hydrogen peroxide or thioredoxin signaling may occur in high light or biotic stress (see Suzuki *et al.* (2011) for a review). The plastidic G6P concentration can be increased by expression of a glucose 6-phosphate/Pi antiporter, GPT2. GPT2 is expressed when sugars accumulate, at high CO_2, and in some starch mutants (Kunz *et al.*, 2010; Leakey *et al.*, 2009; Lloyd and Zakhleniuk, 2004; Weise *et al.*, 2019). When this happens, the concentration gradient of G6P between the plastid and cytosol allows uptake of G6P into the plastid (Gerhardt *et al.*, 1987). This increases the plastidic G6P concentration and stimulates the plastidic shunt.

1.3 PHYSIOLOGICAL IMPLICATIONS OF THE G6P SHUNT

Since the G6P shunt consumes key central metabolites and produces reducing power and CO_2, it is important to consider the physiological ramifications of significant flux through this

pathway in the light. The presence of the G6P shunt may provide an explanation for several unexplained observations such as the source of respiration in the light and a slow-labeling influx of carbon in the Calvin Benson cycle.

1.3.1 Respiration in the light (R_L)

In the light, plants respire non-photorespiratory CO_2, in a process called light respiration (R_L). This is sometimes called day respiration, or R_D. This flux was first identified in oxygen exchange studies in the 1940's, and since then the source of R_L has been debated (Kok, 1948, 1949). A variety of methods have been developed to measure R_L since it is difficult to measure CO_2 release while rubisco is fixing CO_2 (Gong *et al.*, 2018b; Laisk, 1977; Tcherkez *et al.*, 2005; Tcherkez *et al.*, 2017; Yin *et al.*, 2011). Initial studies focused on mitochondrial respiration as the source of CO_2. However, isotopic labeling studies have shown that the tricarboxylic acid (TCA) cycle has very low flux in the light (Calvin and Massini, 1952; Holm-Hansen *et al.*, 1959; Ma *et al.*, 2014; Moses *et al.*, 1959; Tcherkez *et al.*, 2005). The flux leading to R_L has been measured to be at least 10 times greater than that of the TCA cycle (Abadie *et al.*, 2017; Gong *et al.*, 2018a; Loreto *et al.*, 2001; Tcherkez *et al.*, 2009). Glycolysis was proposed as source of respiration, but when labeled glucose is fed to plants, label does not appear in downstream glycolytic products and key enzymatic reactions are downregulated during the day (Lin *et al.*, 1989; Plaxton and Podestá, 2006; Scheible *et al.*, 2000; Stitt, 1990; Vittorio *et al.*, 1954). Non-stoichiometric photorespiration has also been proposed as a source of some R_L, but incomplete labeling is still observed under non-photorespiratory conditions (Cousins *et al.*, 2011; Delwiche and Sharkey, 1993; Mahon *et al.*, 1974). We propose that the G6P shunt is a significant efflux of CO_2 in the light. As described above in section 1.2.2, plastidic G6PDH can be active in the light and cytosolic G6PDH is not redox regulated. This suggests that the G6P shunt is active during the day in both compartments and could account for observations in labeled R_L.

1.3.2 Slow-to-label pool of carbon

It has been reported that photosynthetic intermediates remained only partially labeled (~80%) when leaves were fed $^{13}CO_2$ or $^{14}CO_2$ (Delwiche and Sharkey, 1993; Hasunuma *et al.*, 2010; Ma *et al.*, 2014; Mahon *et al.*, 1974). This is unexpected as turnover times of these intermediates are 0.08-3.2 s^{-1}, yet incomplete labeling persists on the order of minutes to hours (Arrivault *et al.*, 2009; Hasunuma *et al.*, 2010; Ma *et al.*, 2014; Szecowka *et al.*, 2013). This indicates a slow import of unlabeled carbon into the Calvin-Benson cycle from non-recently fixed sources.

One of the characteristics of R_L is that it is an efflux of non-recently fixed carbon (Gauthier *et al.*, 2010; Schnyder *et al.*, 2003; Tcherkez *et al.*, 2012; Tcherkez *et al.*, 2011; Wingate *et al.*, 2007). Methods have utilized this definition of respiration to measure R_L as an efflux of $^{12}CO_2$ in a $^{13}CO_2$ environment (Busch, 2013; Loreto *et al.*, 2001). In the cytosol, hexose phosphates may come from non-recently fixed cytosolic or vacuolar pools and dilute recently fixed carbon that has been exported from the plastid. This would be respired as a mostly unlabeled efflux of CO_2. Respiration and metabolites from the G6P shunt would provide unlabeled carbon that can reenter the Calvin-Benson cycle in three ways:

1) Hexose phosphates can be imported into the plastid via GPT2, a glucose 6-phosphate/phosphate translocator, and enter the plastidic G6P shunt, reentering the Calvin-Benson cycle as pentoses.
2) Unlabeled carbon sources can enter the cytosolic shunt and with the resulting Ru5P being imported into the plastid via XPT (a xylulose 5-phosphate/phosphate translocator) or other transporters.
3) Unlabeled respired CO_2 can be reassimilated by rubisco

While the G6P shunt is not the initial source of unlabeled carbon, it is an essential piece of the pathway that injects non-recently fixed carbon into central metabolism.

1.3.3 Stabilization of photosynthesis in the light

The G6P shunt could serve to stabilize the Calvin-Benson cycle. Previous examples of alternative pathways, such as the rubisco shunt, have been shown to stabilize and maximize carbon efficiency (Schwender *et al.*, 2004). During photosynthesis, the transketolase reaction converts F6P and glyceraldehyde 3-phosphate (GAP) to xylulose 5-phosphate (Xu5P) and erythrose 4-phosphate (E4P). Removal of the phosphate from fructose-1,6-bisphosphate (FBP) makes upstream reactions between GAP and F6P irreversible. In stochastic light or at dawn, GAP pools may become depleted and reactions downstream of F6P may become substrate limited. In this situation, F6P could be converted to G6P and enter the shunt to refill the pentose phosphate pool, allowing the cycle to restart.

1.4 RESEARCH GOALS

Here we propose that the plastidic and cytosolic G6P shunts are active during the day and are a main component of R_L. The first goal of my research is to investigate the kinetic properties of key regulatory enzymes of the plastidic shunt, PGI and G6PDH, to determine if regulation allows for flux through the plastidic shunt. The second goal of my research is to test the hypothesis that the plastidic and cytosolic G6P shunts are the source of respiration in the light. In chapter 2 I report that PGI is a key regulatory enzyme in partioning carbon out of the Calvin-Benson cycle. In chapter 3 I report that plastidic G6PDH can maintain some activity in the light and can be dynamically regulated to increase activity. In chapter 4 I report that the plastidic and cytosolic G6P shunt is responsible for majority of R_L. Finally, I summarize in chapter 5 our current understanding of the G6P shunt and its physiological role in light respiration and propose future directions of research.

APPENDIX

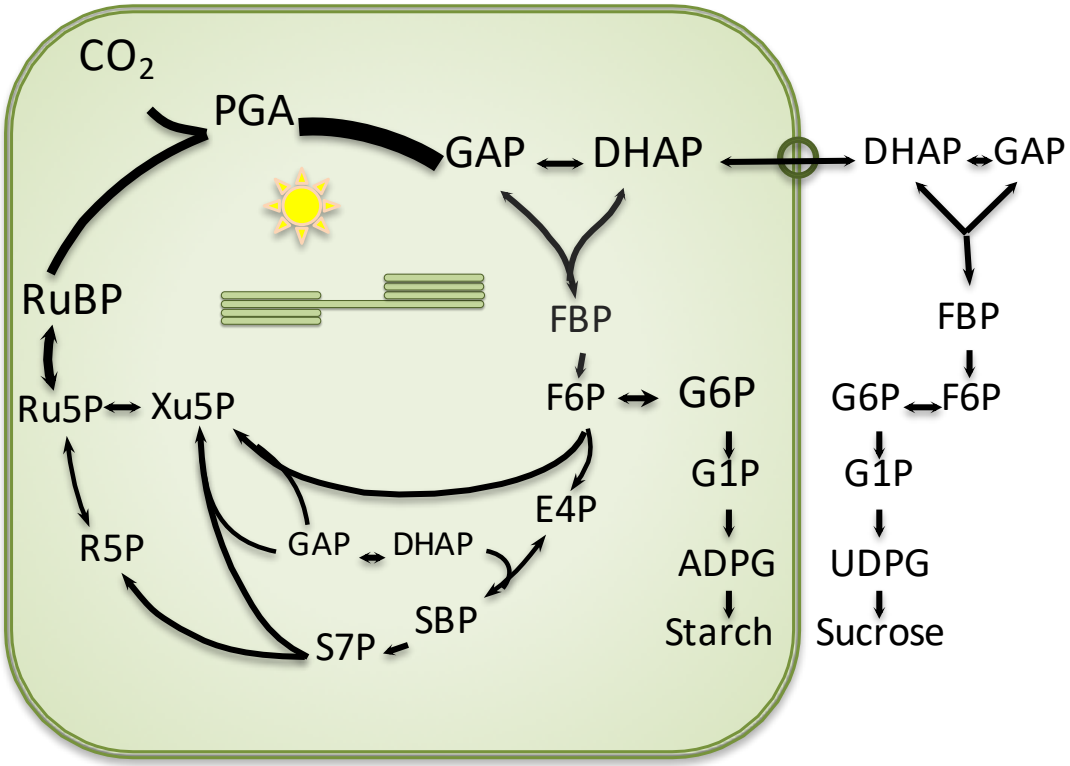

FIGURE 1.1- Carbon flow around the Calvin-Benson cycle.

CO_2 is combined with ribulose bisphosphate (RuBP) by rubisco to produce 3-phosphoglyceric acid (PGA). Triose phosphates (GAP and DHAP) are exported from the cytosol to produce sucrose or continue the cycle. Fructose 6-phosphate (F6P) is isomerized to glucose 6-phosphate (G6P) to enter starch biosynthesis.

FIGURE 1.2- Enzymatic reactions of the G6P shunt.

The G6P shunts are oxidative pentose phosphate pathway reactions. G6P= glucose 6-phosphate, G6PDH = glucose-6-phosphate dehydrogenase, 6PGL = 6-phosphogluconolactone, 6PGLase = 6-phosphogluconolactonase, 6PG = 6-phosphogluconate, 6PGDH = 6-phosphogluconate dehydrogenase, Ru5P = ribulose 5-phosphate.

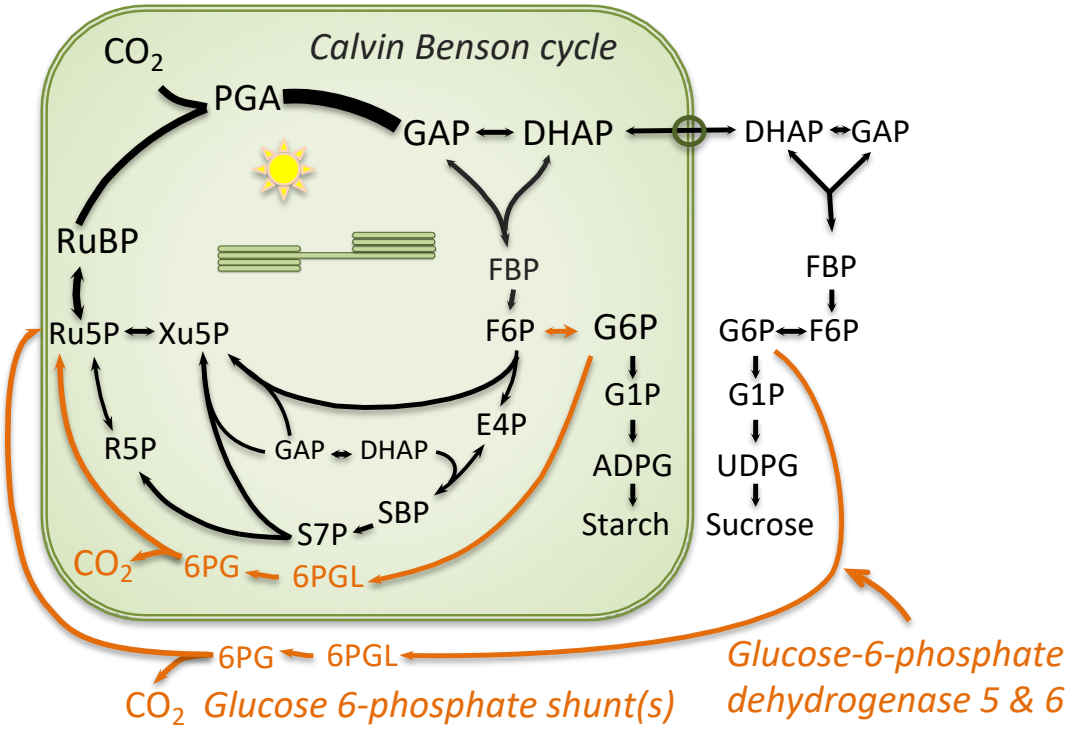

FIGURE 1.3- The G6P shunt in the plastid and cytosol.

The enzymes required for the G6P shunt are present in both compartments. Metabolites in the cytosol can be imported into the plastid either as hexose phosphates via the glucose 6-phosphate/phosphate transporter or pentose phosphates via the xylulose 5-phosphate/phosphate transporter.

LITERATURE CITED

LITERATURE CITED

Abadie C, Blanchet S, Carroll A, Tcherkez G. 2017. Metabolomics analysis of postphotosynthetic effects of gaseous O_2 on primary metabolism in illuminated leaves. *Functional Plant Biology* **44**, 929-940.

Anderson LE, Ng T-CL, Kyung-Eun Yoon P. 1974. Inactivation of pea leaf chloroplastic and cytoplasmic glucose 6-phosphate dehydrogenases by light and dithiothreitol. *Plant Physiology* **53**, 835-839.

Arrivault S, Guenther M, Ivakov A, Feil R, Vosloh D, van Dongen JT, Sulpice R, Stitt M. 2009. Use of reverse-phase liquid chromatography, linked to tandem mass spectrometry, to profile the Calvin cycle and other metabolic intermediates in Arabidopsis rosettes at different carbon dioxide concentrations. *Plant Journal* **59**, 824-839.

Backhausen JE, Jöstingmeyer P, Scheibe R. 1997. Competitive inhibition of spinach leaf phosphoglucose isomerase isoenzymes by erythrose 4-phosphate. *Plant Science* **130**, 121-131.

Bailey-Serres J, Nguyen MT. 1992. Purification and characterization of cytosolic 6-phosphogluconate dehydrogenase isozyme from maize. *Plant Physiology* **100**, 1580-1583.

Bassham JA, Benson AA, Kay LD, Harris AZ, Wilson AT, Calvin M. 1954. The path of carbon in photosynthesis. XXI. The cyclic regeneration of carbon dioxide acceptor. *Journal of the American Chemical Society* **76**, 1760-1770.

Bassham JA, Calvin M. 1957. *The Path of Carbon in Photosynthesis*. Englewood Cliffs, NJ: Prentice-Hall, Inc.

Bauer HP, Srihari T, Jochimas JC, Hofer HW. 1983. 6-Phosphogluconolactonase: purification, properties and activities in various tissues *European Journal of Biochemistry* **133**, 163-168.

Brennan T, Anderson LE. 1980. Inhibition by catalase of dark-mediated glucose-6-phosphate dehydrogenase activation in pea chloroplasts. *Plant Physiology* **66**, 815-817.

Buchanan BB. 1980. Role of light in the regulation of chloroplast enzymes. *Annual Review of Plant Physiology* **31**, 341-374.

Buchanan BB, Gruissem W, Jones RL. 2015. *Biochemistry & Molecular Biology of Plants*. Rockville: American Society of Plant Physiologists.

Busch FA. 2013. Current methods for estimating the rate of photorespiration in leaves. *Plant Biology* **15**, 648-655.

Calvin M, Massini P. 1952. The path of carbon in photosynthesis. XX. The steady-state. *Experimenta* **8**, 445-457.

Cousins A, Walker B, Pracharoenwattana I, Smith S, Badger M. 2011. Peroxisomal hydroxypyruvate reductase is not essential for photorespiration in Arabidopsis but its absence causes an increase in the stoichiometry of photorespiratory CO2 release. *Photosynthesis Research* **108**, 91-100.

Dal Santo S, Stampfl H, Krasensky J, Kempa S, Gibon Y, Petutsching E, Rozhon W, Heuck A, Clausen T, Jonak C. 2012. Stress-induced GSK3 regulates the redox stress response by phosphorylating glucose-6-phosphate dehydrogenase in Arabidopsis. *The Plant Cell* **24**, 3380-3392.

Debnam P, Emes M. 1999. Subcellular distribution of enzymes of the oxidative pentose phosphate pathway in root and leaf tissues. *Journal of Experimental Botany* **50**, 1653-1661.

Delwiche CF, Sharkey TD. 1993. Rapid appearance of ^{13}C in biogenic isoprene when $^{13}CO_2$ is fed to intact leaves. *Plant, Cell & Environment* **16**, 587-591.

Dietz KJ. 1985. A possible rate limiting function of chloroplast hexosemonophosphate isomerase in starch synthesis of leaves. *Biochimica et Biophysica Acta* **839**, 240-248.

Dyson BC, Allwood JW, Feil R, Xu YUN, Miller M, Bowsher CG, Goodacre R, Lunn JE, Johnson GN. 2015. Acclimation of metabolism to light in *Arabidopsis thaliana*: the glucose 6-phosphate/phosphate translocator GPT2 directs metabolic acclimation. *Plant, Cell & Environment* **38**, 1404-1417.

Dyson JED, Noltmann EA. 1968. The effect of pH and temperature on the kinetic parameters of phosphoglucose isomerase. *The Journal of Biological Chemistry* **243**, 1401-1414.

Esposito S, Carfagna S, Massaro G, Vona V, Di Martino Rigano V. 2001. Glucose-6-phosphate dehydrogenase in barley roots: kinetic properties and localisation of the isoforms. *Planta* **212**, 627-634.

Esposito S, Massaro G, Vona V, Di Martino Rigano V, Carfagna S. 2003. Glutamate synthesis in barley root: the role of the plastidic glucose-6-phosphate dehydrogenase. *Planta* **216**, 639-647.

Gauthier PP, Bligny R, Gout E, Mahé A, Nogués S, Hodges M, Tcherkez G. 2010. In folio isotopic tracing demonstrates that nitrogen assimilation into glutamate is mostly independent from current CO_2 assimilation in illuminated leaves of Brassica napus. *New Phytologist* **185**, 988-999.

Gerhardt R, Stitt M, Heldt HW. 1987. Subcellular metabolite levels in spinach leaves. Regulation of sucrose synthesis during diurnal alterations in photosynthetic partitioning. *Plant Physiology* **83**, 399-407.

Gong XY, Tcherkez G, Wenig J, Schäufele R, Schnyder H. 2018a. Determination of leaf respiration in the light: comparison between an isotopic disequilibrium method and the Laisk method. *New Phytologist* **218**, 1371-1382.

Gong XY, Tcherkez G, Wenig J, Schäufele R, Schnyder H. 2018b. Determination of leaf respiration in the light: comparison between an isotopic disequilibrium method and the Laisk method. *New Phytologist* **218**, 1371-1382.

Grazi E, De Flora A, Pontremoli S. 1960. The inhibition of phosphoglucose isomerase by D-erythrose 4-phosphate. *Biochemical and Biophysical Research Communications* **2**, 121-125.

Hasunuma T, Harada K, Miyazawa S-I, Kondo A, Fukusaki E, Miyake C. 2010. Metabolic turnover analysis by a combination of in vivo ^{13}C-labelling from $^{13}CO_2$ and metabolic profiling with CE-MS/MS reveals rate-limiting steps of the C_3 photosynthetic pathway in Nicotiana tabacum leaves. *Journal of Experimental Botany* **61**, 1041-1051.

Hauschild R, von Schaewen A. 2003. Differential regulation of glucose-6-phosphate dehydrogenase isoenzyme activities in potato. *Plant Physiology* **133**, 47-62.

Heldt H-W, Piechulla B. 2005. *Plant Biochemistry*. Burlington MA: Elsevier Academic Press.

Herbert M, Burkhard C, Schnarrenberger C. 1979. A survey for isoenzymes of glucose phosphate isomerase, phosphoglucomutase, glucose 6-phosphate dehydrogenase, and 6-phosphogluconate dehydrogenase in C3-, C4-, and Crassulacean-acid-metabolism plants and green algae. *Planta* **145**, 95-104.

Holm-Hansen O, Nishida K, Moses V, Calvin M. 1959. Effects of mineral salts on short-term incorporation of carbon dioxide in *Chlorella*. *Journal of Experimental Botany* **10**, 109-124.

Hölscher C, Lutterbey M-C, Lansing H, Meyer T, Fischer K, von Schaewen A. 2016. Defects in peroxisomal 6-phosphogluconate dehydrogenase isoform PGD2 Prevent gametophytic interaction in Arabidopsis thaliana. *Plant Physiology* **171**, 192-205.

Hölscher C, Meyer T, Von Schaewen A. 2014. Dual-targeting of Arabidopsis 6-phosphogluconolactonase 3 (PGL3) to chloroplasts and peroxisomes involves interaction with Trx m2 in the cytosol. *Molecular Plant* **7**, 252-255.

Knight JS, Emes MJ, Debnam P. 2001. Isolation and characterisation of a full-length genomic clone encoding a plastidic glucose 6-phosphate dehydrogenase from Nicotiana tabacum. *Planta* **212**, 499-507.

Kok B. 1948. A critical consideration of the quantum yield of *Chlorella* photosynthesis. *Enzymologia* **13**, 1-56.

Kok B. 1949. On the interrelation of respiration and photosynthesis in green plants. *Biochemica et Biophysica Acta* **3**, 625-631.

Krepinsky K, Plaumann M, Martin W, Schnarrenberger C. 2001. Purification and cloning of chloroplast 6-phosphogluconate dehydrogenase from spinach. *European Journal of Biochemistry* **268**, 2678-2686.

Kruger NJ, von Schaewen A. 2003. The oxidative pentose phosphate pathway: structure and organisation. *Current Opionin in Plant Biology* **6**, 236-246.

Kunz HH, Häusler RE, Fettke J, Herbst K, Niewiadomski P, Gierth M, Bell K, Steup M, Flügge UI, Schneider A. 2010. The role of plastidial glucose-6-phosphate/phosphate translocators in vegetative tissues of *Arabidopsis thaliana* mutants impaired in starch biosynthesis. *Plant Biology* **12**, 115-128.

Laisk A. 1977. *Kinetics of Photosynthesis and Photorespiration of C3 Plants, cited in Tcherkez et al. 2017*. Moscow: Nauka.

Leakey ADB, Xu F, Gillespie KM, McGrath JM, Ainsworth EA, Ort DR. 2009. Genomic basis for stimulated respiration by plants growing under elevated carbon dioxide. *Proceedings of the National Academy of Sciences of the United States of America* **106**, 3597-3602.

Lin M, Turnpin DH, Plaxton WC. 1989. Pyruvate kinase isozymes from the green alga *Selenastrum minutum. Archives of Biochemistry and Biophysics* **269**, 228-238.

Lloyd JC, Zakhleniuk OV. 2004. Responses of primary and secondary metabolism to sugar accumulation revealed by microarray expression analysis of the Arabidopsis mutant, pho3. *Journal of Experimental Botany* **55**, 1221-1230.

Loreto F, Velikova V, Di Marco G. 2001. Respiration in the light measured by $^{12}CO_2$ emission in $^{13}CO_2$ atmosphere in maize leaves. *Australian Journal of Plant Physiology* **28**, 1103-1108.

Ma F, Jazmin LJ, Young JD, Allen DK. 2014. Isotopically nonstationary ^{13}C flux analysis of changes in Arabidopsis thaliana leaf metabolism due to high light acclimation. *Proceedings of the National Academy of Sciences* **111**, 16967-16972.

Mahon JD, Fock H, Canvin DT. 1974. Changes in specific radioactivities of sunflower leaf metabolites during photosynthesis in $^{14}CO_2$ and $^{12}CO_2$ at normal and low oxygen. *Planta* **120**, 125-134.

Mathur D, Ahsan Z, Tiwari M, Garg LC. 2005. Biochemical characterization of recombinant phosphoglucose isomerase of *Mycobacterium tuberculosis*. *Biochemical and Biophysical Research Communications* **337**, 626-632.

Medina-Puerta MM, Gallego-Iniesta M, Garrido-Pertierra A. 1988. Kinetic properties from bass liver 6-phosphogluconolactonase. *Biochemistry International* **16**, 571-577.

Meyer T, Hölscher C, Schwöppe C, von Schaewen A. 2011. Alternative tageting of Arabidopsis plastidic glucose-6-phosphate dehydrogenase G6PD1 involves cysteine-dependent interaction with G6PD4 in the cytosol. *The Plant Journal* **66**, 745-758.

Miclet E, Stoven V, Michels PA, Opperdoes FR, Lallemand JY, Duffieux F. 2001. NMR spectroscopic analysis of the first two steps of the pentose-phosphate pathway elucidates the role of 6-phosphogluconolactonase. *Journal of Biological Chemistry* **276**, 34840-34846.

Miernyk JA, MacDougall PS, Dennis DT. 1984. *In vitro* inhibition of the plastid and cytosolic isozymess of 6-phosphogluconate dehydrogenase from developing endosperm of *Ricinus communis* by fructose 2,6-bisphosphate. *Plant Physiology* **76**, 1093-1094.

Miziorko HM, Lorimer GH. 1983. Ribulose-1,5-bisphosphate carboxylase/oxygenase. *Annual Review of Biochemistry* **52**, 507-535.

Moses V, Holm-Hansen O, Bassham JA, Calvin M. 1959. The relationship between the metabolic pools of photosynthetic and respiratory intermediates. *Journal of Molecular Biology* **1**, 21-29.

Née G, Aumont-Nicaise M, Zaffagnini M, Nessler S, Valerio-Lepiniec M, Bourguet-Issakidis E. 2014. Redox regulation of chloroplastic G6PDH activity by thioredoxin occurs through structural changes modifying substrate accessibility and cofactor binding. *Biochem J* **457**, 117-125.

Née G, Zaffagnini M, Trost P, Issakidis-Bourguet E. 2009. Redox regulation of chloroplastic glucose-6-phosphate dehydrogenase: A new role for f-type thioredoxin. *FEBS Letters* **583**, 2827-2832.

Noltmann EA. 1964. Isolation of crystalline phosphoglucose isomerase from rabbit muscle. *The Journal of Biological Chemistry* **239**, 1545-1550.

Olavarría K, Valdés D, Cabrera R. 2012. The cofactor preference of glucose-6-phosphate dehydrogenase from *Escherichia coli* - modelling the physiological production of reduced cofactors. *FEBS Journal* **279**, 2296-2309.

Plaxton WC, Podestá FE. 2006. The functional organization and control of plant respiration. *Critical Reviews in Plant Sciences* **25**, 159-198.

Preiser AL, Fischer N, Banerjee A, Sharkey T. 2019. Plastidic glucose-6-phosphate dehydrogenase is regulated to maintain activity in the light. *Biochemical Journal* **476**, 1539-1551.

Reumann S, Ma C, Lemke S, Babujee L. 2004. AraPerox. A database of putative Arabidopsis proteins from plant peroxisomes. *Plant Physiology* **136**, 2587-2608.

Salas M, Viñuela E, Sols A. 1964. Spontaneous and enzymatically catalyzed anomerization of glucose 6-phosphate and anomeric specificity of related enzymes. *The Journal of Biological Chemistry* **240**, 561-568.

Scheibe R. 1990. Light/dark modulation: Regulation of chloroplast metabolism in a new light. *Botanica Acta* **103**, 327-334.

Scheibe R, Geissler A, Fickenscher K. 1989. Chloroplast glucose-6-phosphate dehydrogenase: K_m shift upon light modulation and reduction. *Archives of Biochemistry and Biophysics* **274**, 290-297.

Scheible WR, Krapp A, Stitt M. 2000. Reciprocal diurnal changes of phosphoenolpyruvate carboxylase expression and cytosolic pyruvate kinase, citrate synthase and NADP-isocitrate dehydrogenase expression regulate organic acid metabolism during nitrate assimilation in tobacco leaves. *Plant, Cell & Environment* **23**, 1155-1167.

Schleucher J, Vanderveer P, Markley JL, Sharkey TD. 1999. Intramolecular deuterium distributions reveal disequilibrium of chloroplast phosphoglucose isomerase. *Plant, Cell & Environment* **22**, 525-533.

Schnarrenberger C, Flechner A, Martin W. 1995. Enzymatic evidence for a complete oxidative pentose phosphate pathway in chloroplasts and an incomplete pathway in the cytosol of spinach leaves. *Plant Physiology* **108**, 609-614.

Schnarrenberger C, Oeser A. 1974. Two isoenzymes of glucosephosphate isomerase from spinach leaves and their intracellular compartmentation. *European Journal of Biochemistry* **45**, 77-82.

Schnarrenberger C, Oeser A, Tolbert NE. 1973. Two enzymes each of glucose-6-phosphate dehydrogenase and 6-phosphogluconate dehydrogenase in spinach leaves. *Archives of Biochemistry and Biophysics* **154**, 438-448.

Schnyder H, Schaüfele R, Lötscher M, Gebbing T. 2003. Disentangling CO_2 fluxes: direct measurements of mesocosm-scale natural abundance $^{13}CO_2/^{12}CO_2$ gas exchagne, ^{13}C discrimination, and labelling of CO_2 exchange flux components in controlled environments. *Plant, Cell & Environment* **26**, 1863-1874.

Schofield PJ, Sols A. 1976. Rat liver 6-phosphogluconolactonase: a low K_m enzyme. *Biochemical and Biophysical Research Communications* **71**, 1313-1318.

Schwender J, Goffman F, Ohlrogge JB, Shachar-Hill Y. 2004. Rubisco without the Calvin cycle improves the carbon efficiency of developing green seeds. *Nature* **432**, 779-782.

Scopes RK. 1985. 6-Phosphogluconolactonase from *Zymomonas mobilis*: an enzyme of high catalytic efficiency *FEBS Journal* **193**, 185-188.

Semenikhina AV, Popova A, Matasova LV. 1999. Catalytic properties of glucose-6-phosphate dehydrogenase from pea leaves. *Biochemistry* **64**, 863-866.

Sharkey TD, Vassey TL. 1989. Low oxygen inhibition of photosynthesis is caused by inhibition of starch synthesis. *Plant Physiology* **90**, 385-387.

Sharkey TD, Weise SE. 2016. The glucose 6-phosphate shunt around the Calvin-Benson Cycle. *Journal of Experimental Botany* **67**, 4067-4077.

Shreve DS, Levy HR. 1980. Kinetic mechanism of glucose-6-phosphate dehydrogenase from the lactating rat mammary gland. *Journal of Biological Chemistry* **255**, 2670-2677.

Signorini M, Bregoli AM, Caselli L, Bergamini CM. 1995. Purification and properties of 6-phosphogluconate dehydrogenase from beet leaves. *Biochemistry and Molecular Biology International* **35**, 669-675.

Simcox DP, Dennis DT. 1978. 6-phosphogluconate dehydrogenase isoenzymes from the developing endosperm of *Ricinus conmunis* L. *Plant Physiology* **62**, 287-290.

Stitt M. 1990. Fructose-2,6-bisphosphate as a regulatory molecule in plants. *Annual Review of Plant Physiology and Plant Molecular Biology* **41**, 153-185.

Suzuki N, Koussevitzky S, Mittler R, Miller G. 2011. ROS and redox signalling in the response of plants to abiotic stress. *Plant Cell and Environment* **35**, 259-270.

Szecowka M, Heise R, Tohge T, Nunes-Nesi A, Vosloh D, Huege J, Feil R, Lunn J, Nikoloski Z, Stitt M, Fernie AR, Arrivault S. 2013. Metabolic fluxes in an illuminated Arabidopsis rosette. *The Plant Cell Online* **25**, 694-714.

Tcherkez G, Cornic G, Bligny R, Gout E, Ghashghaie J. 2005. *In vivo* respiratory metabolism of illuminated leaves. *Plant Physiology* **138**, 1596-1606.

Tcherkez G, Gauthier P, Buckley TN, Busch FA, Barbour MM, Bruhn D, Heskel MA, Gong XY, Crous KY, Griffin K, Way D, Turnbull M, Adams MA, Atkin OK, Farquhar GD, Cornic G. 2017. Leaf day respiration: low CO_2 flux but high significance for metabolism and carbon balance. *New Phytologist* **216**, 986-1001.

Tcherkez G, Mahé A, Gauthier P, Mauve C, Gout E, Bligny R, Cornic G, Hodges M. 2009. *In folio* respiratory fluxomics revealed by 13C isotopic labeling and H/D isotope effects highlight the noncyclic nature of the tricarboxylic acid 'cycle' in illuminated leaves. *Plant Physiology* **151**, 620-630.

Tcherkez G, Mahé A, Guérard F, Boex-Fontvieille ERA, Gout E, Lamothe M, Barbour MM, Bligny R. 2012. Short-term effects of CO_2 and O_2 on citrate metabolism in illuminated leaves. *Plant, Cell & Environment* **35**, 2208-2220.

Tcherkez G, Mauve C, Lamothe M, Le Bras C, Grapin A. 2011. The $^{13}C/^{12}C$ isotopic signal of day-respired CO_2 in varigated leaves of *Pelargonium x horotum*. *Plant, Cell & Environment* **34**, 270-283.

Vittorio PV, Krotkov G, Reed GB. 1954. Synthesis of radioactive sucrose by tobacco leaves from ^{14}C uniformly labelled glucose and glucose-1-phosphate. *Canadian Journal of Botany* **32**, 369-377.

Wakao S, Benning C. 2005. Genome-wide analysis of glucose-6-phosphate dehydrogenases in Arabidopsis. *The Plant Journal* **41**, 243-256.

Weise SE, Liu T, Childs KL, Preiser AL, Katulski HM, Perrin-Porzondek C, Sharkey TD. 2019. Transcriptional regulation of the glucose-6-phosphate/phosphate translocator 2 is related to carbon exchange across the chloroplast envelope. *Frontiers in Plant Science* **10**, 827.

Weise SE, Schrader SM, Kleinbeck KR, Sharkey TD. 2006. Carbon balance and circadian regulation of hydrolytic and phosphorolytic breakdown of transitory starch. *Plant Physiology* **141**, 879-886.

Wenderoth I, Scheibe R, von Schaewen A. 1997. Identification of the cysteine residues involved in redox modification of plant plastidic glucose-6-phosphate dehydrogenase. *Journal of Biological Chemistry* **272**, 26985-26990.

Wendt UK, Wenderoth I, Tegeler A, von Schaewen A. 2000. Molecular characterization of a novel glucose-6-phosphate dehydrogenase from potato (*Solanum tuberosum L.*). *The Plant Journal* **23**, 723-733.

Wingate L, Seibt U, Moncrieff JB, Jarvis PG, Lloyd J. 2007. Variations in ^{13}C discrimination during CO_2 exchange by *Picea sitchensis* branches in the field. *Plant, Cell & Environment* **30**, 600-616.

Xiong Y, DeFraia C, Williams D, Zhang X, Mou Z. 2009. Characterization of Arabidopsis 6-phosphogluconolactonase T-DNA insertion mutants reveals an essential role for the oxidative section of the plastidic pentose phosphate pathway in plant growth and development. *Plant and Cell Physiology* **50**, 1277-1291.

Yin X, Sun Z, Struik PC, Gu J. 2011. Evaluating a new method to estimate the rate of leaf respiration in the light by analysis of combined gas exchange and chlorophyll fluorescence measurements. *Journal of Experimental Botany* **62**, 3489-3499.

CHAPTER 2

Phosphoglucoisomerase plays a key regulatory role in starch synthesis and degradation

This research was done in collaboration with Dr. Aparajita Banerjee, Dr. Sean Weise, Dr. Luciana Renna, and Alan McClain. S.W. designed the recombinant PGI and transient expression constructs. A.B. purified the recombinant PGI and performed some kinetic assays. L.R. helped with YFP imaging. A.M. wrote scripts for collecting and analyzing

2.1 ABSTRACT

Phosphoglucoisomerase (PGI) isomerizes fructose 6-phosphate (F6P) and glucose 6-phosphate (G6P) in starch and sucrose biosynthesis. Both plastidic and cytosolic isoforms are found in plant leaves. Previous studies have attempted to determine the K_m for F6P and G6P for these isoforms (Schnarrenberger and Oeser, 1974; Backhausen et al., 1997) and to find significant inhibitors (Backhausen *et al.*, 1997; Dietz, 1985; Mathur *et al.*, 2005; Sharkey and Weise, 2016). Using recombinant enzymes and isolated chloroplasts, we have characterized plastidic and cytosolic isoforms of PGI. We have found that the plastidic PGI has at least a 3-fold higher K_m for G6P compared to that for F6P. Our results, in combination with the observation that plastidic PGI is not in equilibrium (Backhausen *et al.*, 1997; Gerhardt *et al.*, 1987; Schnarrenberger and Oeser, 1974; Sharkey and Vassey, 1989; Szecowka *et al.*, 2013), support the conclusion the stromal G6P is kept low and PGI acts like a one-way valve, allowing carbon to leave the Calvin-Benson cycle but not reenter. We also found that misexpression of PGI disrupts starch accumulation and degradation. We conclude that PGI is a key regulatory enzyme in starch synthesis and degradation.

2.2 INTRODUCTION

In the light, plants synthesize and store transient starch in the plastid to breakdown as energy reserves during the night. Starch is accumulated linearly throughout the day and carbon must be carefully partitioned out of the Calvin-Benson cycle in order to not deplete metabolite pools needed for continuation of the Calvin-Benson cycle while still accumulating adequate amounts of starch to survive the night. Therefore, regulation of the enzymes involved in partitioning carbon out of the cycle is essential to understand.

There are several key enzymes in starch synthesis. First, in order to export carbon from the Calvin-Benson cycle, phosphoglucoisomerase (PGI) isomerizes fructose 6-phosphate (F6P) and glucose 6-phosphate (G6P). This reaction is reversible but is displaced from equilibrium (Backhausen *et al.*, 1997; Gerhardt *et al.*, 1987; Schnarrenberger and Oeser, 1974; Sharkey and Vassey, 1989; Szecowka *et al.*, 2013). Loss of PGI decreases starch by 98.5% (Yu *et al.*, 2000). There is an additional isoform of PGI in the cytosol that isomerizes F6P and G6P in the sucrose synthesis pathway. Unlike the plastidial isoform, the G6P/F6P ratio in the cytosol is at equilibrium (Gerhardt *et al.*, 1987; Sharkey and Vassey, 1989; Szecowka *et al.*, 2013). In the plastid, G6P is converted to glucose-1-phosphate (G1P) by phosphoglucomutase (PGM). This reaction is also reversible and has a K_m for G6P of 47 μM and 8.5 μM for G1P (Lowry and Passonneau, 1969; Ray and Roscelli, 1964). Next, G1P is metabolized to activated ADP-glucose by ADP-glucose pyrophosphorylase (AGPase), which has a K_m for G1P of 0.13-0.25 mM (Kavakli *et al.*, 2002; Salamone *et al.*, 2002). The equilibrium for PGM lies far in favor of G6P and measured G1P concentrations in the chloroplast are ~40 μM, making AGPase activity very sensitive to the supply of G1P (discussed in Sharkey and Weise (2012)). AGPase is activated by 3-phosphoglyceric acid (PGA), inhibited by phosphate, and is post-translationally modified by cysteine bridges in oxidizing conditions (Hendriks *et al.*, 2003; Preiss *et al.*, 1995). Loss-of-

function in both PGM and AGPase results in starchless plants (Caspar *et al.*, 1985; Hanson and McHale, 1988; Kofler *et al.*, 2000; Lin *et al.*, 1988). Finally, after the glucose moiety is activated by the addition of ADP, it is attached to the growing starch granule by the work of starch synthases and branching and debranching enzymes (Preiss *et al.*, 1991; Tetlow and Emes, 2014).

While starch synthesis has been well-studied for decades, our knowledge of the regulation of the entire pathway remains incomplete. Particularly, it is unknown why the plastidic PGI is displaced from equilibrium and appears to be regulated, despite catalyzing an easily reversible reaction. Our goal in this study was to confirm the kinetics of both plastidic and cytosolic PGI and to examine the inhibition of PGI by Calvin-Benson cycle metabolites. We confirmed that plastidic PGI has a higher K_m for G6P than for F6P and that the cytosolic enzyme does not have this limitation (Dyson and Noltmann, 1968; Schnarrenberger and Oeser, 1974). We also found that previous reports of PGA inhibiting PGI are incorrect (Backhausen *et al.*, 1997; Dietz, 1985; Mathur *et al.*, 2005; Sharkey and Weise, 2016). PGI is instead inhibited by erythrose 4-phosphate (E4P) and 6-phosphogluconate (6PG). Additionally, we sought to understand the importance of PGI regulation by using transgenic expression in *Nicotiana tabacum* to mislocalize cytosolic PGI, which has similar K_m's for F6P and G6P, in the plastid. We found that expression of misregulated PGI increases starch accumulation and disrupts starch degradation. From this work, we conclude that, despite catalyzing a reversible reaction, PGI is a key point of regulation in starch synthesis by acting as a one-way value to export carbon from the Calvin-Benson cycle and as a rate-limiting step in starch synthesis.

2.3 MATERIALS AND METHODS

2.3.1 Overexpression and purification of recombinant enzymes

N-terminal His-tagged *Arabidopsis thaliana* plastidic and cytosolic PGI genes were commercially synthesized by GenScript (https://www.genscript.com). Both plasmid constructs

were overexpressed in *E. coli* strain BL21. Cells were grown at 37ºC to an OD_{600} of 0.6 to 1.0 and induced with 0.5 mM isopropyl β-D-1 thiogalactopyranoside at room temperature overnight. Cells were centrifuged and resuspended in lysis buffer (5 mL lysis buffer/g of pellet; 50 mM sodium phosphate, pH 8.0, 300 mM NaCl) containing 1 mg mL^{-1} lysozyme, 1 µg mL^{-1} of DNAseI, and 1x protease inhibitor cocktail (Sigma Aldrich, www.sigmaaldrich.com). Cells were then lysed by sonication (Branson Sonifier 250, us.vwr.com). The sonicator was set at 50% duty cycle and an output level of 1. The cells were sonicated using five steps where each step consisted of a 15 s pulse followed by 15 s on ice. The lysate was centrifuged and supernatant collected. Ni-NTA resin (0.25 volume of lysate; Qiagen, https://www.qiagen.com) was added to the crude lysate with gentle stirring for 1 h. The mixture was loaded into a column and allowed to settle, then washed with wash buffer (50 mM sodium phosphate, pH 8.0, 300 mM NaCl, 10 mM imidazole) until the OD_{280} of the effluent was less than 0.05. Protein was eluted with six volumes of elution buffer (50 mM sodium phosphate pH 8.0, 300 mM NaCl, 250 mM imidazole) containing 1x protease inhibitor cocktail (Sigma Aldrich, www.sigmaaldrich.com). The Ni-NTA column purification was performed in a cold room at 4˚C. For all purified proteins, protein concentration was determined using a Pierce 660 nm protein assay reagent kit (ThermoFisher Scientific, www.thermofisher.com) using a bovine serum albumin standard and fractions containing >95% of total protein of interest were combined and concentrated using Amicon Ultra 0.5 ml centrifugal filters (molecular weight cut off 3 kDa). Glycerol was added to the concentrated protein to obtain a final protein solution with 15% glycerol. The glycerol stock of the proteins was aliquoted into small volumes, frozen in liquid nitrogen, and stored at -80˚C. Final preparations of purified protein were run on a 12% SDS-polyacrylamide gel and stained with Coomassie Blue to check the purity of the enzymes and concentration was determined as

described above. Molecular weights were estimated from the protein construct using Vector NTI (ThermoFisher Scientific, www.thermofisher.com).

2.3.2 Coupled spectrophotometric assay for PGI (F6P to G6P reaction)

The activity of the purified plastidic and cytosolic PGI was studied using coupled spectrophotometric assays. Concentrations of G6P and F6P were measured spectrophotometrically using NADPH-linked assays (Lowry and Passonneau, 1972). All assays were validated by demonstrating linear product formation, proportional to the time of the assay and amount of enzyme added. All coupling enzymes were added in excess so that no change in product formation was seen when varying the coupling enzyme. PGI assays were done in 50 mM bicine buffer pH 7.8, containing 4.8 mM DTT, 0.6 mM $NADP^+$, 2 U G6PDH (from *Leuconostoc mesenteroides*), varying concentrations of F6P as indicated below, and 1.31 ng plastidic or cytosolic PGI. The reaction was:

$$\mathrm{F6P} \rightleftarrows \mathrm{G6P} + \mathrm{NADP^+} \longrightarrow 6-\mathrm{phosphogluconate} + \mathrm{NADPH} + \mathrm{H^+}.$$

The concentrations used to study the K_m of PGI for F6P were 0-4.8 mM. Under these conditions, less than 5% of the non-limiting substrate was consumed over the duration of the assay. The assay mixtures were prepared by adding all the components except the enzyme. Activity was recorded with a dual wavelength filter photometer (Sigma ZFP2) as the increase in absorbance at 334 nm minus absorbance at 405 nm caused by $NADP^+$ reduction to NADPH using an extinction coefficient of 6190 M^{-1} cm^{-1}. These wavelengths were used because they correspond to emission wavelengths of the lamp used in the filter photometer.

2.3.3 Mass spectrometry assay for PGI (G6P to F6P reaction)

The activity of the purified plastidic and cytosolic PGI in the G6P to F6P direction was studied using a coupled mass spectrometer assay. The assay mixture contained 50 mM Tris pH 7.8, 2.5 mM $MgCl_2$, 1 mM ATP, 5 mM DTT, 0.15 U phosphofructokinase (from *Bacillus*

stearothermophilus), varying concentrations of G6P from 0-3.6 mM, and 1.6 ng of plastidic or cytosolic PGI.

The reaction was:

$$\text{G6P} \rightleftarrows \text{F6P} \longrightarrow \text{FBP}.$$

The assay mixtures were prepared by adding all the components except the enzyme. The reaction was initiated upon addition of the enzyme. After five min, the reaction was quenched with four volumes of 100% ice-cold methanol. The concentration of FBP produced was shown to be linear for up to ten min. Five nmol of D-[UL-$^{13}C_6$] fructose 1,6-bisphosphate was added as an internal standard for quantification, and the sample was heated for 5 min at 95˚C. Six volumes of 10 mM tributylamine, pH 5.0, was added and the sample was filtered through a Mini-UniPrep 0.2 µm Syringeless Filter Device (GE Healthcare Life Sciences, Whatman). LC/MS-MS was carried out on a Waters Quattro Premier XE system and was operated in electrospray negative ion mode with both multiple reaction monitoring (Table 2.1). The capillary voltage was 2.75 kV; the cone voltage, 50 V; the extractor voltage, 5 V. The source temperature was 120˚C and the desolvation temperature was 350˚C. Gas flow for the desolvation and cone was set to 800 and 50 L h^{-1}, respectively. MassLynx software and the Acquity UPLC Console were used to control the instrument. Samples were passed through an Aquity UPLC BEH Column (Waters) with a multi-step gradient with eluent A (10 mM tributylamine with 5% methanol, adjusted to pH 6 with 500 mM acetic acid) and eluent B (methanol): 0-1 min, 95-85% A; 1-3 min, 85%-65% A; 3-3.5 min, 65-40% A; 3.5-4 min, 40-0% A; 4-8.50 min, 0% A; 8.5-10 min, 100% A. The flow rate was 0.3 mL min^{-1}. FBP peaks were integrated using QuanLynx software and the concentration of the metabolites was quantified by comparing the peak response to an external calibration curve.

2.3.4 Kinetic characterization

Enzymes were assayed at varying concentrations of substrate as described above. The K_m values for plastidic and cytosolic PGI were determined by fitting the data with non-linear regression using the Hill function in OriginPro 8.0 (OriginLab Corporation).

2.3.5 Inhibition studies

Different metabolites of the Calvin-Benson cycle were tested for their effect on PGI activity. All the metabolites were purchased from Sigma Aldrich (Sigma Aldrich, www.sigmaaldrich.com). In metabolite screening assays, metabolites were assayed at a 1:1 ratio with the substrate. To determine the K_i of PGI for different metabolites, the assay was carried out in presence of various concentrations of F6P or G6P and the inhibitory metabolite. Assay mixtures were prepared as described above. In inhibition assays, 0-0.98 mM F6P or 0-1.5 mM G6P was used. The concentration range used to study the K_i of PGI for E4P was 0-0.05 mM and that for 6PG was 0-1.5 mM. The mechanism of inhibition was determined from Hanes-Woolf plots. The K_i was determined from the non-linear least squares fitting of the activity vs. concentration plot using Solver in Excel using the standard equation for competitive inhibition as described below:

$$\boldsymbol{v} = \frac{\boldsymbol{V_{max}}*\boldsymbol{S}}{\boldsymbol{K_m}\left(1+\frac{I}{\boldsymbol{K_i}}\right)+S} \quad \text{Eq. 2.1}$$

where V_{max} is the maximum velocity, S is the subtrate concentration, K_m is the Michaelis constant, and K_i is the inhibition constant. For non-competitive inhibition, the equation below was used.

$$\boldsymbol{v} = \frac{\boldsymbol{V_{max}}*\boldsymbol{S}/\left(1+\frac{I}{\boldsymbol{K_i}}\right)}{\left(\boldsymbol{K_m}\left(1+\frac{I}{\boldsymbol{K_i}}\right)/\left(1+\frac{I}{\boldsymbol{K_i}}\right)+\boldsymbol{S}\right)} \quad \text{Eq. 2.2}$$

2.3.6 Plant material

Fresh *Spinacia oleracea* (So) was purchased at a local market for use that day. Spinach was either dark or light treated for 1.5 h before beginning isolation and petioles were kept in water to prevent wilting.

Arabidopsis thaliana (At) Col-0 was grown on soil in a growth chamber at a 12 h light at 120 µmol m^{-2} s^{-1}, 23˚C and 12 h dark at 21˚C. Plants were harvested either midday for light samples or midnight for dark samples.

Nicotiana tabacum seeds were planted in SureMix soil (Michigan Grower Products, Inc., Galesburg, MI, U.S.A.). The plants were grown in the greenhouse, starting in October 2019 with an average daytime temperature of 27˚C nighttime temperature of 20˚C Plants were fertilized twice per week with commercially available Peters 20-20-20 fertilizer (ICL Specialty Fertilizers, https://www.icl-sf.com) at 100 ppm. Experiments were done when plants were 5-12 weeks old on the fifth to seventh fully expanded leaves.

2.3.7 Chloroplast isolation

Chloroplasts were isolated using a Percoll gradient (Weise *et al.*, 2004). Leaves were placed in a chilled blender with grinding buffer (330 mM mannitol, 50 mM Hepes, pH 7.6, 5 mM $MgCl_2$, 1 mM $MnCl_2$, 1 mM EDTA, 5 mM ascorbic acid, 0.25% BSA), blended, and then filtered through four layers of cheese cloth. Filtered liquid was centrifuged, and the pellet was resuspended in resuspension buffer (330 mM mannitol, 50 mM Hepes, pH 7.6, 5 mM $MgCl_2$, 1 mM $MnCl_2$, 1 mM EDTA, 0.25% BSA). The resuspended pellet was layered on top of a 20-80% Percoll gradient which was centrifuged at 1200 g for 7 min. The bottom band in the gradient containing the intact chloroplasts was collected. One volume of resuspension buffer was added to the collected chloroplasts and centrifuged at 1200 g for 2 min. The pellet was resuspended in 50 µL of water and vortexed to lyse the chloroplasts. One volume of 2x buffer (100 mM Hepes, pH

7.6, 10 mM $MgCl_2$, 2 mM $MnCl_2$, 2 mM EDTA, 2 mM EGTA, 60% glycerol, 0.2% Triton X-100, 0.2% PVPP) was added. Samples were stored at -80˚C until used for further analysis. Chlorophyll was quantified by lysing 50 µL of purified chloroplasts by sonication and adding supernatant to 1 mL of 95% ethanol. OD_{654} was used to calculate the chlorophyll concentration (Wintermans and DeMots, 1965):

$$\text{mg Chl} = OD * 0.0398 * 0.050\ \mu\text{L} \qquad \text{Eq. 2.3}$$

Assays that used isolated chloroplasts were normalized by mg of chlorophyll added to the assay mixture.

2.3.8 Transient expression of PGI in N. Tabacum

A fusion gene was generated using the transit peptide of the Arabidopsis chloroplast PGI1 (At4g24620). This was determined by ChloroP (http://www.cbs.dtu.dk/services/ChloroP/) to be the first 144 bp starting at the ATG codon. The transit peptide was placed in front of the Arabidopsis cytosol PGI2 (At5g42740) cDNA with the ATG from the PGI2 sequence omitted for a total length of 1824 bp. A second fusion gene was made by placing a YFP gene sequence at the end of the gene directly before the TGA stop codon. A third fusion gene was made by placing the YFP gene sequence at the N-terminus between the transit peptide and the PGI2 cDNA sequence. These constructs were synthesized by Bio Basic Inc. (Markham Ontario, Canada) and placed in the pUC57 plasmid vector. The construct was then transferred to the pEAQ-HT-DEST1 destination vector containing the P19 suppressor of silencing (Sainsbury *et al.*, 2009). The pEAQ-HT-DEST1 vector constructs were transformed into *Agrobacterium* strain GV3101 by electroporation. All constructs and transformed *E. coli* and agrobacterium were confirmed with PCR.

Agrobacterium containing the desired construct was grown in LB media in a 5 mL culture tube at 28˚C overnight. The next day cells were pelleted by centrifugation at 7000 *g* for 5 min at

20˚C and washed twice with infiltration buffer (2 mM trisodium phosphate, 50 mM MES, 25 mM glucose, 200 mM acetosyringone). The OD_{600} was measured and used to calculate the necessary volume of agrobacterium to dilute to an OD_{600} of 0.05, 0.025, or 0.01 for initial controls and 0.025 for all subsequent experiments. *N. tabacum* leaves were gently infiltrated using a 1 mL syringe without a needle. All experiments, except for initial controls, were done at two days post-infiltration.

2.3.9 Confirmation of localization of misexpressed PGI

Protein transient expression was performed using 4-week-old *N. tabacum* plants and *Agrobacterium tumefaciens* (strain GV3101) with an OD_{600} of 0.05. according to (Batoko *et al.*, 2000). Both N-terminal and C-terminal YFP fusion constructs were used.

Confocal images acquisitions were performed using an inverted laser scanner confocal microscope Nikon A1RSi on tobacco two days post-infiltration on leaf epidermal cells. Images were acquired using a 60X oil λS DIC N2 objective. YFP was excited by the 514 nm line of an argon ion laser and emission collected at 530-560 nm. Chlorophylls autofluorescence were excited at 647 nm line and emission was collected at 680-750 nm (Mehrshahi *et al.,* 2013).

2.3.10 Starch time course

N. tabacum leaves were infiltrated as described above. Starting 48 h post-infiltration, leaf punches were collected at 4:40 PM (+10:40 h after lights on), 10:00 PM (lights off), 12:40 PM (+2:40 h after lights off), 3:20 AM (+5:20 h after lights off), 6:00 AM (lights on), and 11:20 AM (+5:20 h after lights on). These times corresponded with lights on, lights off, and two points evenly spaced in between each change in light conditions. Samples were collected in 2 mL pre-weighed microcentrifuge tubes, frozen immediately in liquid nitrogen, and stored at -80˚C. Fresh weight was determined before any further analysis.

Frozen plant material was ground using a ball mill (Retsch, https://www.retsch.com) and was suspended in ice-cold 3.5% perchloric acid solution (50% w/v of plant tissue), homogenized, and incubated on ice for 5 min. Samples were then centrifuged at 28000 *g* for 10 min at 4˚C. The pellet was washed twice with both 80% ethanol and deionized water and then dried in a Savant AES 1010 SpeedVac (ThermoFisher Scientific, https://www.thermofischer.com) for 15 min to remove any remaining ethanol. The dried pellet was resuspended in 500 µL of 0.2 M KOH and incubated at 95˚C for 30 min to gelatinize the starch. Acetic acid was added to a final concentration of approximately 150 mM to bring the solution to a pH of 5. Fifty U of α-amylase and 0.2 U of amyloglucoside were added to the sample. The starch solution was incubated for two days at room temperature on a shaker to convert the starch to glucose. Two hunderd µL of an assay mixture of 110 mM HEPES, 500 nmol $NADP^+$, 500 nmol ATP, and 0.4 U G6PDH was added to wells in an assay plate. Twenty µL of the broken-down starch sample was added to each well and was measured at 340 nm on a FilterMax F5 Plate Reader (Molecular Devices, https://moleculardevices.com) until a stable baseline was obtained. A starting OD_{340} was measured. One U of hexokinase was added to each well, quickly shaken, and monitored at 340 nm until the reaction was completed. An endpoint OD_{340} was measured and starch (glucose equivalents) was determined using the ΔOD.

Significance of linearity for starch degradation at night was determined by linear regression statistics in OriginPro 8.0 (OriginLab Corporation).

2.3.11 Starch and sucrose partitioning with $^{14}CO_2$

N. tabacum leaves were infiltrated as described above. Two days post-infiltration, plants were placed in a LI-COR 6800 with the multiphase flash fluorometer (LI-COR Biosciences, https://www.licor.com) with 600 µmol m^{-2} s^{-1} of light, 42 Pa CO_2 and 2.1 kPa of water vapor in the incoming air. Leaf temperature was 25˚C. Plants were acclimated until photosynthesis and

stomatal conductance were steady, approximately 30 min to 1 h. After acclimation,42 Pa $^{14}CO_2$ was fed to the plant using a custom built gas mixing apparatus for a 10 min pulse and 5 min chase during which the CO_2 concentration remained constant as described in Sharkey *et al.* (1985). Leaf samples were immediately collected and frozen in liquid nitrogen. Samples were weighed to determine fresh weight and stored at -80˚C.

Frozen plant material from either the time course or radioactive labelling experiments were ground using a ball mill (Retsch, https://www.retsch.com) and was suspended in a formic acid extraction solution (4% formic acid, 71% ethanol; 50% w/v of plant tissue), homogenized, and centrifuged at 28000 g for 10 min at 4˚C. The pellet was treated as described above in "Starch Time Course in Transiently Expressing *Nicotiana tabacum*". The supernatant of the original extraction containing soluble sugars was dried using a FreeZone Triad Freeze Dryer (Labconco, https://labconco.com). Once dried, the material was resuspended in 700 µL of deionized water. 250 µL of the sugar solution was applied to a Dowex 1 (Cl^- form) and then Dowex 50 (H^+ form) ion exchange columns. Both columns had a bed volume of approximately 2 mL. After the soluble fraction was loaded on the column, the first 1 mL of flow-through was discarded and the next 4 mL collected. The columns were then washed with 5 mL of deionized water. All ionic compounds (amino acids, Calvin-Benson cycle intermediates, malate, fumarate, etc.) were removed by the columns and the final flow through was assumed to contained sucrose and other neutral compounds. The collected flow-through from the columns was dried using a FreeZone Triad Freeze Dryer (Labconco, https://labconco.com) and resuspended in 250 µL of deionized water. Two hundred µL of the starch sample, 100 µL of the total soluble sample or 250 µL of the neutral sample were added to approximately 3 mL scintillation cocktail (Research Products International Corp.) Samples were counted for ^{14}C radioactivity for 10 min using a 1450 Microbeta Trilux scintillation counter (Perkin Elmer, https://www.perkinelmer.com). Proportions

of counts metabolites relative to total counts were multiplied by the photosynthetic rate of each plant as described in Sharkey et al. (1985). Linear regression was determined by method of least squares.

2.3.12 Measuring cyclic electron flow

N. tabacum leaves were infiltrated as described above. Forty-eight h post-infiltration, plants were clamped into a modified LI-COR 6800 with a clear-top chamber with 607 µmol m^{-2} s^{-1} of light. The air entering the chamber had 42 Pa CO_2 and 2.1 kPa of water. Leaf temperature was set to 25˚C. Plants were acclimated until photosynthesis and stomatal conductance were steady, approximately 30 min to 1 h. Afterwards, at each new light intensity in the protocol, the plant was acclimated for 2 min. When light was below 200 µmol m^{-2} s^{-1}, seven 500-msec DIRKs (dark interval relaxation kinetics transients) were measured at 20 s intervals to measure the electrochromic shift (the change in absorbance of carotenoids at 518 nm, a measure of the proton-motive force (Takizawa *et al.*, 2007; Witt, 1979)). When light was above 200 µmol m^{-2} s^{-1}, five DIRKs were used. Twenty s after the DIRKs, we gave a saturating flash of approximately 10,000 µmol m^{-2} s^{-1} of light to obtain maximum fluorescence. DIRKs for each light intensity were averaged and analyzed according to Kiirats *et al.* (2009). The initial decay of the electrochromic shift represents the velocity of protons across the thylakoid membrane, v_{H+}. We fit this linearly from the first three points of the averaged curve. Linear electron flow (LEF) was calculated as below:

$$LEF = PAR \cdot \Phi II \cdot \alpha \cdot \beta \quad \text{Eq. 2.4}$$

where ΦII is the efficiency of photosystem 2, α is the partitioning of photons between PSI and PSII and assumed to be 0.5, and β is the effective absorptance of the leaf, assumed to be 0.89. We plotted v_{H+} vs. LEF and fitted the line with a linear regression. The difference in slope of the

linear fit between the control and treated plants indicates the proportion of protons contributed by cyclic electron flow compared to LEF (Avenson *et al.*, 2005).

2.4 RESULTS

2.4.1 Purification of recombinant PGI

Final concentration of purified plastidic PGI was 15.3 mg/mL and that of cytosolic PGI was 13.8 mg/mL. The molecular weight of His-tagged recombinant plastidic and cytosolic PGI were ~62.9 kDa and ~62.5 kDa respectively. The specific activity was 787 µmol mg^{-1} protein min^{-1} for plastidic PGI and 1522 µmol mg^{-1} protein min^{-1} for cytosolic PGI.

2.4.2 Kinetic characterization of plastidic and cytosolic PGI

Table 2.2 shows the K_m (for both F6P and G6P) of plastidic and cytosolic PGI (Figure S2.2). For plastidic AtPGI, the K_m for G6P was ~2.9-fold higher than that for F6P. The K_m's for F6P and G6P of the cytosolic enzyme were the same. We did not calculate the V_{max} value of G6P and F6P for both isoforms since initial results did not uphold the Haldane relation:

$$K_{eq} = {}^{k_{cat\ F6P\rightarrow G6P}}/_{k_{cat\ G6P\rightarrow F6P}} * {}^{K_{m\ G6P\rightarrow F6P}}/_{K_{m\ F6P\rightarrow G6P}} \qquad \text{Eq. 2.5}$$

Therefore, we concluded that the measured V_{max} was not accurate, either due to differences in methodology for measuring G6P or F6P kinetics or storage in the freezer. This may be addressed by preparing new purified proteins daily, however this was impractical due to the time needed to purification and assays. Using the determined K_{eq} of 3.70, we can calculate that the ratio of ${}^{k_{cat\ F6P\rightarrow G6P}}/_{k_{cat\ G6P\rightarrow F6P}}$ is 1.65 for the plastidic isoform and 4.75 for the cytosolic isoform. DTT did not significantly influence the specific activity of plastidic or cytosolic PGI (Figure S2.3).

2.4.3 E4P and 6PG inhibition of PGI

We tested different metabolites for their effect on PGI activity. Inhibition with either substrate was similar for both plastidic and cytosolic AtPGI. Erythrose 4-phosphate (E4P), 3-phosphoglyceric acid (PGA), dihydroxyacetone phosphate (DHAP), and 6-phosphogluconate (6PG) were screened (Figure 2.1). Only E4P and 6PG showed significant inhibition of PGI activity. Figure 2.2 shows the activity of plastidic AtPGI over a range of F6P and E4P concentrations. Activity of cytosolic AtPGI was analyzed in a similar manner as shown for plastidic AtPGI. The calculated K_i values of E4P and 6PG are shown in Table 2.2. The K_i values for 6PG were between 31 and 203 μM, depending on the isoform and substrate. E4P was shown to be more inhibitory with K_i's between 1.5 and 6 μM. Based on the Hanes-Woolf plots (Figure S2.4), E4P was shown to be competitive, except above 0.04 mM, with G6P. 6PG was identified as competitive with F6P, except above 1.0 mM, and non-competitive with G6P.

2.4.4 Regulation of PGI in isolated chloroplasts

Plastidic SoPGI activity from chloroplasts from dark-treated spinach leaves had a higher K_m for G6P compared to light-treated chloroplasts (Figure 2.3). The K_m of SoPGI for F6P did not change in the light or dark.

2.4.5 Subcellular localization of mis-localized PGI

We used YFP expression to observe cellular distribution of our misexpressed PGI construct. YFP fluorescence was seen in the chloroplast for both the N-terminal and C-terminal constructs, confirming that our PGI construct was targeted as intended (Figure S2.5).

2.4.6 Transient expression of PGI

After infiltrating *N. tabacum* with agrobacterium transformed with the modified PGI construct, we collected samples once every 24 h for 3 days. Using qPCR, we found that expression of the construct was highest on the second day after infiltration (Fig S2.6a). We also

found that a density of agrobacteria of 0.025 OD_{600} had the highest expression of the construct. Photosynthetic assimilation was ~50% of pre-infiltration values (Fig S2.6b). After two days both expression and photosynthesis declined. Based on this, we used two days post-infiltration as the time point for all future experiments.

2.4.7 Time course of starch accumulation in transiently expressing N. tabacum

Starting 48 h after infiltration, we measured starch content in *N. tabacum* that transiently expressed either the mislocalized PGI construct or an empty vector. We found that at the end of day and end of night, PGI plants had significantly more starch. End-of-day starch content was approximately 1.65-fold more than controls while end-of-night starch content was approximately 1.98-fold more than controls (Figure 2.6a). We found that PGI plants did not linearly breakdown starch at night ($R^2 = 0.648$), while empty vector plants did ($R^2 = 0.998$) (Figure 2.6b). The Prob(F) value (likelihood that the regression parameters are zero) for the linear regression of empty vector plants was $7.64*10^{-4}$ while Prob(F) for PGI plants was 0.20 indicating linearity for the empty vector plants but not plants expressing PGI. Daytime synthesis of starch did not increase consistently throughout the day and was not further analyzed. Plants were grown in greenhouse conditions and the experiment took place on a cloudy day. Lights came on in the greenhouse late in the day (5:00 pm) and caused an increase in light compared to daytime intensity for the last five hours of the photoperiod. Therefore, we focused on end of day, end of night, and night degradation values.

2.4.8 Starch and sucrose partitioning with $^{14}CO_2$ in N. tabacum *transiently expressing PGI*

We measured partitioning to starch, sucrose, and ionic metabolites in both mislocalized PGI and empty vector plants. We found there was no difference (Table 2.3).

2.4.9 Cyclic electron flow in transiently expressing N. tabacum

We measured cyclic electron flow in both mislocalized PGI and empty vector plants and found there was no difference (Figure 2.5).

2.5 DISCUSSION

2.5.1 Role of PGI in regulating starch synthesis

We propose that PGI is a key regulatory point in carbon export from the Calvin-Benson cycle by acting as both a one-way valve to prevent re-entry of carbon into the Calvin-Benson cycle and as a rate-limiting enzymatic reaction in starch synthesis.

The G6P/F6P ratio at equilibrium has been reported to be 3.70 at 25˚C (Dyson and Noltmann, 1968). However, measurements from plastidic plant extracts show the ratio of G6P/F6P in the stroma to be close to 1 (Backhausen *et al.*, 1997; Gerhardt *et al.*, 1987; Schnarrenberger and Oeser, 1974; Sharkey and Vassey, 1989; Szecowka *et al.*, 2013). This disequilibrium is not seen for the cytosolic PGI. The cytosolic G6P/F6P ratio is 2.4-4.7 (Gerhardt *et al.*, 1987; Sharkey and Vassey, 1989; Szecowka *et al.*, 2013). Kinetic isotope effects in starch, but not sucrose, also support the conclusion that plastidic PGI, but not cytosolic PGI, is unable to maintain equilibrium (Schleucher *et al.*, 1999). This disequilibrium, which results in lower steady-state G6P concentrations than would be expected, combined with the higher K_m for G6P for the plastidic enzyme, makes this reaction functionally irreversible. The difference in K_m is seen in both recombinant plastidic AtPGI and in isolated plastidic SoPGI, but not in recombinant cytosolic AtPGI.

In addition to controlling directionality of flux between F6P and G6P, PGI is also a regulatory step in starch synthesis. It is often assumed that enzymes catalyzing highly reversible reactions, like isomerases or mutases, do not exhibit control over pathway flux. It is thought that ADP-glucose pyrophosphorylase (AGPase) exhibits most, if not all, of regulatory control over the

starch synthesis pathway (Ballicora *et al.*, 2004; Preiss and Sivak, 1998; Tiessen *et al.*, 2002). Discussion of key enzymes and regulation of starch synthesis and computational models of starch synthesis often leave early steps of the starch synthetic pathway, i.e. PGI and PGM, focusing instead on formation of the ADP-glucose (ADPG) pool by AGPase and attachment of soluble ADPG to the growing starch chain (Preiss and Sivak, 1998; Sonnewald and Kossmann, 2014; Tetlow *et al.*, 2004; Wu *et al.*, 2014). However, calculated flux-control coefficients for enzymes in starch synthesis are 0.35, 0.21, 0.64, and 0.13 for PGI, PGM, AGPase, and branching enzyme, respectively (Neuhaus and Stitt, 1990). Multiple enzymes have control over the starch synthesis pathway and PGI exerts the second largest control. Additionally, it has been shown that a loss of 50% of plastidic PGI reduces starch synthesis by 50% while loss of 64% of cytosolic PGI has a negligible effect on sucrose synthesis, reinforcing the rate-limiting role of the plastidic isoform (Kruckeberg *et al.*, 1989). Our findings support this key role of PGI. Figure 2.4 shows that misexpressing PGI in the plastid to increase overall activity leads to increased starch accumulation by end of day.

2.5.2 Regulation of the plastidic G6P pool and the G6P shunt

G6P produced by PGI in the plastid can be used for more than just starch synthesis. G6P can also be oxidized by glucose-6-phosphate dehydrogenase to 6-phosphogluconolactone, the first step in the oxidative branch of the pentose phosphate pathway (Meyer *et al.*, 2011; Wakao and Benning, 2005). It has been hypothesized that G6PDH could initiate a shunt around the Calvin-Benson cycle (Sharkey and Weise, 2016). The G6P shunt would oxidize and decarboxylate G6P to synthesize ribulose 5-phosphate (Ru5P) and release a CO_2. The G6P shunt has also been hypothesized to be correlated with increased cyclic electron flow, as it consumes 3 net ATP for every turn of the cycle but no net reducing power. Increased concentrations of plastidic G6P could stimulate the shunt by overcoming the increased K_m of reduced G6PDH (Preiser *et al.*,

2019). Therefore, we measured cyclic electron flow in our plants with misregulated PGI, but we did not find any difference compared to empty vector controls. We conclude that while increasing expression of PGI can increase overall flux through the starch synthesis pathway, it does not increase the plastidic G6P concentration enough to stimulate the G6P shunt.

2.5.3 Role of PGI in regulating starch degradation

We found that mislocalization and expression of PGI in the plastid disrupted degradation of starch. Phosphorylytic starch breakdown results in the production of G6P from starch and has been shown to be a significant contribution of carbon to the plastid (Weise *et al.*, 2006). Misexpressed PGI could increase degradation of starch by the phosphorylytic pathway by providing a pathway to enzymatic reactions that would not normally be available, in addition to the oxidative pentose phosphate pathway. This indicates that even at night PGI is an important regulatory point in starch metabolism and is a rate-limiting step that prevents early starch degradation through the night.

2.5.4 Inhibition of PGI

We previously assumed that PGA is a strong inhibitor of PGI (e.g. Sharkey and Weise 2016) based on the report by Dietz (1985). Surprisingly, we did not observe this to be the case. Examination of data from Dietz (1985) shows that in PGA inhibition assays, 6PG was also present in the reaction mixture at 50 μM. The G6P/F6P disequilibrium in chloroplasts was proportional to PGA (Dietz, 1985) but PGA was not tested alone for its effect on PGI. We found that the K_i of plastidic PGI for 6PG with limiting F6P was 31 μM or with limiting G6P was 203 μM. Based on our findings, we propose that PGI is not inhibited by PGA, and the previously reported inhibition can be explained by presence of 6PG or E4P. *In vivo* plastidic concentrations of 6PG are not known, therefore, the extent of inhibition of PGI *in vivo* by 6PG cannot be currently determined.

PGI is inhibited by μM concentrations of E4P (Backhausen *et al.*, 1997; Grazi *et al.*, 1960; Salas *et al.*, 1964). E4P may be inhibitory to both isoforms of PGI because it is a competitive inhibitor and the active sites of both isoforms may be similar (Backhausen *et al.*, 1997). Presumably there is no E4P in the cytosol since it lacks crucial enzymes in the non-oxidative branch of the pentose phosphate pathway (Schnarrenberger *et al.*, 1995). Measurements and estimations of plastidic E4P concentrations *in vivo* show E4P to be ~17-20 μM (Backhausen *et al.*, 1997; Bassham and Krause, 1969; Heldt *et al.*, 1977). This is well above the K_i of E4P for plastidic PGI. Backhausen *et al.* (1997) propose that this regulation is necessary in order to keep photosynthetic pool sizes stable during changes in light intensity.

In addition to stabilizing the Calvin-Benson cycle, we propose that inhibition of PGI by E4P can provide insight into the phenomenon of reverse sensitivity to CO_2 and O_2 of photosynthetic CO_2 assimilation rate observed by Sharkey and Vassey (1989). They found that when potato leaves were switched to decreased partial pressure of oxygen, rates of photosynthetic CO_2 assimilation decreased as a result of decreased starch synthesis. Sharkey and Vassey (1989) proposed this was an effect of PGA inhibition of PGI, but because we did not find PGA to be inhibitory, we now suggest that the decrease in starch synthesis is due to an increase in E4P concentrations (or possibly 6PG).

2.6 CONCLUSION

We conclude that PGI is an important regulatory enzyme in both starch synthesis and degradation. Previous analyses of the starch pathways have overlooked this key role. Additionally, we have re-examined previous knowledge of PGI inhibition and have found that it was mistakenly thought that PGI is inhibited by PGA and is instead inhibited by E4P.

2.7 ACKNOWLEDGEMENTS

We thank Michigan State University Research Technology Support Facility Mass Spectrometry Core for providing the facility for the LC-MS/MS work. We also thank George Lomonossoff for allowing us to use the vectors for transient expression. This research was funded by U.S. Department of Energy Grant DE-FG02-91ER20021 (T.D.S., A.L.P., S.E.W., A.B., and L.R.). A.L.P was partially supported and A.M.M is fully supported by a fellowship from Michigan State University under the Training Program in Plant Biotechnology for Health and Sustainability (T32-GM110523). T.D.S received partial salary support from Michigan AgBioResearch.

APPENDIX

TABLE 2.1- Parameters used for detection of FBP and the internal standard with LC/MS/MS.

Parameters were optimized using 10 μM standards before analyzing samples.

Metabolite	Cone (V)	Collision (V)	+0 Parent (m/z)	Daughter (m/z)
FBP	26	18	339	97
D-[UL-$^{13}C_6$] FBP	26	18	345	97

TABLE 2.2- Kinetic constants and inhibition constants for plastidic and cytosolic AtPGI as determined by NADPH-linked spectrophotometric assays and LC-MS/MS assays.

K_m and k_{cat} were determined by fitting the Michalis-Menten equation. Data points used in model fitting were different preparations (n=3). For inhibition constants, each number was determined from the fitted curves as described in the methods. Errors shown are S.E. (n=3). Sum of least-squares for inhibition parameters were determined using Solver in Excel.

	F6P → G6P		G6P → F6P	
	Plastidic PGI	Cytosolic PGI	Plastidic PGI	Cytosolic PGI
K_m (μM)	73 ± 46	203 ± 7	164 ± 25	158 ± 49
E4P K_i (μM)	2.3	1.5	6.0	3.7
6PG K_i (μM)	31	106	245	149

TABLE 2.3- Starch and sucrose and ionic fraction partitioning in mislocalized pPGI and empty vector *N. tabacum.*

Data points are mean ± standard deviation with N = five different plants. There was no statistical difference between treatments.

	Mislocalized cytosolic PGI	Empty Vector
Starch	45% ± 7	37% ± 8
Sucrose	26% ± 2	25% ± 8
Ionic	29% ± 7	38% ± 6

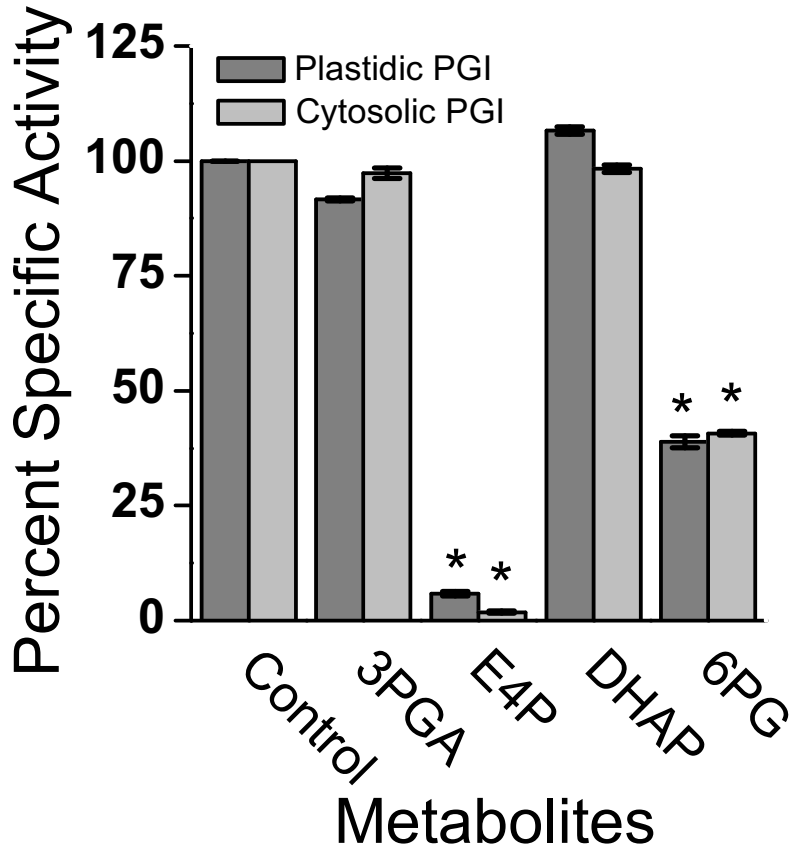

FIGURE 2.1- Comparison of specific activity of plastidic and cytosolic AtPGI with various metabolites.

Each bar represents mean and error bars represent S.E. (n=3). All metabolites were screened at 1:1 F6P substrate to metabolite. Data with an asterisk (*) are significantly different from the control as determined by Student's t-test ($P < 0.05$).

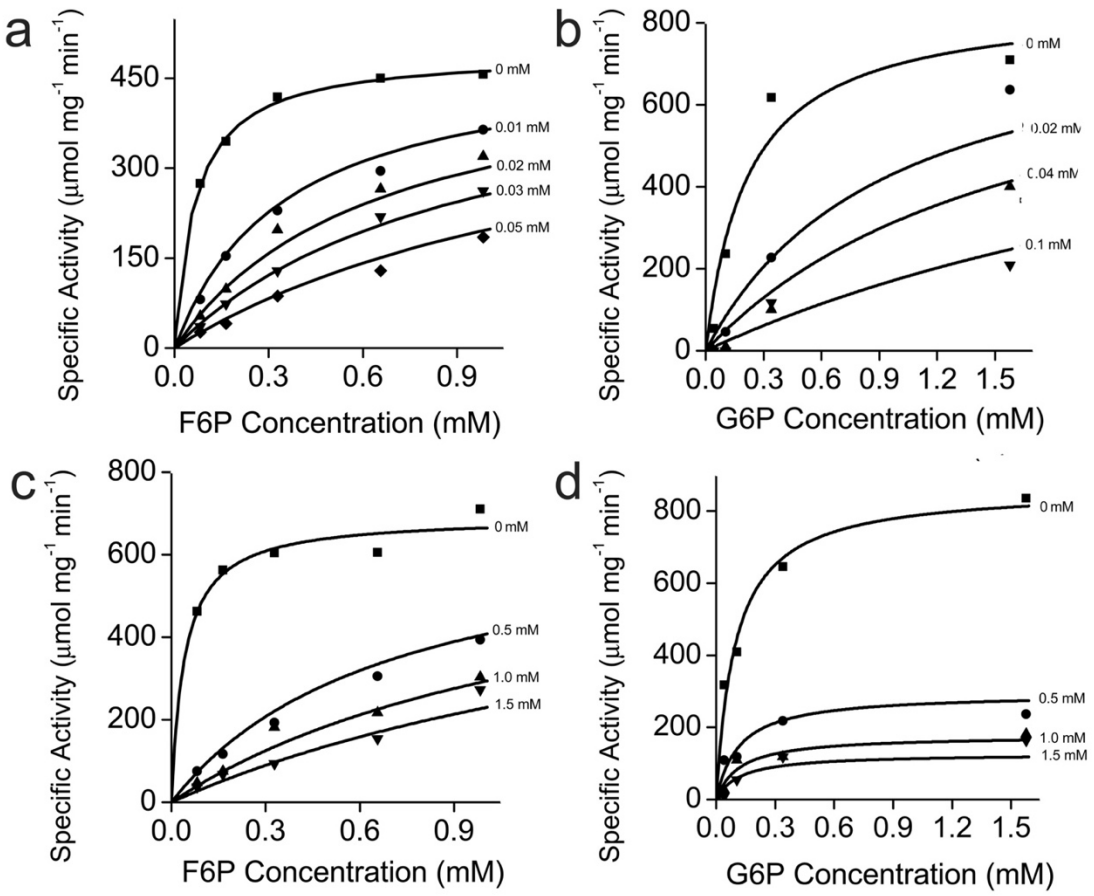

FIGURE 2.2- Effect of erythrose 4-phosphate (E4P) and 6-phosphogluconate (6PG) on plastidic AtPGI.

We measured the effect of E4P (a, b) and 6PG (c, d) on AtPGI. Different symbols represent different concentrations of inhibitor. PGI was more inhibited by E4P than by 6PG. Lines represent data fit to Eq. 2.3.

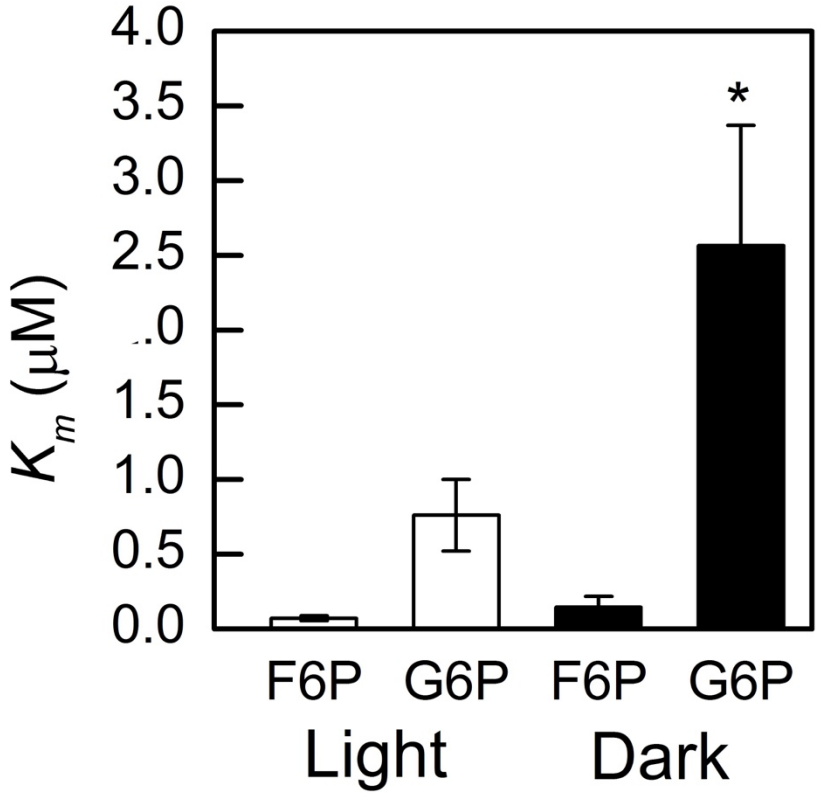

FIGURE 2.3- Comparison of F6P and G6P K_m in plastidic SoPGI in dark and light-treated isolated spinach chloroplasts.

Each bar represents mean and error bars represent S.E. (n=3). The K_m for G6P increased in dark treated compared to light treated isolated chloroplasts. Bars with an asterisk (*) are significantly different from corresponding light treated samples as determined by Student's t-test ($P < 0.05$).

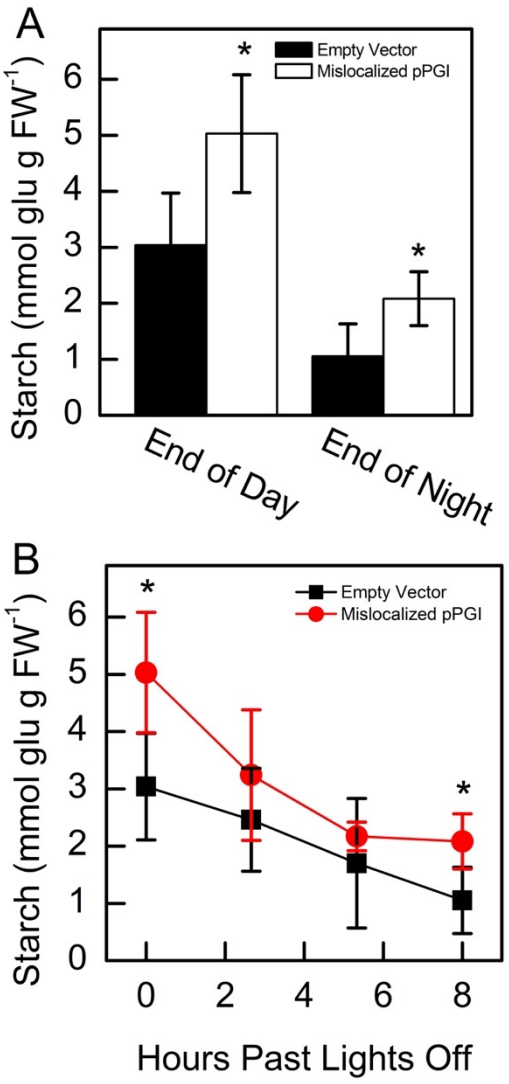

FIGURE 2.4- Starch amounts at end of day and end of night (a) and degradation of starch (b) in *N. tabacum* expressing mislocalized pPGI.

Starch in plants with mislocalized pPGI was significantly higher than empty vector control plants. Starch breakdown in empty vector plants was linear through the night, however, starch breakdown was non-linear in mislocalized pPGI plants. Each bar or data point represents mean and error bars represent S.E. (n=5). Bars or data points with an asterisk (*) are significantly different from corresponding empty vector samples as determined by Student's t-test ($P < 0.05$). Significance for linearity was determined by Prob(F) of the linear regressions.

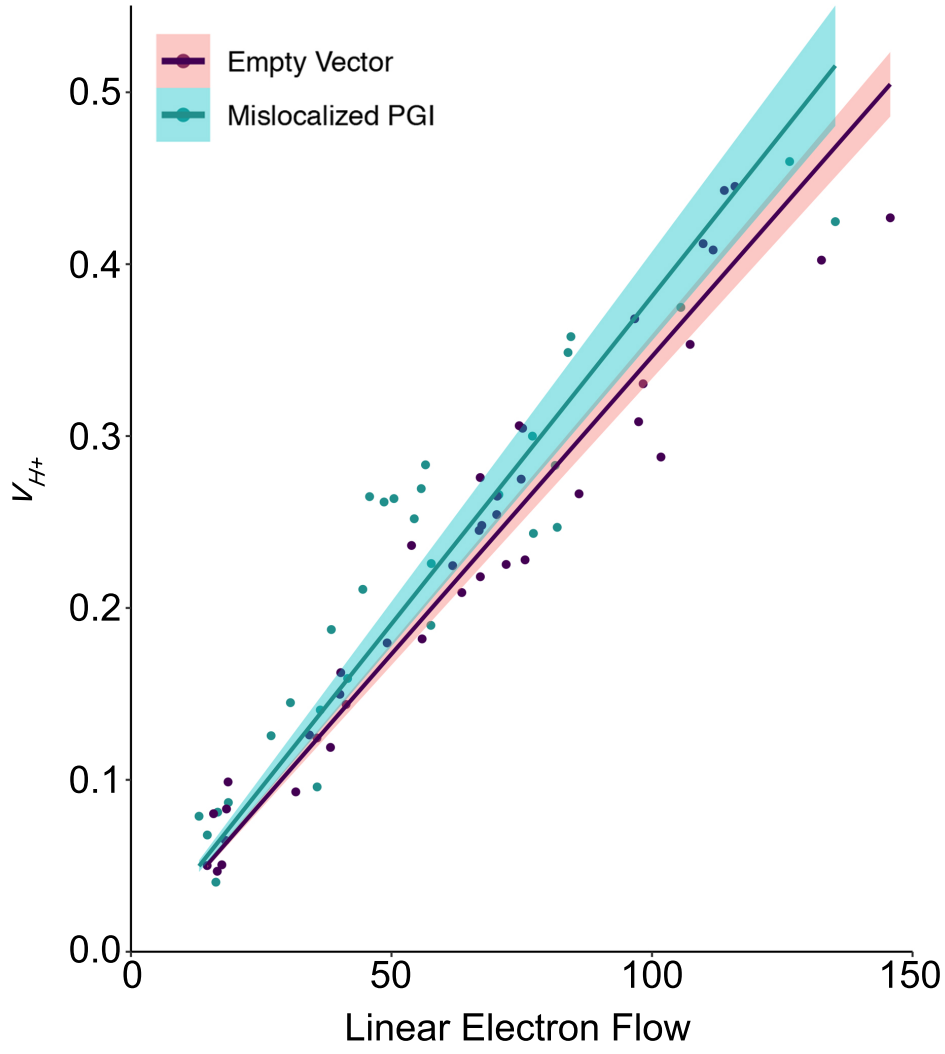

FIGURE 2.5- Cyclic electron flow in *N. tabacum* expressing mislocalized pPGI and empty vector.

Cyclic electron flow was measured 48 h post-infiltration. Blue represents the mislocalized PGI and red represents empty vector controls, N = 5. The line represents the line of best fit. The colored area represents the 95% confidence interval. An increase of v_{H+} relative to linear electron flow indicates an increase in cyclic electron flow. There was no statistical difference between the treatments.

TABLE S2.1- Transient expression construct sequences

Construct	Sequence
Cytosolic PGI	Gcgtcatcaaccgctttgatttgtgataccgaagcgtggaaggatttgaagggacatgtagaagatatt aagaagactcatttgcgtgatttgatgagtgatgctaatagatgccagtccatgatgatggagtttgatgg gttgctgttggattattctcgacagcgtgcaactgttgagacaatggacaagcttttgaacttggcaaagg cttctcaattgacagagaagatcagccgcatgttcaatggggagcatattaacagtacagagaacagat cagttcttcatgttgcgctccgtgctccaaaggatgcagttatcaaggctgatggaatgaatgtggttcca gaagtgtggaacgttctagataagatcaaggaattttctgacaaaattcgctctggttcatgggttggagc cactggcaaaccgctgaaagatgtcattgcgattggtattggtggtagcttcttaggtccactgtttgtcca cacggctctccaaacagatcctgaagctctagagtctgctaaaggacgccagctgcgatttcttgcaaat attgatcctgttgatgttgctagaaatatcagtggactaaatccagaaactactctagttgtggtggtctcga aaacgtttacaacagctgaaacaatgcttaacgccagaacattgagggaatggataacagctgctcttgg ggcttcagctgttgcaaaacatatggttgctgtcagcactaatcttgcgttagtagagaagtttggtattgac ccgaacaatgcatttgcattttgggactgggttggtggaaggtacagtgtttgcagtgcggttggagtctta cctttgtctctgcagtatggcttctccatggttgagaagtttttgaagggagcttcaagcattgatcagcattt ccagtccacaccgttcgagaagaatatacctgtgcttttagggttgttgagtgtatggaatgtatcatttcttg gatatcctgctagggccatcttaccttattcgcaagcccttgagaaatttgctccacacattcaacaggtta gtatggagagtaatggaaagggagtctcaattgatggtctacctctcccgttcgagactggtgagattgat tttggtgaacctggaacaaatggtcaacacagcttttaccaactcattcaccagggacgcgtaatcccttgt gatttcattggcattgtgaagagtcagcaacctgtgtaccttaagggagaggtggtcagtaaccacgacg agctcatgtcaaacttttttgcacagcctgatgctcttgcatatggaaaaactcctgaacagctgcagaaag agaatgtttcagaaaatctcattccccataagacattctctggaaatcgaccttctcttagccttctacttcca gaattgactgcttacaatgttggccagttgttggctatctatgaacacagagtagcagttcaaggctttgtg tggggtatcaattcgtttgaccagtggggcgttgagctaggaaaagttctggctactcaggtcaggaaac agcttcattcatcacgcactcaaggaaccgctcccgagggattcaattacagtaccaccacacttttgaaa cgatatctggagacaagttccgagccccagatg
YFP	Gtgagcaagggcgaggagctgttcaccggggtggtgcccatcctggtcgagctggacggcgacgtaaa Cggccacaagttcagcgtgtccggcgagggcgagggcgacgccacctacggcaagctgaccctgaa Gttcatctgcaccaccggcaagctgcccgtgccctggcccaccctcgtgaccaccttcggctacggcctg Aagtgcttcgcccgctaccccgaccacatgaagcagcacgacttcttcaagtccgccatgcccgaaggct Acgtccaggagcgcaccatcttcttcaaggacgacggcaactacaagacccgcgccgaggtgaagttcg Agggcgacaccctggtgaaccgcatcgagctgaagggcatcgacttcaaggaggacggcaacatcctgg Ggcacaagctggagtacaactacaacagccacaacgtctatatcatggccgacaagcagaagaacggcat Caaggtgaacttcaagatccgccacaacatcgaggacggcagcgtgcagctcgccgaccactaccagca Gaacacccccatcggcgacggccccgtgctgctgcccgacaaccactacctgagctaccagtccgccctg Agcaaagaccccaacgagaagcgcgatcacatggtcctgctggagttcgtgaccgccgccgggatcactc tcggcatggacgagctctacaagtga
Transit peptide	Atggcctctctctcaggcctatactcttcttctccatctctcaaacctgccaaaaaccattcctttaaagcattgc cggcgcaatctagagattccttctctttcccacatacctccaaacccaccaatctaccgttgactctc

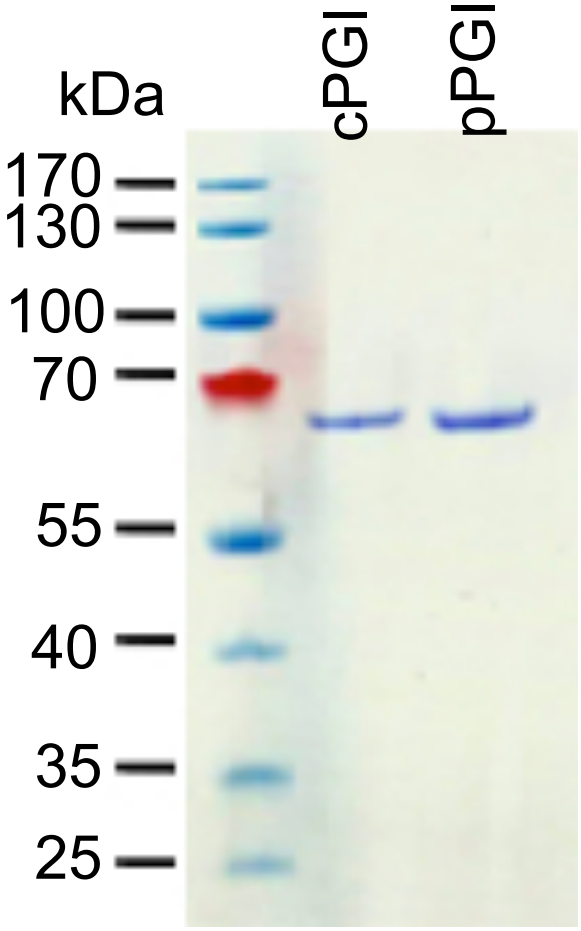

FIGURE S2.1- SDS-PAGE of purified PGI proteins, stained with Coomassie blue.

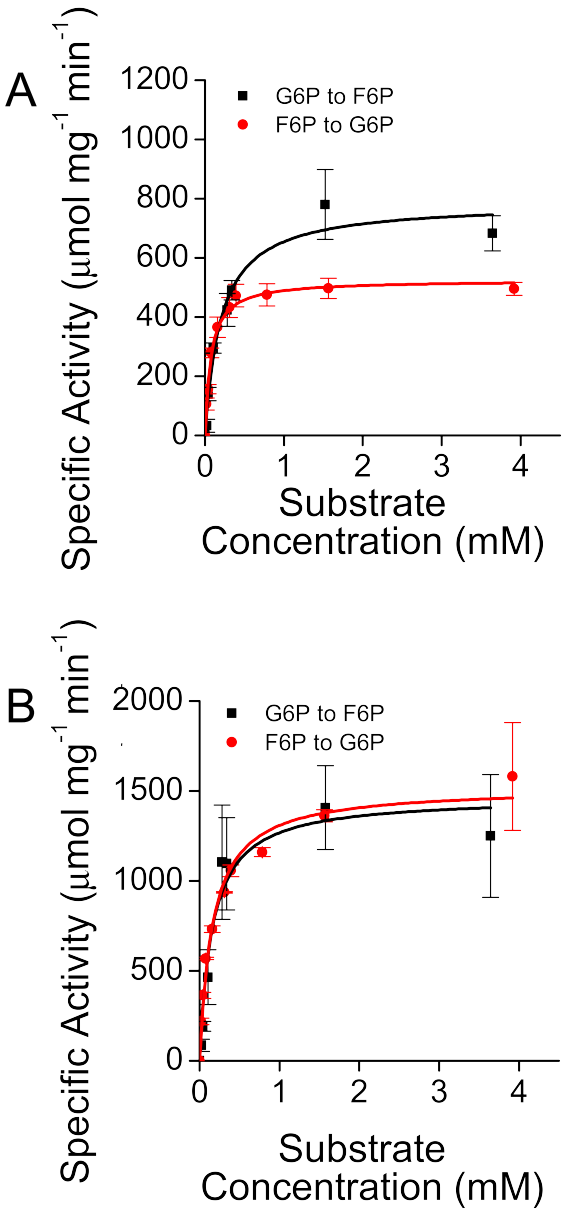

FIGURE S2.2- Effect of F6P and G6P on plastidic (A) and cytosolic (B) AtPGI specific activity.

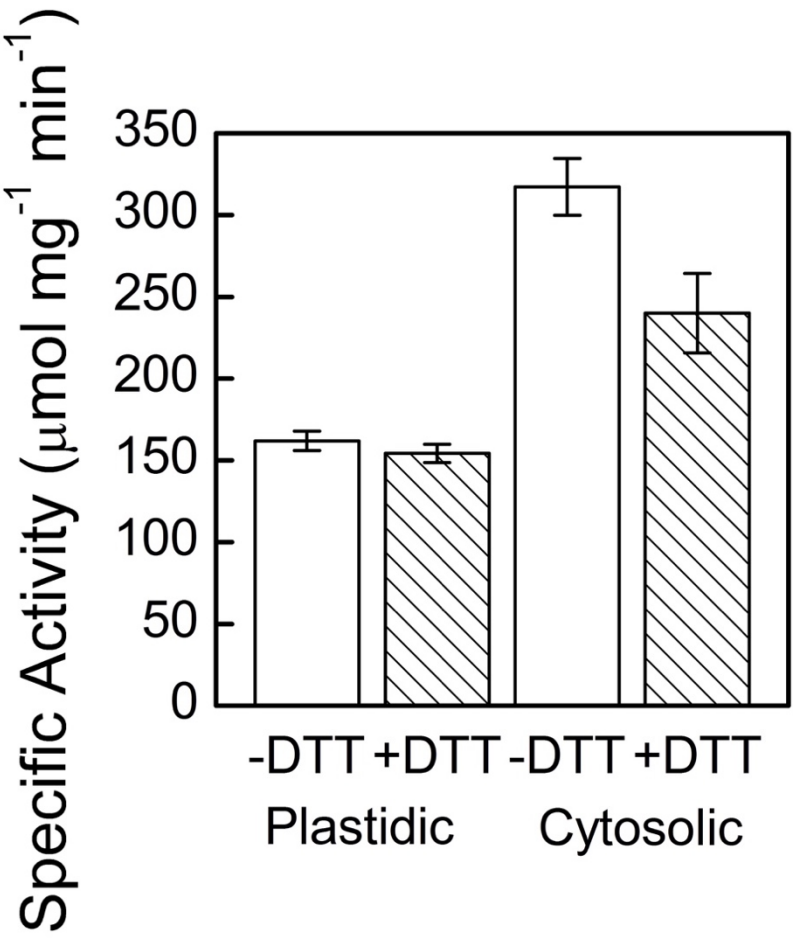

FIGURE S2.3- Specific activity of plastidic and cytosolic AtPGI with and without 10 mM DTT. The activities were not statistically different.

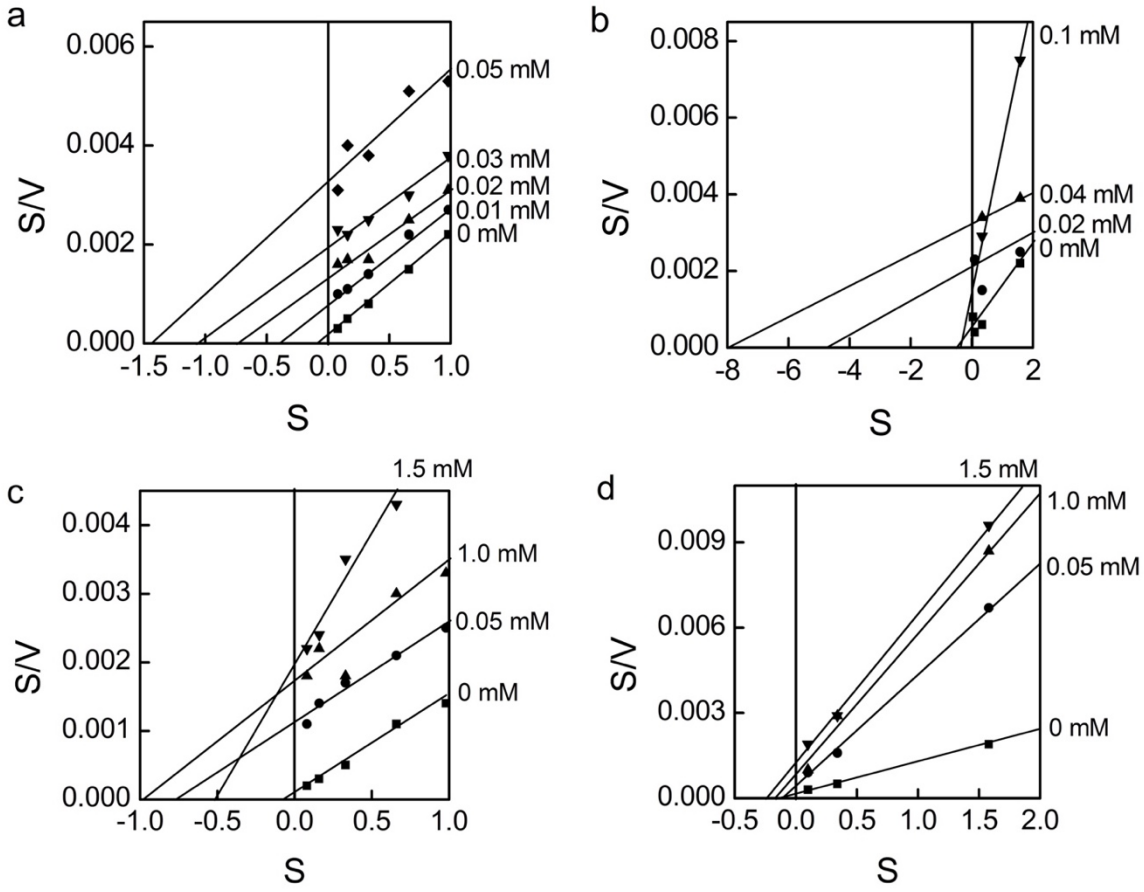

FIGURE S2.4- Hanes-Woolf plots of E4P (a, b) and 6PG (c, d) inhibition of plastidic AtPGI with G6P as a substrate.

Lines represent linear regression by least squared error.

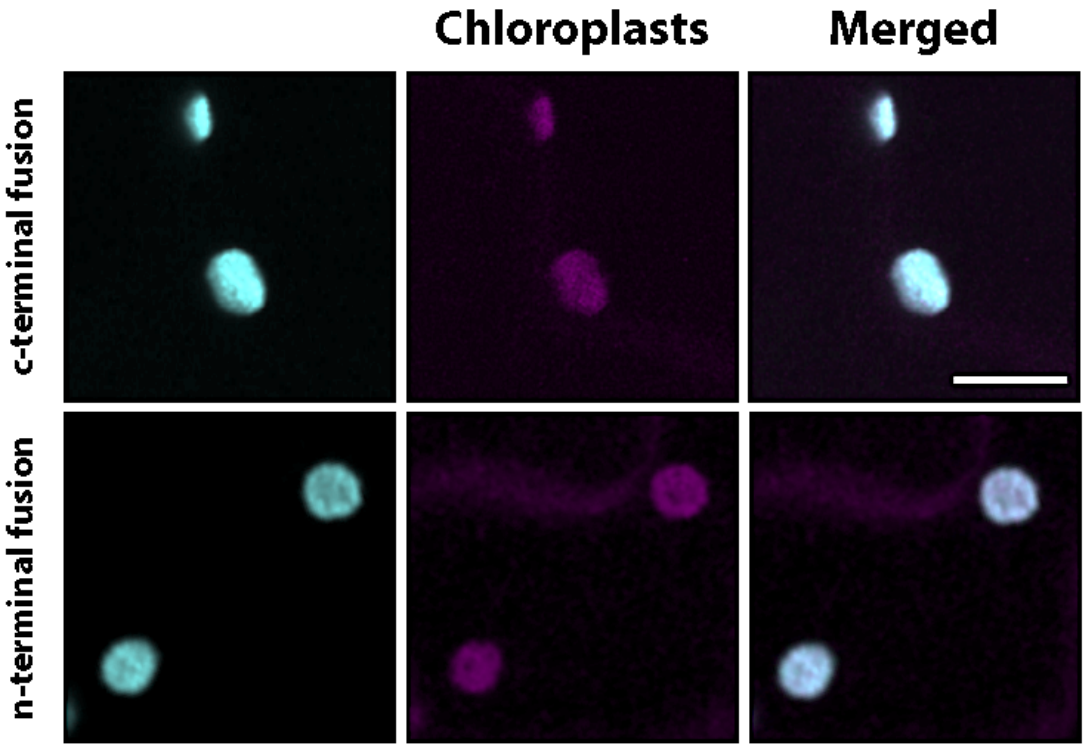

FIGURE S2.5- Localization of modified pPGI to the chloroplast.

Confocal images of *Nicotiana tabacum* epidermal cell transiently expressing N- or C-terminal tagged mislocalized PGI. Both fluorescent fusions localize at the chloroplasts (cyan) as the co-localization (merge channel) shows with the chloroplast autofluorescence (magenta). Scale bar 10 μm.

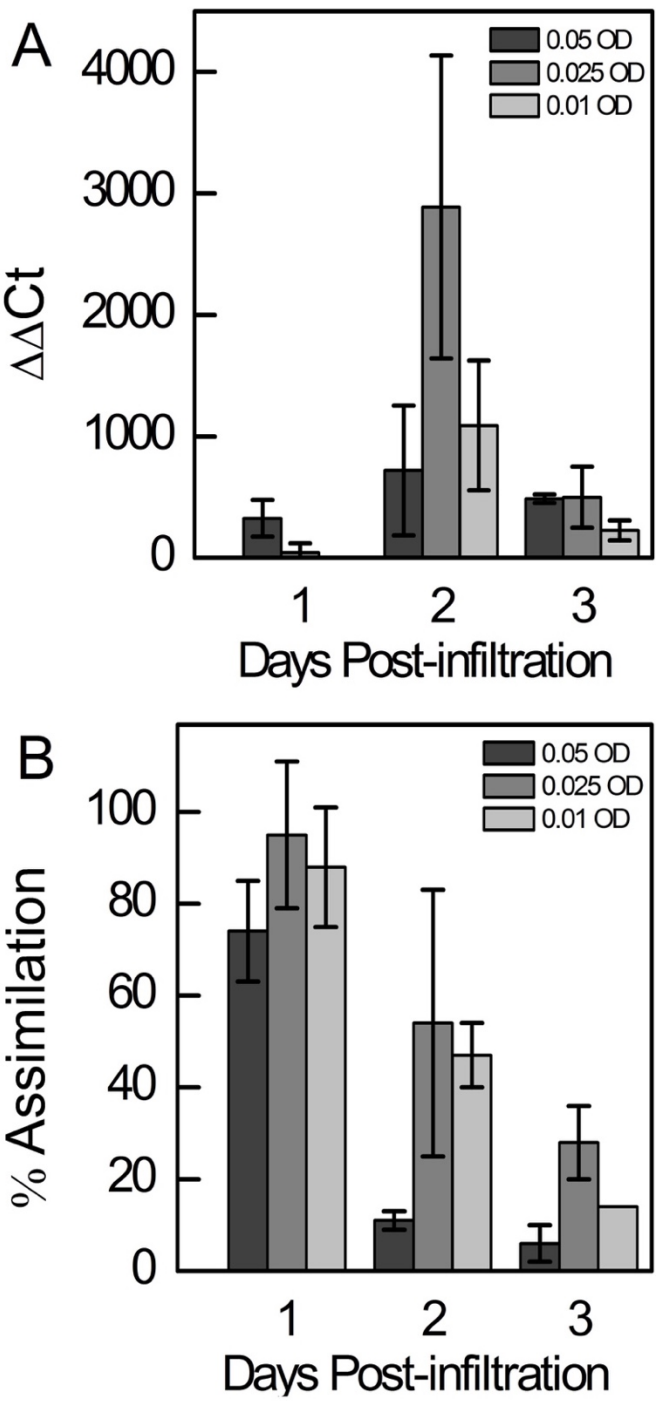

FIGURE S2.6- qPCR (A) and rates of assimilation (B) for *N. tabacum* infiltrated with mislocalized pPGI.

All values are relative to pre-infiltration samples from the same plant.

LITERATURE CITED

LITERATURE CITED

Avenson TJ, Kanazawa A, Cruz JA, Takizawa K, Ettinger WE, Kramer DM. 2005. Integrating the proton circuit into photosynthesis: progress and challenges. *Plant, Cell & Environment* **28**, 97-109.

Backhausen JE, Jöstingmeyer P, Scheibe R. 1997. Competitive inhibition of spinach leaf phosphoglucose isomerase isoenzymes by erythrose 4-phosphate. *Plant Science* **130**, 121-131.

Ballicora MA, Iglesias AA, Preiss J. 2004. ADP-glucose pyrophosphorylase: a regulatory enzyme for plant starch synthesis. *Photosynthesis Research* **79**, 1-24.

Bassham JA, Krause GH. 1969. Free energy changes and metabolic regulation in steady-state photosynthetic carbon reduction. *Biochimica et Biophysica Acta* **189**, 207-221.

Batoko H, Zheng HQ, Hawes C, Moore I. 2000. A rab1 GTPase is required for transport between the endoplasmic reticulum and golgi apparatus and for normal golgi movement in plants. *Plant Cell* **11**, 2201-2218.

Caspar T, Huber SC, Somerville C. 1985. Alterations in growth, photosynthesis, and respiration in a starchless mutant of *Arabidopsis thaliana* (L.) deficient in chloroplast phosphoglucomutase activity. *Plant Physiology* **79**, 11-17.

Dietz KJ. 1985. A possible rate limiting function of chloroplast hexosemonophosphate isomerase in starch synthesis of leaves. *Biochimica et Biophysica Acta* **839**, 240-248.

Dyson JED, Noltmann EA. 1968. The effect of pH and temperature on the kinetic parameters of phosphoglucose isomerase. *The Journal of Biological Chemistry* **243**, 1401-1414.

Gerhardt R, Stitt M, Heldt HW. 1987. Subcellular metabolite levels in spinach leaves. Regulation of sucrose synthesis during diurnal alterations in photosynthetic partitioning. *Plant Physiology* **83**, 399-407.

Grazi E, De Flora A, Pontremoli S. 1960. The inhibition of phosphoglucose isomerase by D-erythrose 4-phosphate. *Biochemical and Biophysical Research Communications* **2**, 121-125.

Hanson KR, McHale NA. 1988. A starchless mutant of *Nicotiana sylvestris* containing a modified plastid phosphoglucomutase. *Plant Physiology* **88**, 838-844.

Heldt HW, Chon CJ, Maronde D, Herold A, Stankovic ZS, Walker DA, Kraminer A, Kirk MR, Heber U. 1977. Role of orthophosphate and other factors in the regulation of starch formation in leaves and isolated chloroplasts. *Plant Physiology* **59**, 1146-1155.

Hendriks JHM, Kolbe A, Gibon Y, Stitt M, Geigenberger P. 2003. ADP-glucose pyrophosphorylase is activated by posttranslational redox-modification in response to light and to sugars in leaves of Arabidopsis and other plant species. *Plant Physiology* **133**, 838-849.

Kavakli IH, Kato C, Choi SB, Kim KH, Salamone PR, Ito H, Okita TW. 2002. Generation, characterization, and heterologous expression of wild-type and up-regulated forms of Arabidopsis thaliana leaf ADP-glucose pyrophosphorylase. *Planta* **215**, 430-439.

Kiirats O, Cruz JA, Edwards GE, Kramer DM. 2009. Feedback limitation of photosynthesis at high CO2 acts by modulating the activity of the chloroplast ATP synthase. *Functional Plant Biology* **36**, 893-901.

Kofler H, Häusler RE, Schulz B, Gröner F, Flügge UI, Weber A. 2000. Molecular characterisation of a new mutant allele of the plastid phosphoglucomutase in *Arabidopsis* , and complementation of the mutant with the wild-type cDNA. *Molecular and General Genetics* **263**, 978-986.

Kruckeberg AL, Neuhaus HE, Feil R, Gottlieb LD, Stitt M. 1989. Decreased-activity mutants of phosphoglucose isomerase in the cytosol and chloroplast of *Clarkia xantiana*. Impact on mass-action ratios and fluxes to sucrose and starch, and estimation of flux control coefficients and elasticity coefficients. *Biochemical Journal* **261**, 457-467.

Lin TP, Caspar T, Somerville C, Preiss J. 1988. Isolation and characterization of a starchless mutant of *Arabidopsis thaliana* (L.) Heynh lacking ADPglucose pyrophosphorylase activity. *Plant Physiology* **86**, 1131-1135.

Lowry OH, Passonneau JV. 1969. Phosphoglucomutase kinetics with the phosphates of fructose, glucose, mannose, ribose, and galactose. *Journal of Biological Chemistry* **244**.

Lowry OH, Passonneau JV. 1972. *A flexible system of enzymatic analysis*. Orlando: Academic Press.

Mathur D, Ahsan Z, Tiwari M, Garg LC. 2005. Biochemical characterization of recombinant phosphoglucose isomerase of *Mycobacterium tuberculosis*. *Biochemical and Biophysical Research Communications* **337**, 626-632.

Mehrshahi P, Stefano G, Andaloro JM, Brandizzi F, Froehlich JE, DellaPenna D. 2013 Transorganellar complementation redefines the biochemical continuity of endoplasmic reticulum and chloroplasts. *Proceedings of the National Academy of Science* **110**, 12126-12131.

Meyer T, Hölscher C, Schwöppe C, von Schaewen A. 2011. Alternative tageting of Arabidopsis plastidic glucose-6-phosphate dehydrogenase G6PD1 involves cysteine-dependent interaction with G6PD4 in the cytosol. *The Plant Journal* **66**, 745-758.

Neuhaus HE, Stitt M. 1990. Control analysis of photosynthate partitioning. Impact of reduced activity of ADP-glucose pyrophosphorylase or plastid phosphoglucomutase on the fluxes to starch and sucrose in *Arabidopsis thaliana* (L.) Heynh. *Planta* **182**, 445-454.

Preiser AL, Fischer N, Banerjee A, Sharkey T. 2019. Plastidic glucose-6-phosphate dehydrogenase is regulated to maintain activity in the light. *Biochemical Journal* **476**, 1539-1551.

Preiss J, Ballicora MA, Laughlin MJ, Fu Y-B, Okita TW. 1995. Studies on the starch biosynthetic enzymesfor manipulation of starch content and quality. In: Madore MA, Lucas WJ, eds. *Carbon partitioning and source-sink interactions in plants*. Rockville, MD: American Society of Plant Physiologists, 91-99.

Preiss J, Hutney J, Smith-White B, Li L, Okita TW. 1991. Regulatory mechanisms involved in the biosynthesis of starch. *Journal of Pure and Applied Chemistry* **63**, 535-544.

Preiss J, Sivak MN. 1998. Biochemistry, molecular biology, and regulation of starch synthesis. *Genetic Engineering*. Berlin: Springer, 177-223.

Ray WJ, Roscelli GA. 1964. A kinetic study of the phosphoglucomutase pathway. *Journal of Biological Chemistry* **239**, 1228-1236.

Sainsbury F, Thuenemann EC, Lomonossoff GP. 2009. pEAQ: versatile expression vectors for easy and quick transient expression of heterologous proteins in plants. *Plant Biotechnology Journal* **7**, 682-693.

Salamone PR, Kavakli IH, Slattery CJ, Okita TW. 2002. Directed molecular evolution of ADP-glucose pyrophosphorylase. *Proceedings of the National Academy of Sciences of the United States of America* **99**, 1070-1075.

Salas M, Viñuela E, Sols A. 1964. Spontaneous and enzymatically catalyzed anomerization of glucose 6-phosphate and anomeric specificity of related enzymes. *The Journal of Biological Chemistry* **240**, 561-568.

Schleucher J, Vanderveer P, Markley JL, Sharkey TD. 1999. Intramolecular deuterium distributions reveal disequilibrium of chloroplast phosphoglucose isomerase. *Plant, Cell & Environment* **22**, 525-533.

Schnarrenberger C, Flechner A, Martin W. 1995. Enzymatic evidence for a complete oxidative pentose phosphate pathway in chloroplasts and an incomplete pathway in the cytosol of spinach leaves. *Plant Physiology* **108**, 609-614.

Schnarrenberger C, Oeser A. 1974. Two isoenzymes of glucosephosphate isomerase from spinach leaves and their intracellular compartmentation. *European Journal of Biochemistry* **45**, 77-82.

Sharkey TD, Berry JA, Raschke K. 1985. Starch and sucrose synthesis in *Phaseolus vulgaris* as affected by light, CO2 and abscisic acid. *Plant Physiology* **77**, 617-620.

Sharkey TD, Vassey TL. 1989. Low oxygen inhibition of photosynthesis is caused by inhibition of starch synthesis. *Plant Physiology* **90**, 385-387.

Sharkey TD, Weise SE. 2012. Autotrophic carbon dioxide fixation. In: Eaton-Rye JJ, Tripathy B, Sharkey TD, Sharkey TD, eds. *Photosynthesis: Plastid Biology, Energy Conversion and Carbon Assimilation*. Dordrecht: Springer Academic Publications, 649-672.

Sharkey TD, Weise SE. 2016. The glucose 6-phosphate shunt around the Calvin-Benson Cycle. *Journal of Experimental Botany* **67**, 4067-4077.

Sonnewald U, Kossmann J. 2014. Starches—from current models to genetic engineering. *Plant Biotechnology* **11**, 223-232.

Szecowka M, Heise R, Tohge T, Nunes-Nesi A, Vosloh D, Huege J, Feil R, Lunn J, Nikoloski Z, Stitt M, Fernie AR, Arrivault S. 2013. Metabolic fluxes in an illuminated Arabidopsis rosette. *The Plant Cell Online* **25**, 694-714.

Takizawa K, Cruz JA, Kanazawa A, Kramer DM. 2007. The thylakoid proton motive force in vivo. Quantitative, non-invasive probes, energetics, and regulatory consequences of light-induced pmf. *Biochimica et Biophysica Acta* **1767**, 1233-1244.

Tetlow IJ, Emes MJ. 2014. A review of starch-branching enzymes and their role in amylopectin biosynthesis. *IUBMB Life* **66**, 546-558.

Tetlow IJ, Morell MK, Emes MJ. 2004. Recent developments in understanding the regulation of starch metabolism in higher plants. *Journal of Experimental Botany* **55**, 2131-2145.

Tiessen A, Hendriks JHM, Stitt M, Branscheid A, Gibon Y, FarrÇ EM, Geigenberger P. 2002. Starch synthesis in potato tubers is regulated by post-translational redox modification of ADP-glucose pyrophosphorylase: A novel regulatory mechanism linking starch synthesis to the sucrose supply. *The Plant Cell* **14**, 2191-2213.

Uematsu K, Suzuki N, Iwamae T, Inui M, Yukawa H. 2012. Expression of Arabidopsis plastidial phosphoglucomutase in tobacco stiumulates photosynthetic carbon flow into starch synthesis. *Journal of Plant Physiology* **169**, 1454-1462.

Wakao S, Benning C. 2005. Genome-wide analysis of glucose-6-phosphate dehydrogenases in Arabidopsis. *The Plant Journal* **41**, 243-256.

Weise SE, Schrader SM, Kleinbeck KR, Sharkey TD. 2006. Carbon balance and circadian regulation of hydrolytic and phosphorolytic breakdown of transitory starch. *Plant Physiology* **141**, 879-886.

Weise SE, Weber A, Sharkey TD. 2004. Maltose is the major form of carbon exported from the chloroplast at night. *Planta* **218**, 474-482.

Wintermans JGFM, DeMots A. 1965. Spectrophotometric characteristics of chlorophylls a and b and their pheophytins in ethanol. *Biochimica et Biophysica Acta* **109**, 448-453.

Witt HT. 1979. Energy conversion in the functional membrane of photosynthesis. Analysis by light pulse and electric pulse methods. The central role of the electric field. *Biochimica et Biophysica Acta* **505**, 355-427.

Wu AC, Ral J-P, Morell MK, Gilbert RG. 2014. New perspectives on the role of α- and β-amylases in transient starch synthesis. *PLOS ONE* **9**, e100498.

Yu TS, Lue WL, Wang SM, Chen J. 2000. Mutation of Arabidopsis plastid phosphoglucose isomerase affects leaf starch synthesis and floral initiation. *Plant Physiology* **123**, 319-326.

CHAPTER 3

Plastidic glucose-6-phosphate dehydrogenases are regulated to maintain activity in the light

This research was originally published in the Biochemical Journal. Alyssa L. Preiser, Nicholas Fisher, Aparajita Banerjee and Thomas D. Sharkey. 2019. Plastidic glucose-6-phosphate dehydrogenases are regulated to maintain activity in the light. *Biochemical Journal* **476,** 1539-1551. https://doi.org/10.1042/BCJ20190234

This research was done in collaboration with Dr. Nicholas Fisher and Dr. Aparajita Banerjee, A.B. designed the recombinant G6PDH. N.F. helped design and analyze the midpoint potential experiments.

3.1 ABSTRACT

Glucose-6-phosphate dehydrogenase (G6PDH) can initiate the glucose-6-phosphate (G6P) shunt around the Calvin-Benson cycle. To understand the regulation of flux through this pathway we have characterized the biochemical parameters and redox regulation of the three functional plastidic isoforms of Arabidopsis G6PDH. When purified, recombinant proteins were measured, all three exhibited significant inhibition by G6P but not $NADP^+$, making the determination of enzyme kinetic parameters complex. We found that the half-saturation concentration of the G6PDH isoform 1 is increased under reducing conditions. The other two isoforms exhibit less redox regulation, however, isoform 2 is strongly inhibited by NADPH. Redox regulation of G6PDH1 can be partially reversed by hydrogen peroxide or protected against by the presence of its substrate, G6P. Overall, our results support the conclusion that G6PDH can have significant activity throughout the day and can be dynamically regulated to allow or prevent flux through the glucose-6-phosphate shunt.

3.2 INTRODUCTION

Glucose-6-phosphate (G6P) is the first product out of the Calvin–Benson cycle in the starch synthesis pathway. However, it can also enter the oxidative pentose phosphate pathway creating a G6P shunt that bypasses the nonoxidative pentose phosphate pathway reactions that make up a significant part of the Calvin–Benson cycle. This pathway is generally considered to occur only in the dark because of the redox regulation of glucose-6-phosphate dehydrogenase (G6PDH) (Anderson *et al.*, 1974; Buchanan, 1980; Buchanan *et al.*, 2015; Heldt and Piechulla, 2005; Née *et al.*, 2014; Scheibe *et al.*, 1989). To estimate flux through this alternative pathway and conditions where it may be important, it is critical to characterize the regulation of G6PDH activity in the light.

The substrate of G6PDH, G6P, can be produced or consumed by three other reactions in the plastid: phosphoglucoisomerase (PGI), phosphoglucomutase (PGM), and glucose-6-phosphate/phosphate translocator 2 (GPT2). PGI reversibly isomerizes fructose-6-phosphate (F6P) and G6P. Analysis of mutant lines of *Clarkia xantiana* indicated that PGI is not in great excess (Kruckeberg *et al.*, 1989). There are two isoforms of PGI in Arabidopsis, one targeted to the plastid and the other found in the cytosol. The plastid PGI, in particular, is likely limiting, given that G6P/F6P ratios in the plastid are significantly displaced from equilibrium and much lower than in the cytosol (Backhausen *et al.*, 1997; Gerhardt *et al.*, 1987; Schnarrenberger and Oeser, 1974; Sharkey and Vassey, 1989; Szecowka *et al.*, 2013). Plants with loss-of-function mutations in the plastidic enzyme have 98.5% less starch in leaves (Yu *et al.*, 2000). Loss-of-function mutants in the cytosolic enzyme result in increased starch and decreased sucrose (Kunz *et al.*, 2014). Second, PGM is an important reaction in starch synthesis that catalyzes the reversible reaction of G6P to glucose 1-phosphate (G1P). The K_m for G6P is 47 mM and 8.5 mM for G1P with a V_{max} of 115 and 328 mmol mg^{-1} min^{-1}, respectively (Lowry and Passonneau,

1969; Ray and Roscelli, 1964). Hanson and McHale (1988) showed that PGM had similar activity to PGI in *Nicotiana sylvestris*. Knockouts of PGM result in starchless plants (Caspar *et al.*, 1985; Hanson and McHale, 1988; Kofler *et al.*, 2000). Finally, GPT2 is a glucose-6-phosphate/phosphate antiporter in the chloroplast membrane that is not normally present in green tissue (Kammerer *et al.*, 1998; Kunz *et al.*, 2010). This is corroborated by the large concentration gradient in G6P between the chloroplast and cytosol (Gerhardt *et al.*, 1987; Sharkey and Vassey, 1989; Szecowka *et al.*, 2013).

However, GPT2 is important in acclimation to light (Dyson *et al.*, 2015), is expressed in plants grown in high CO_2 (Leakey et al., 2009), and is increased when starch synthesis is repressed by knocking out starch synthesis genes (Kunz *et al.*, 2010). When GPT2 is present, the gradient of G6P would result in G6P import into the plastid (Gerhardt *et al.*, 1987; Sharkey and Vassey, 1989; Szecowka *et al.*, 2013).

Here, we focus on the characterization and biochemical regulation of the plastidic G6PDH isoforms due to its key role in the G6P shunt. There are six isoforms of G6PDH in Arabidopsis. Four of these are predicted to be targeted to the chloroplast and three of these are functional (Meyer *et al.*, 2011; Wakao and Benning, 2005). All three plastidic isoforms are expressed in leaf tissue. G6PDH1 and 2 have the highest relative expression (Wakao and Benning, 2005). It has been hypothesized that during the day, G6PDH initiates a G6P shunt around the Calvin–Benson cycle (Sharkey and Weise, 2016). The G6P shunt oxidizes and decarboxylates G6P to synthesize ribulose-5-phosphate (Ru5P). While the G6P shunt is a futile cycle, it has been proposed to play an important role in stabilization of photosynthesis.

Our goal was to characterize the kinetics and biochemical parameters of oxidized and reduced G6PDH isoforms and the key regulators of G6PDH. Novel findings indicate that G6PDH can remain fairly active during the day. We conclude that a G6P shunt is allowed and even likely in

light of the kinetic parameters of G6PDH and that its activity could be modulated during the day to regulate flux through the G6P shunt.

3.3 MATERIALS AND METHODS

3.3.1 Expression and purification of recombinant enzymes

C-terminal Strep-tagged (Meyer *et al.*, 2011; Wakao and Benning, 2005; Wendt *et al.*, 2000) plastidic G6PDH1, 2, and 3 genes were commercially synthesized by GenScript (https://www.genscript.com). All of the plasmid constructs were overexpressed in *Escherichia coli* strain BL21. Cells were grown at 37°C to an OD_{600} of 0.6–1 and induced with 0.5 mM isopropyl β-D-1 thiogalactopyranoside (IPTG) at room temperature. Cells were grown overnight at room temperature after the addition of IPTG. Cells were then centrifuged and resuspended in cold Buffer W (IBA, www.iba-lifesciences.com) with 1 mg ml^{-1} lysozyme, 1 mg ml^{-1} of DNAseI, and 1x protease inhibitor cocktail (Sigma, www.sigmaaldrich.com). Cells were then lysed by sonication (Branson Sonifier 250, us.vwr.com). The sonicator was set at 50% duty cycle and an output level of 1. The cells were sonicated using five steps where each step consisted of 15 s pulses and 15 s on ice. The lysate was centrifuged and the supernatant collected. Protein was purified on a Strep-Tactin column (IBA) according to the manufacturer's instructions. For all purified proteins, SDS–PAGE was carried out and fractions containing >95% of total protein of interest were combined and concentrated using Amicon Ultra 0.5 ml centrifugal filters (molecular mass cutoff 3 kDa). Glycerol was added to the concentrated protein to obtain a final protein solution with 15% glycerol. The glycerol stock of the proteins was aliquoted into small volumes, frozen in liquid nitrogen, and stored at −80°C. The concentration of the proteins was determined using Pierce 660 nm Protein Assay Reagent Kit (Thermo Fisher Scientific, www.thermofisher.com) using a bovine serum albumin standard. Final preparations of purified protein were run on an SDS-polyacrylamide gel and stained with Coomassie Blue to check the

purity of the enzymes. Molecular masses were estimated from the protein constructs using Vector NTI (Thermo Fisher Scientific, www.thermofisher.com).

3.3.2 Coupled spectrophotometric assay for G6PDH

The activity of the purified G6PDH1, 2, and 3 was studied using coupled spectrophotometric assays. The concentration of G6P was determined using NADPH-linked assays measured spectrophotometrically. The purity of G6P was verified by untargeted LC–MS/MS. All assays were validated by demonstrating linear product formation, proportional to the time of the assay, and amount of enzyme added. The assay was performed in 150 mM HEPES buffer (pH 7.2) containing varying concentrations of $NADP^+$, G6P, and G6PDH. 8.3 ng of G6PDH1, 20 ng of G6PDH2, and 44 ng of G6PDH3 were used. At these concentrations, G6PDH isoforms had similar, measurable, and sensitive activity for the methods that we used.

The concentrations used to study the half-saturation concentration of G6PDH for G6P were 0–44.2 mM, and the concentrations used to study K_m for $NADP^+$ were 0–11 mM in a total volume of 800 ml. The concentrations were chosen to result in many data points spanning the range of activity up to enzyme saturation based on preliminary assays. When G6PDH was assayed with varied G6P, 0.6 mM $NADP^+$ was added. The chosen concentration of $NADP^+$ was in large excess and the concentration of $NADP^+$ would change very little during the assay at this concentration. When G6PDH was assayed varying $NADP^+$, 7.6 mM G6P was added for G6PDH1 and 3 and 15.4 mM for G6PDH2 since these were approximately the concentrations that gave maximal activity for each enzyme. Under these conditions, <5% of the substrates were consumed over the course of the assay. The assay mixtures were initially prepared by adding all the components except the enzyme and obtaining a stable baseline. The enzyme was added to start the reaction. The activity was recorded using a dual wavelength filter photometer (Sigma

ZFP2) as the change in absorbance at 334 nm relative to 405 nm caused by $NADP^+$ reduction to NADPH using an extinction coefficient of 6190 M^{-1} cm^{-1}. These wavelengths were used because they correspond to mercury emission wavelengths of the lamp used in the filter photometer. By using two wavelengths, the sensitivity of the assay was greatly increased allowing measurements at low enzyme concentrations that caused very little change in substrate concentrations, even during long assays.

When assaying redox sensitivity, G6PDH was incubated with 10 mM DTT or 10 mM hydrogen peroxide at room temperature for 30 min before addition to the assay. The assay mixture was prepared with $NADP^+$ and enzyme. After obtaining a stable baseline, 0.3 mM G6P for G6PDH1 and 3 and 1.6 mM G6P for G6PDH2 were added to initiate the reaction. For G6P protection assays, a stable baseline was obtained with G6PDH1 and 0.6 mM $NADP^+$. The reactions were initiated by adding 10 mM DTT and 0.3 mM G6P. The activity was measured 30 or 60 min later to allow time for DTT deactivation. During an hour of incubation, <5% of added G6P and $NADP^+$ was consumed and activity was still linear in response to time.

3.3.3 Kinetic characterization

Enzymes were assayed at varying concentrations of the substrate while keeping the concentration of other substrates constant as described above. All G6PDH isoforms showed substrate inhibition for G6P; therefore, we estimated regression lines and kinetic constants by finding the minimum of the sum of the squared residuals from the following equation using Solver in Excel, where v is the specific activity of the enzyme in mmol mg^{-1} min^{-1}, X is the number of bound inactivating substrate molecules, and H is the Hill cooperativity coefficient (Gray *et al.*, 2011) [28]:

$$v = \frac{V_{max} + V_i\left(S^x / K_{is}^x\right)}{1 + \frac{K_m^H}{S^H} + \frac{S^x}{K_{is}^x}}. \qquad \text{Eq. 3.1}$$

As recommended by LiCata and Allewell (1997), X was constrained to be ≤ 2 in order to prevent unrealistic values of parameters giving good fits. However, because it is difficult to estimate K_m in the presence of substrate inhibition, we determined the half-saturation concentration from the maximum velocity seen in the assays ($S_{0.5}$) of G6PDH. $NADP^+$ kinetics were estimated using standard Michaelis–Menten kinetics.

3.3.4 Inhibition studies

Different metabolites of the Calvin–Benson cycle were tested for their effect on G6PDH activity. All the metabolites were purchased from Sigma–Aldrich. In metabolite screening assays, metabolites were assayed at a 1:1 ratio with the substrate. To determine the K_i of G6PDH for different metabolites, the assay was carried out in the presence of various concentrations of G6P and NADPH. Assay mixtures were prepared as described above with different concentrations of substrate. The G6P concentration was varied between 0 and 3.8 mM. The concentration of $NADP^+$ in G6PDH assays was held constant at 600 mM. The concentration range used to study the K_i of G6PDH1 and 3 was 0–0.3 mM NADPH and 0–14.5 mM NADPH for the G6PDH2 assays based on preliminary assays. The mechanism of inhibition was determined from Hanes–Woolf plots. The K_i was determined from the non-linear least squares fitting of the activity versus NADPH concentration plot using Solver in Excel using the standard equation for competitive inhibition as described below.

$$v = \frac{V_{max} * S}{K_m\left(1 + \frac{I}{K_i}\right) + S}. \quad \text{Eq. 3.2}$$

where V_{max} is the maximum velocity, S is the G6P concentration, K_m is the Michaelis constant, and K_i is the inhibition constant. Sum of least squares for Solver regressions for inhibition constants are shown in Table 1.

3.3.5 Midpoint potential of G6PDH1

As G6PDH1 was the most redox-sensitive of the three enzymes under study, we performed a series of oxidation–reduction titrations with purified G6PDH1. Fully reduced DTT was prepared daily by combining 100 mM DTT with 200 mM sodium borohydride. The mixture was incubated on ice for 20 min and then neutralized by adding concentrated HCl to a final concentration of 0.2 M. The mixture was brought to a pH of 8 and diluted to a final concentration of 50 mM DTT. Oxidized DTT and buffers used in the assay were also pH 8. We used mixtures of oxidized and reduced DTT at different redox potentials, ranging from −420 to −124 mV in order to span the range from fully reduced enzyme to fully oxidized. The total concentration of DTT was 1–8.5 mM. 4.1 ng of G6PDH1 was incubated in the DTT mixture with 1 mg ml^{-1} BSA (pH 8) for 1 h at 25°C in an anaerobic environment. The activity of G6PDH was measured as described in 'Coupled spectrophotometric assay for G6PDH' using 0.3 mM G6P to initiate the reaction. The data were fit with the Nernst equation for a two-electron process. We used the E_m of DTT as determined by Hutchison and Ort (1995), −391 mV at pH 8. Oxidized and reduced DTT was quantified using modified protocols from Cho *et al.* (2005) and Charrier and Anastasio (2013) to calculate the potential.

$$E_h = E_m + 2.303\left({}^{RT}/_{nF}\right) * log_{10}\left({}^{DTT_{ox}}/_{DTT_{red}}\right). \quad \text{Eq. 3.3}$$

3.3.6 Leaf extract assays

Arabidopsis Col-0 was grown on soil in a growth chamber with 12 h light at 120 mmol m^{-2} s^{-1}, 23°C and 12 h dark at 21°C. Plants were treated at 0 or 200 mmol m^{-2} s^{-1} for 1 h.

Approximately, 300 mg of leaf samples were collected in a 2 ml microfuge tube and immediately frozen by plunging in liquid nitrogen. Frozen samples were ground in a Retsch mill with 4 mm silicon carbide particles (BioSpec Products, www.biospec.com). About 1 ml of cold extraction buffer (45 mM HEPES, pH 7.2, 30 mM NaCl, 10 mM mannitol, 2 mM EDTA, 0.5% Triton X-100, 1% polyvinylpolypyrrolidone, 0.5% casein, and 1% protease inhibitor cocktail) was added to the sample and vortexed for 30 s. The sample was centrifuged for 30 s at maximum speed and immediately placed on ice. G6PDH activity was assayed as described in 'Coupled spectrophotometric assay for G6PDH'. Assays that used leaf extracts were normalized by amount of chlorophyll added to the assay mixture. Chlorophyll was quantified by lysing 50 ml of purified chloroplasts by sonication and adding supernatant to 1 ml of 95% ethanol. Chlorophyll concentration was calculated based on the OD_{654} (Wintermans and DeMots, 1965):

$$\text{mg Chl} = OD * 0.0398 * 0.050\ \mu\text{l}. \qquad \text{Eq. 3.4}$$

3.3.7 Chloroplast isolation

Arabidopsis Col-0 was grown on soil in a growth chamber with 12 h light at 120 mmol m^{-2} s^{-1}, 23°C and 12 h dark at 21°C. Chloroplasts were isolated using a Percoll gradient (Weise *et al.*, 2004). Leaves were placed in a chilled blender with cold grinding buffer (330 mM mannitol, 50 mM HEPES, pH 7.6, 5 mM $MgCl_2$, 1 mM $MnCl_2$, 1 mM EDTA, 5 mM ascorbic acid, 0.25% BSA), blended, and then filtered through four layers of cheesecloth. Filtered liquid was centrifuged and the pellet was resuspended in resuspension buffer (330 mM mannitol, 50 mM HEPES, pH 7.6, 5 mM $MgCl_2$, 1 mM $MnCl_2$, 1 mM EDTA, 0.25% BSA). The resuspended pellet was layered on top of a 20–80% Percoll gradient which was centrifuged at 1200 g for 7 min. The bottom band in the gradient containing the intact chloroplasts was collected. One volume of resuspension buffer was added to collected chloroplasts and centrifuged at 1200 g for 2 min. The pellet was resuspended in 50 ml of water and vortexed to lyse the chloroplasts. One

volume of 2x buffer (100 mM HEPES, pH 7.6, 10 mM $MgCl_2$, 2 mM $MnCl_2$, 2 mM EDTA, 2 mM EGTA, 60% glycerol, 0.2% Triton X-100, and 0.2% PVPP) was added. Samples were stored at −80°C until used for further analysis.

When chloroplast isolations were used to assess the activity of fully oxidized and reduced plastidic G6PDH, isolated plastids were treated with 0 or 200 mmol m^{-2} s^{-1} of light for 1 h, on ice to limit protease activity, to oxidize or reduce G6PDH before assaying activity. Assays that used isolated chloroplasts were normalized by the amount of chlorophyll added to the assay mixture as described in 'Leaf extract assays'.

3.4 RESULTS

3.4.1 Purification of recombinant G6PDH

The final concentration of G6PDH1 was 1.66 mg ml^{-1}, G6PDH2 was 1.90 mg ml^{-1}, and G6PDH3 was 0.177 mg ml^{-1} (Supplementary Figure 3.1). The molecular mass of Strep-tagged recombinant G6PDH1 was ~65.2 kDa, G6PDH2 was ~70.2 kDa, and G6PDH3 was ~70.5 kDa. The maximum specific activity was ~55 mmol mg^{-1} protein min^{-1} for G6PDH1, ~22 mmol mg^{-1} protein min^{-1} for G6PDH2, and ~11 mmol mg^{-1} protein min^{-1} for G6PDH3. Maximum specific activities were determined from fitting varying $NADP^+$ and 7.6 mM G6P for G6PDH1 and 3 and 15.4 mM for G6PDH2. One preparation of each recombinant enzyme was aliquoted and a fresh aliquot was used each day for all experiments that day. Each experiment described below consists of three technical replicates prepared from separate dilutions of enzyme aliquots.

3.4.2 Kinetic characterization of G6PDH isoforms

We determined the oxidized (fully active) biochemical parameters of G6PDH1, 2, and 3. Table 1 shows the K_m and $S_{0.5}$ (for both G6P and $NADP^+$), G6P K_i, k_{cat}, NADPH K_i, and other determined kinetic parameters of all three G6PDH isoforms. All three oxidized G6PDH isoforms

showed substrate inhibition (Figure 3.1a). G6PDH1 had a $S_{0.5}$ of 0.3 mM and G6PDH3 had a $S_{0.5}$ of 0.3 mM G6P while G6PDH1 had the highest k_{cat} for G6P of 51.8 s^{-1}. For $NADP^+$ (Figure 3.1b), G6PDH1 had the highest k_{cat}.

3.4.3 G6PDH is inhibited by NADPH

Since the activity of an enzyme is also dependent on the presence of metabolic inhibitors, we tested ribulose-1,5-bisphosphate (RuBP), Ru5P, F6P, PGA, DHAP, E4P, NADPH, and 6PG for their effect on G6PDH activity. Only NADPH showed inhibition. While NADPH inhibited all three isoforms, G6PDH2 was the most inhibited. The calculated K_i values for NADPH are shown in Table 1. Sum of least squares for Solver regressions for inhibition constants are shown in Table 1. NADPH was found to be competitive for all isoforms based on the Hanes–Woolf plots, except above 14.5 mM for G6PDH2 and above 0.15 mM for G6PDH3 (Supplementary Figure 3.2).

3.4.4 G6PDH1 is redox-regulated

All isoforms of G6PDH were susceptible to deactivation by DTT, but G6PDH1 was the most deactivated after half an hour, losing ~90% of its activity (Figure 3.2a). Kinetic characterization of G6PDH1 incubated with 10 mM DTT showed that decreased activity in G6PDH1 was due to both a decrease in k_{cat} and an increase in $S_{0.5}$. However, the k_{cat} was less affected than the $S_{0.5}$ (Table 3.1, Figure 3.2b). Comparison of our results to those of Née *et al.* (2009), who used thioredoxins to deactivate G6PDH1, show that DTT is an acceptable mimic of thioredoxins to deactivate G6PDH1. Both results show that G6PDH1 will lose ~90% of activity when fully reduced. G6PDH2 and 3 did not significantly change the k_{cat} or $S_{0.5}$. G6PDH2 retained ~60% of activity and G6PDH3 retained ~80% of activity. Redox deactivation of G6PDH1 can be partially rescued by the addition of hydrogen peroxide equimolar to DTT in vitro (Figure 3.3a). However, G6PDH1 does not fully recover, returning to only ~65% of its original activity. Presumably,

there are additional mechanisms for fully reactivating G6PDH1 in vivo. G6PDH1 activity reached approximately 64% activity while 79% of the DTT was still reduced (Figure 3.3b). The calculated E_m at this time point was −407 mV. Based on our determined midpoint potential of G6PDH1 (see 'The midpoint potential of G6PDH1 is −378 mV at pH 8'), we predict G6PDH1 would have <5% activity at the redox potential in the assay. Therefore, we conclude the addition of hydrogen peroxide did not result in the reactivation of G6PDH1 by oxidizing DTT but that hydrogen peroxide was directly activating G6PDH1.

Redox deactivation of G6PDH1 was decreased when G6P was present. When G6P was present at 0.3 mM during incubation with DTT, the activity of reduced G6PDH was higher than when G6P was not present (Figure 3.4). Substrate interaction with other redox-regulated chloroplast enzymes has been reported before (Leegood *et al.*, 1982; Woodrow and Walker, 1983).

3.4.5 The midpoint potential of G6PDH1 is −378 mV at pH 8

In addition to determining that G6PDH1 is susceptible to redox deactivation, we determined the midpoint potential of G6PDH1 (Figure 3.5). The data were fit with the Nernst equation for a two-electron process. Incubation of G6PDH1 at higher redox potentials (−300 to −140 mV) did not increase activity any further. The midpoint potential of G6PDH1 at pH 8 was −378 mV. This corresponds to a midpoint potential of −318 mV at pH 7. We measured the amount of reduced DTT present at the beginning and end of an hour incubation with 3 mg ml^{-1} BSA. The measured amount of DTT did not change within the time of incubation. Additionally, the presence of 1 mg ml^{-1} or 3 mg ml^{-1} BSA did not change the measured amount of DTT, and hence the redox potential, within the first 5 min.

3.4.6 G6PDH is active in isolated chloroplasts and leaf extracts

As well as performing in vitro characterization, we used rapid leaf extract assays and chloroplast isolations to determine the activity of redox-regulated G6PDH in the leaf. After illumination at 200 mmol m^{-2} s^{-1} for 1 h, G6PDH activity in Arabidopsis leaf extracts decreased by ~30% (Figure 3.6). When isolated chloroplasts were illuminated at 200 mmol m^{-2} s^{-1} for 1 h, G6PDH activity decreased by 40%. Each chloroplast isolation and leaf extract had three biological replicates. The recombinant enzyme kinetic constants we determined indicate that a significant amount of the activity of G6PDH seen during the day can be caused by plastidial forms of the enzyme. Lendzian and Ziegler (1970) showed similar results with spinach showing that this phenomenon is not restricted to Arabidopsis.

3.5 DISCUSSION

Here we have investigated two questions: (1) what are the kinetic parameters of both oxidized and reduced G6PDH1 and (2) what are the key regulators of plastidic G6PDH enzyme in order to understand how these factors impact G6PDH activity in the light and therefore flux through the G6P shunt.

3.5.1 G6PDH activity is highly sensitive to G6P concentration in the plastid

The activity of G6PDH (and thus the G6P shunt) is sensitive to stromal G6P concentration by four mechanisms.

1. Deactivation of G6PDH in reducing conditions is primarily due to an increase in $S_{0.5}$ (Scheibe *et al.*, 1989).
2. G6P protects G6PDH from deactivation in reducing conditions (Figure 3.4) and catalytic site inhibition by diethyl decarbonate (Née *et al.*, 2014)
3. All isoforms of plastidic G6PDH show G6P substrate inhibition (Figure 3.1a).

4. G6P has been shown to relieve the inhibition of G6PDH by NADPH, as well as decrease the K_m and increases the k_{cat} of G6PDH in assays where $NADP^+$ is varied (Olavarría *et al.*, 2012; Shreve and Levy, 1980).

Our data corroborate previous research that shows G6PDH is in a reduced, less active form in the light, most likely to reduce futile cycling in leaves (Née *et al.*, 2014; Scheibe *et al.*, 1989; Wakao and Benning, 2005). However, while the enzyme is less active in the light (Anderson *et al.*, 1974; Buchanan, 1980; Buchanan *et al.*, 2015; Heldt and Piechulla, 2005; Née *et al.*, 2014; Scheibe *et al.*, 1989), our results show that it can retain significant activity. While there is a slight decrease in k_{cat}, G6PDH1 is predominately regulated by an increase in K_m, agreeing with data from Scheibe *et al.* (1989) in pea. Née *et al.* (2014) have also characterized the kinetics of G6PDH1 but found a higher $S_{0.5}$ and k_{cat} than described here. Additionally, they propose that changes in $NADP^+$ binding play a role in G6PDH redox regulation. The G6P concentration in the plastid is estimated to be approximately 1.4 mM (Dietz, 1985; Gerhardt *et al.*, 1987; Sharkey and Vassey, 1989). G6PDH regulation via a K_m shift allows for up to ~30% maximal activity with increased substrate concentration, even in reducing conditions. Under some conditions the plastid G6P concentration might increase. For example, when plants are grown in high CO_2, exposed to an increase in light intensity, or in plant deficient in starch synthesis (Dyson *et al.*, 2015; Kunz *et al.*, 2010; Leakey *et al.*, 2009), G6P concentrations may increase to the point where reduced G6PDH can readily consume G6P. However, the substrate inhibition of G6PDH limits the maximal activity of the enzyme at high substrate concentrations to possibly reduce futile cycling. While enzyme activity is generally dependent on the concentration of its substrate, because of the four ways that G6P can regulate G6PDH enzyme activity, G6PDH is particularly sensitive to the concentration of G6P.

3.5.2 G6PDH1 redox regulation allows modulation of G6PDH activity in the light

We determined the midpoint potential of G6PDH to be −378 mV at pH 8. Née *et al.* (2009) found a midpoint potential of 330 mV. Just over 10% of the difference may result from the difference in pH (8.0 in our study, 7.9 in Née *et al.* (2009). We went to considerable lengths to ensure the DTT was fully reduced and to exclude oxygen during the incubations. In what follows we assume that the midpoint potential of G6PDH1 is −378 mV. This is close to the midpoint potential of other redox regulated enzymes in the Calvin-Benson cycle and electron transport (Cammack *et al.*, 1977; Hirasawa *et al.*, 1998; Hirasawa *et al.*, 2000; Hirasawa *et al.*, 1999; Knaff, 2000; Née *et al.*, 2009; Strand *et al.*, 2016).

Assuming equilibrium and the midpoint potential of G6PDH1 at pH 8 as a reference, using the Nernst equation, we calculate that all Calvin-Benson cycle enzymes and electron transport proteins are almost fully reduced and thus active while G6PDH maintains 50% of its activity (Table 2). Exceptions are ferredoxin and malate dehydrogenase (MDH), which are predicted to be oxidized at -378 mV. Ferredoxin should be oxidized during the day to accept electrons from photosystem I (PSI). MDH has maximal activity when fully reduced, but it has been shown that MDH activity is not fully active during the day (Nakamoto and Edwards, 1983a, b). Our prediction that NADPH would be 46% reduced is consistent with findings from Lendzian (1980), which show the ratio of NADPH to $NADP^+$ to be ∼1 in a reconstituted spinach chloroplast. Although there may be deviations from redox equilibrium within the stroma, from these approximations we conclude that the midpoint potential of G6PDH1 is in a range to allow dynamic regulation of G6PDH and that it is theoretically possible to have flux through the Calvin-Benson cycle and the G6P shunt at the same time.

We have also shown that G6PDH can be activated upon addition of hydrogen peroxide. Brennan and Anderson (1980) and Née *et al.* (2009) previously demonstrated a role for hydrogen

peroxide regulation of G6PDH both *in vivo* and *in vitro* in the presence of thioredoxin. Additionally, in conditions where hydrogen peroxide can accumulate, such as high light, hydrogen peroxide can act on G6PDH directly to reverse G6PDH deactivation and modulate the consumption of G6P by the G6P shunt. It has been shown that hydrogen peroxide can be produced in situ in isolated chloroplasts and can transiently accumulate for signaling (Smirnoff and Arnaud, 2019). The activity of G6PDH can be modulated by redox status of the plastid, G6P concentration, and hydrogen peroxide. Hydrogen peroxide can also stimulate cyclic electron flow (Strand *et al.*, 2015), which could make up for the loss of ATP in the G6P shunt.

Redox regulation of dominant isoforms of G6PDH is found in many species, including Arabidopsis, pea, potato, spinach, and barley (Scheibe *et al.*, 1989; Schnarrenberger *et al.*, 1973; Semenikhina *et al.*, 1999; Wenderoth *et al.*, 1997; Wendt *et al.*, 2000; Wright *et al.*, 1997). We have shown that plastidic G6PDH from isolated Arabidopsis chloroplasts retains ~50% of its total activity, even in high light conditions. Additionally, cytosolic G6PDH could convert G6P in the cytosol to pentose phosphate and to be imported into the plastid by the xylulose-5-phosphate transporter (Eicks *et al.*, 2002).

Oxidative stress might also stimulate the G6P shunt. Drought or high light can result in an accumulation of hydrogen peroxide and other ROS products (see Suzuki *et al.* (2011) for a review). Based on current findings, we propose that, with the accumulation of hydrogen peroxide, the $S_{0.5}$ of G6PDH1 can decrease, increasing the flux through the G6P shunt. Sharkey and Weise (2016) proposed that the shunt can induce cyclic electron flow, which may help protect PSI. Photoprotective mechanisms of PSII (photosystem II), for example, state transitions of the antenna complex or energy-dependent quenching, are usually sufficient to safely dissipate excess excitation energy at PSII (Derks *et al.*, 2015). However, with high light, in fluctuating light (Allahverdiyeva *et al.*, 2014), and at low temperature (Sonoike, 2011), excess energy or

electrons could still be passed on to PSI and result in PSI photoinhibition. Unlike PSII, the proteins of PSI have a low turnover rate and damage to PSI is considered more severe than damage to PSII (Lima-Melo *et al.*, 2018; Scheller and Haldrup, 2005; Sonoike, 2011). Coupling ATP consumption in the G6P shunt with cyclic electron flow would dissipate light energy at PSI (Miyake *et al.*, 2004; Munekage *et al.*, 2004; Strand and Kramer, 2014).

3.6 CONCLUSION

Our data support the conclusion that G6PDH can retain significant activity during the day and therefore allow flux through the G6P shunt in the light. This is particularly relevant in conditions where the redox status of the plastid or the plastidic concentration of G6P may be changing. G6PDH is still partially deactivated, reducing the loss of carbon while still maintaining regulatory flexibility to increase and decrease the G6P shunt (Figure 3.7) as needed. However, in vivo flux measurements are not yet available for the G6P shunt. Characterization of G6PDH mutants and quantification of flux through this pathway is essential to understand the physiological importance of the shunt.

3.7 ACKNOWLEDGMENTS

We thank Michigan State University Research Technology Support Facility Mass Spectrometry Core for providing the facility for doing the LC–MS/MS work. This research was funded by U.S. Department of Energy Grant DE-FG02-91ER2002 (T.D.S. and A.L.P) and DE-FG02-11ER16220 (N.F.). A.L.P is partially supported by a fellowship from Michigan State University under the Training Program in Plant Biotechnology for Health and Sustainability (T32-GM110523). Partial salary support for T.D.S. came from Michigan AgBioResearch.

APPENDIX

TABLE 3.1- Kinetic constants and inhibition constants of G6PDH1, 2, and 3 as determined by NADPH-linked spectrophotometric assays.

K_m and k_{cat} were determined by fitting the Michalis-Menten equation. Other parameters were determined from a modified Michalis-Menten equation which includes substrate inhibition. Data points used in model fitting were n=3 different preparations. For inhibition constants, each number was determined from the fitted curves as described in the methods. Errors shown are S.E. (n=3). Sum of least-squares for inhibition parameters of G6PDH that were determined using Solver in Excel. RMSE- square root of mean squared error.

		G6PDH1	G6PDH2	G6PDH3
G6P K_m (mM)	Oxidized	0.4±0.03	1.6±0.5	0.3±0.06
	Reduced	1.8±0.6	1.4±0.4	0.5±0.1
G6P K_i (mM)	Oxidized	17.1±6.0	22.4±4.5	33.1±2.0
	Reduced	56.2±6.4	3.7±1.1	44.9±11.9
k_{cat} (s^{-1})	Oxidized	49.2±1.6	27.1±2.8	11.6±0.4
	Reduced	22.6±3.3	26.1±4.4	12.3±2.6
NADP K_m (µM)		0.6±0.2	1.3±0.03	0.6±0.06
Binding inhibitor molecules *(X)*		2.0±0.0	2.0±0.0	1.7±0.3
Hill cooperativity coefficient *(H)*		1.0±0.0	1.0±0.0	1.0±0.0
Catalytic Efficiency G6P (mM^{-1} s^{-1})		125.1±8.5.	23.1±11.2	51.8±14.3
Catalytic Efficiency NADP (μM^{-1} s^{-1})		109.7±38.8	21.0±2.5	20.1±1.6
NADPH K_i (µM)		59	0.9	112
NADPH K_i RMSE		15.8	3.3	2.1

TABLE 3.2- Midpoint potentials and percent reduction of key Calvin-Benson cycle enzymes and electron transport proteins at -378 mV at pH 8, assuming equilibrium.

Calvin-Benson cycle enzymes are mostly active at the midpoint potential of G6PDH. One electron chemistry is assumed for ferredoxin and two electron chemistry for all others.

Enzyme or metabolite	Midpoint potential, E_m (mv) at pH 8	% reduced at -378 mV
G6PDH	-378	50.0
Ferredoxin	-410	7.0
NADPH	-380	46.0
Thioredoxin *f*	-350	90.6
Thioredoxin *m*	-360	81.1
NADP-MDH	-390	27.5
FBPase	-375	56.0
PRK	-355	86.5
Cyclic electron flow	-330	98.0

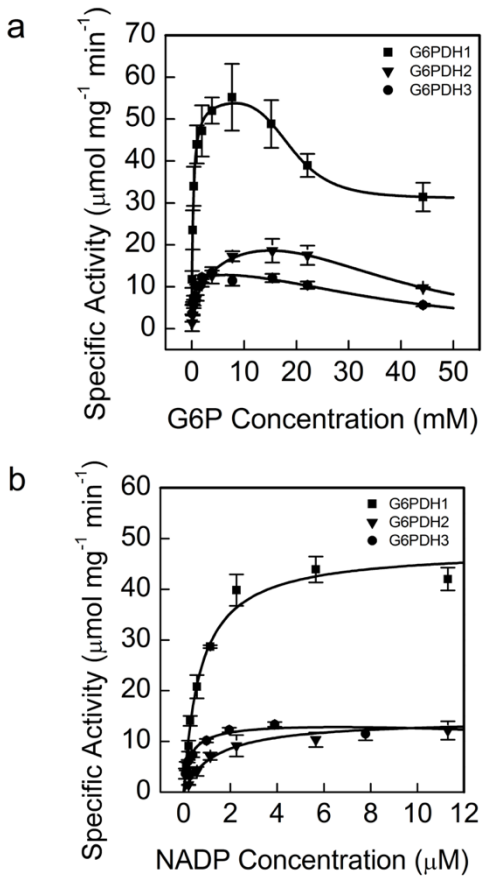

FIGURE 3.1- Activity of G6PDH1, 2, and 3 at different G6P and $NADP^+$ concentrations.

All three isoforms of oxidized G6PDH showed substrate inhibition for G6P. G6PDH1 and 3 showed the greatest affinity for G6P (a) and G6PDH3 had the greatest affinity for $NADP^+$(b). During the G6P experiments, $NADP^+$ was 0.6 mM and during the $NADP^+$ experiment assays were done with 7.6 mM G6P for G6PDH1 and 3 and 15.4 mM for G6PDH2 since these were approximately the concentrations that gave maximal activity for each enzyme. In (a) lines represent data fit with Eq (2) and in (b) lines represent data fit with the Michaelis–Menten equation. Each data point represents mean and error bars represent S.E. (n = 3).

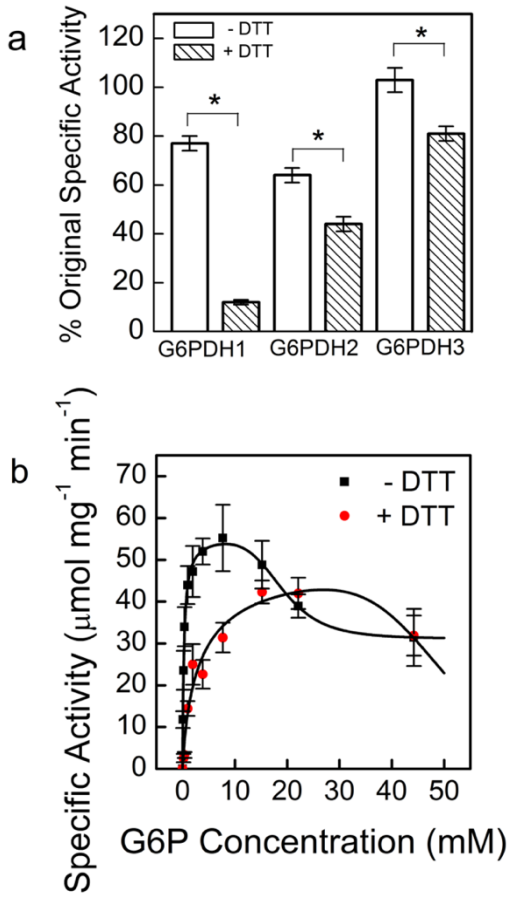

FIGURE 3.2- Activity of G6PDH 1, 2, and 3 with and without DTT treatment and $S_{0.5}$ shift with DTT in G6PDH 1.

G6PDH1 was the most affected by DTT treatment. White bars indicate controls incubated without DTT for 30 min and shaded bars represent incubation with 10 mM DTT for 30 min (a). Single point assays were done at $S_{0.5}$ concentrations, 0.3 mM G6P for G6PDH1 and 3 and 1.6 mM for G6PDH2 (b). Bars with an asterisk (*) are significantly different from corresponding controls as determined by Student's t-test ($P < 0.05$). In (b), the lines represent data fit with Eq. 2, and there are two overlapping data points at the highest G6P concentration. Each bar or data point represents mean and error bars represent S.E. (n = 3).

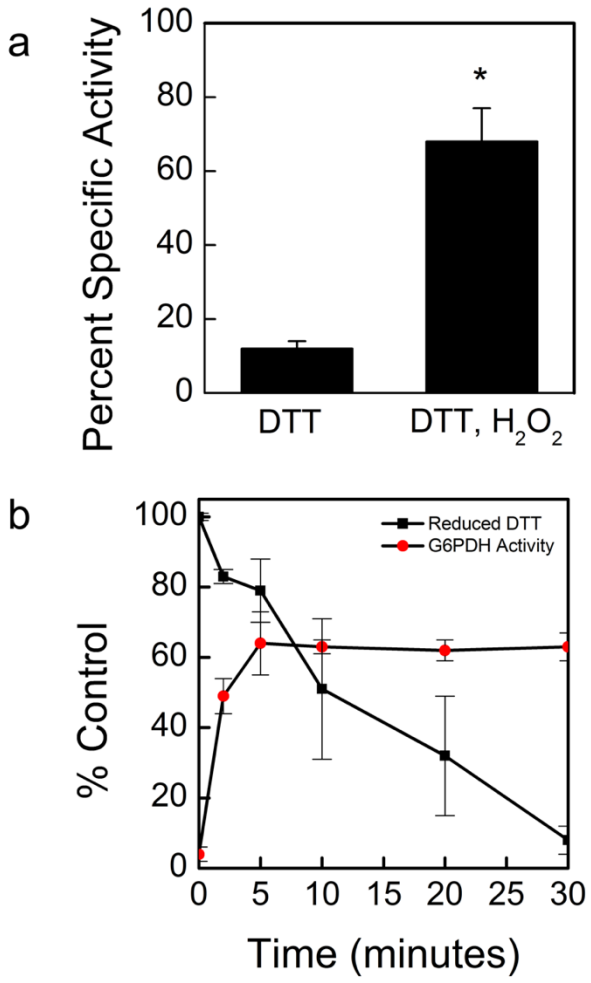

FIGURE 3.3- Partial reactivation of DTT-deactivated G6PDH1 with hydrogen peroxide.

G6PDH1 deactivation by DTT could be partially recovered by addition of equimolar hydrogen peroxide. (a) Reactivation is not through DTT oxidation, but rather hydrogen peroxide directly affects G6PDH1 (b). In (b), at each time point, G6PDH activity was assayed DTT concentrations were quantified using protocols from Cho *et al.* (2005) and Charrier and Anastasio (2013). Assays were done with 0.3 mM G6P. Each bar or data point represents mean and error bars represent S.E. (n = 3). Bars with an asterisk (*) are significantly different as determined by two-tailed Student's t-test ($P < 0.05$).

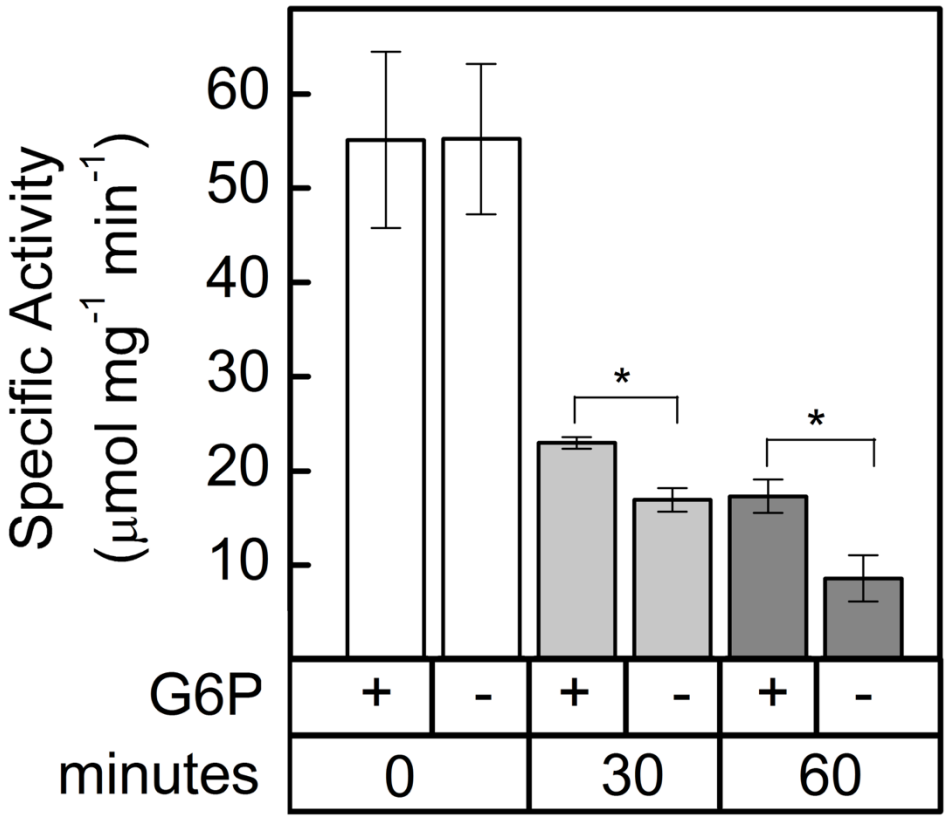

FIGURE 3.4- G6PDH1 protection from deactivation by G6P.

G6PDH1 is less deactivated by DTT after 30 and 60 min when G6P is present at 0.3 mM. Each bar represents the mean and error bars represent S.E. (n = 3). Bars with asterisk (*) are significantly different as determined by two-tailed Student's t-test ($P < 0.05$).

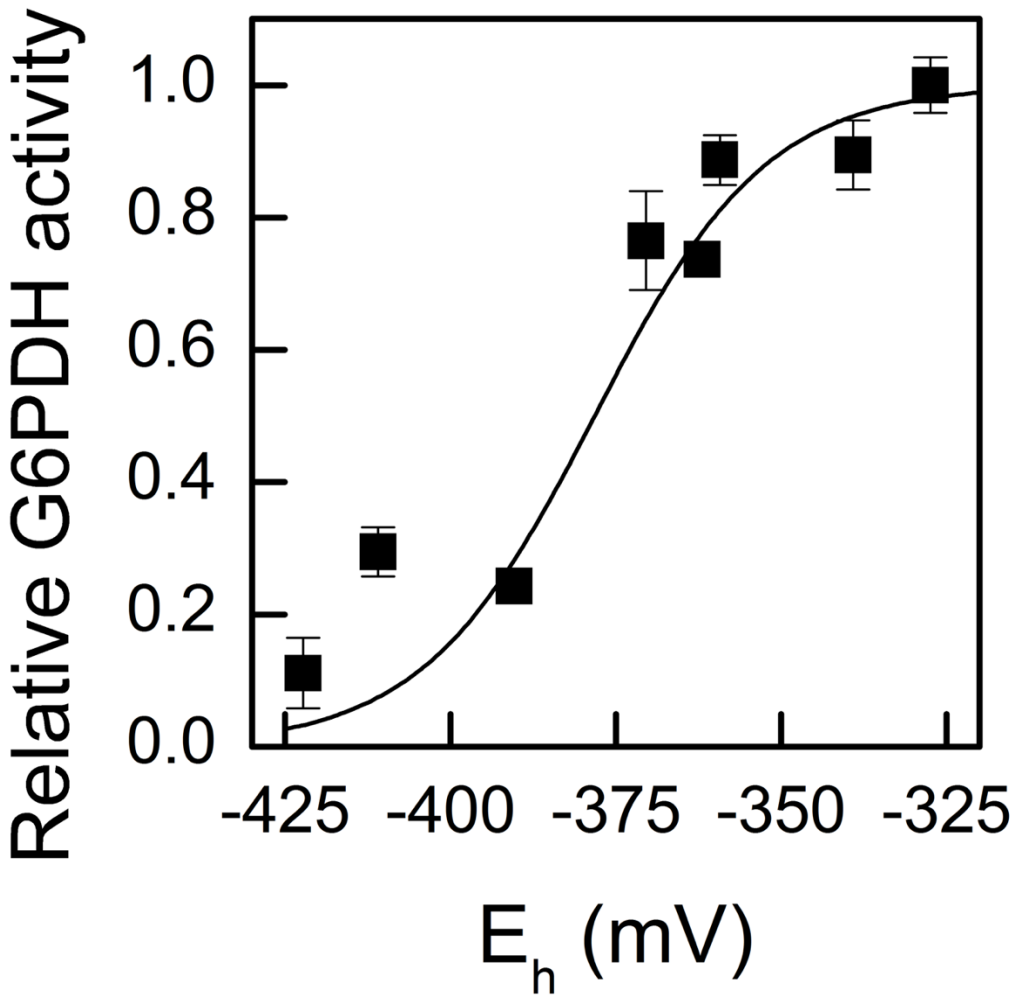

FIGURE 3.5- G6PDH1 midpoint potential.

The midpoint potential of G6PDH1 was determined to be −378 mV at pH 8. Assays were done at the $S_{0.5}$ concentration of G6P for oxidized G6PDH1, 0.3 mM. Each data point represents the mean and error bars represent S.E. (n = 3). The solid line represents the Nernst equation for a two-electron process.

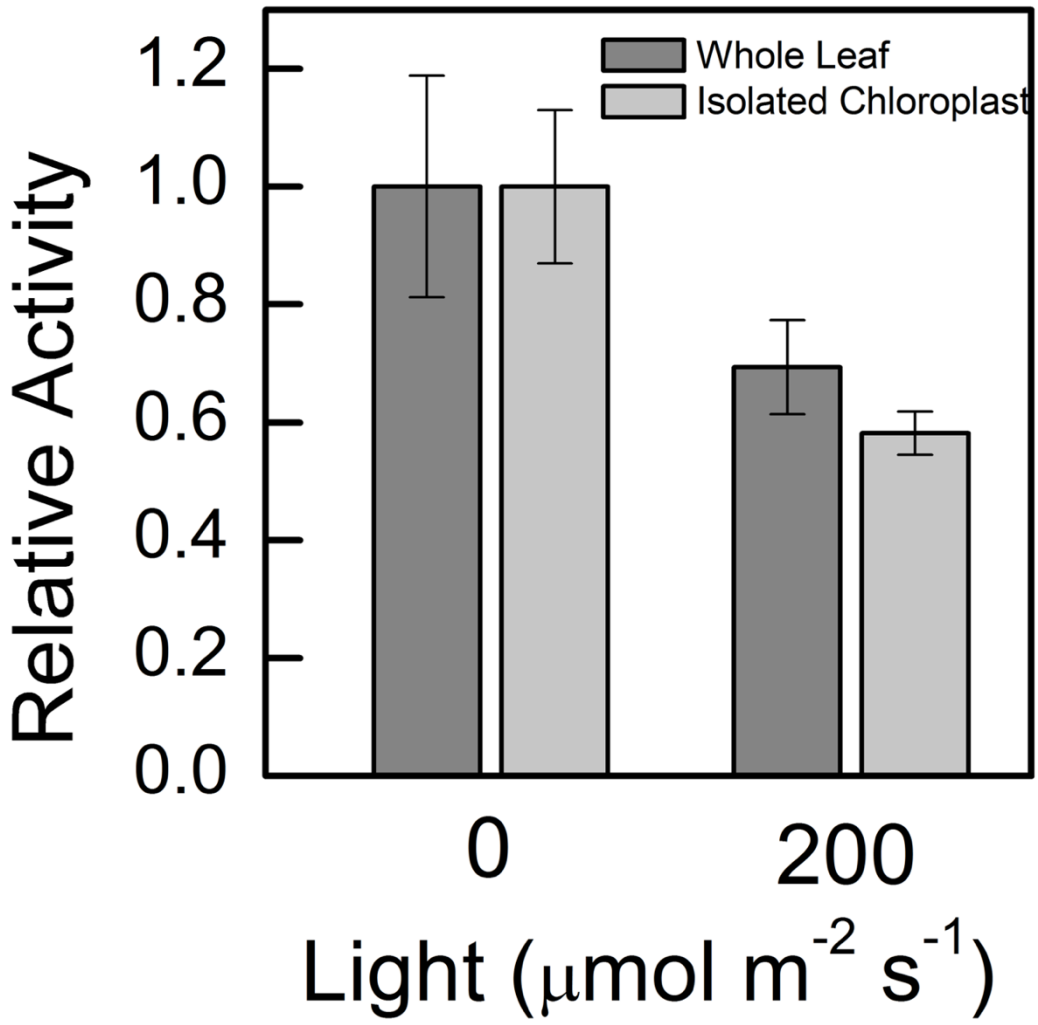

FIGURE 3.6- Whole leaf and chloroplast activity of G6PDH in Arabidopsis.

Whole leaf activity of G6PDH decreased 35% after illumination at 200 mmol m^{-2} s^{-1} for 1 h. This represents the total redox-sensitive G6PDH fraction in Arabidopsis leaves. Chloroplast G6PDH activity decreased 50% after illumination at 200 mmol m^{-2} s^{-1} for 1 h. Samples were normalized by amount of chlorophyll added to the assay mixture. Assays were done with 5 mM G6P. Each bar represents the mean and error bars represent S.E. (n = 3).

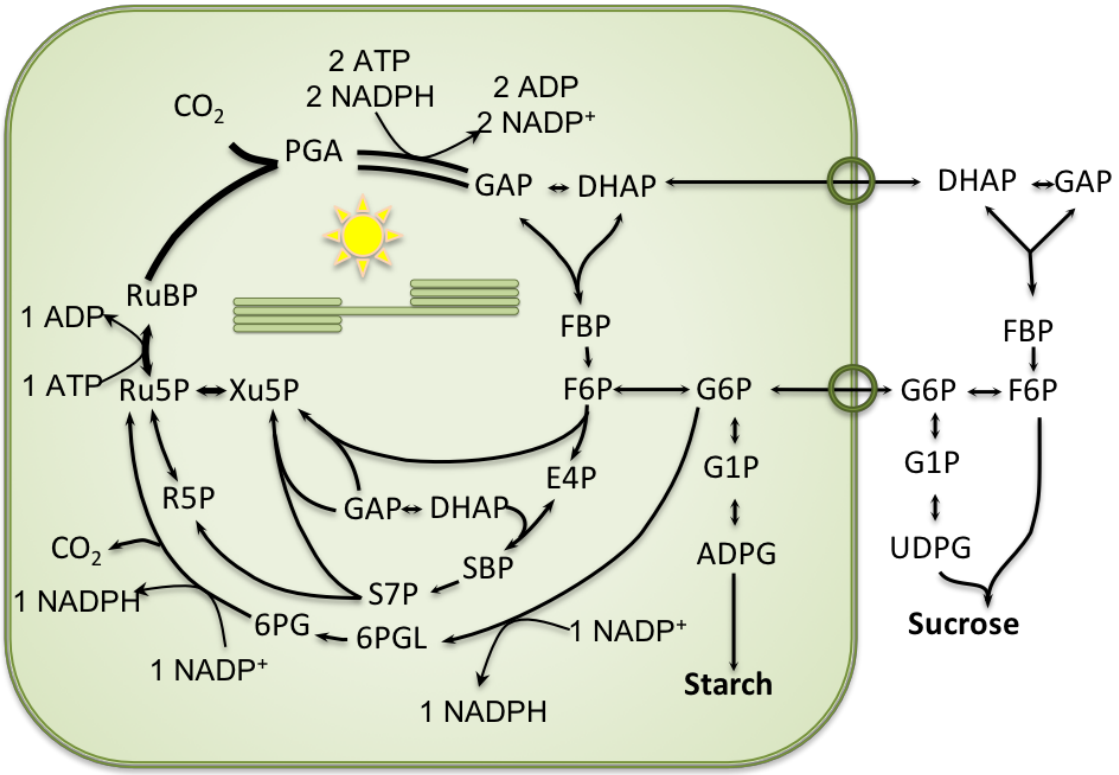

FIGURE 3.7- The glucose-6-phosphate (G6P) shunt.

G6P is consumed by G6PDH to enter the G6P shunt.G6P re-enters the Calvin–Benson cycle as ribulose 5-phosphate (Ru5P). Overall, the shunt consumes three ATP and two $NADP^+$ and produces two NAPDH. One CO_2 molecule is lost for every G6P that enters the shunt.

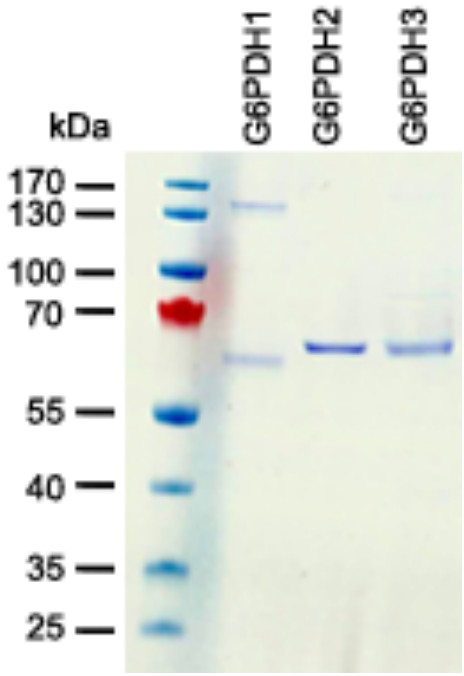

FIGURE S3.1- SDS page of the purified G6PDH proteins, stained with Coomassie blue.

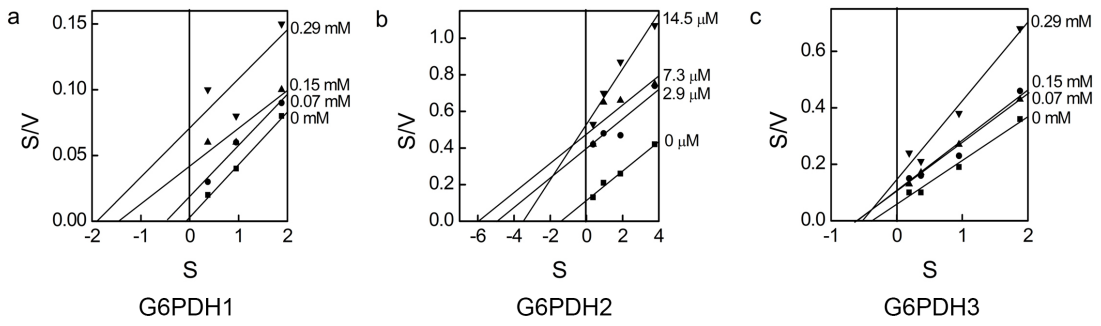

FIGURE S3.2- Hanes-Woolf plots of NADPH effect on G6PDH1, 2, and 3.

LITERATURE CITED

LITERATURE CITED

Anderson LE, Ng T-CL, Kyung-Eun Yoon P. 1974. Inactivation of pea leaf chloroplastic and cytoplasmic glucose 6-phosphate dehydrogenases by light and dithiothreitol. *Plant Physiology* **53**, 835-839.

Backhausen JE, Jöstingmeyer P, Scheibe R. 1997. Competitive inhibition of spinach leaf phosphoglucose isomerase isoenzymes by erythrose 4-phosphate. *Plant Science* **130**, 121-131.

Brennan T, Anderson LE. 1980. Inhibition by catalase of dark-mediated glucose-6-phosphate dehydrogenase activation in pea chloroplasts. *Plant Physiology* **66**, 815-817.

Buchanan BB. 1980. Role of light in the regulation of chloroplast enzymes. *Annual Review of Plant Physiology* **31**, 341-374.

Buchanan BB, Gruissem W, Jones RL. 2015. *Biochemistry & Molecular Biology of Plants*. Rockville: American Society of Plant Physiologists.

Cammack R, Rao KK, Bargeron CP, Hutson KG, Andrew PW, Rogers LJ. 1977. Midpoint redox potentials of plant and algal ferredoxins. *Biochemical Journal* **168**, 205-209.

Caspar T, Huber SC, Somerville C. 1985. Alterations in growth, photosynthesis, and respiration in a starchless mutant of *Arabidopsis thaliana* (L.) deficient in chloroplast phosphoglucomutase activity. *Plant Physiology* **79**, 11-17.

Charrier JG, Anastasio C. 2013. On dithiothreitol (DTT) as a measure of oxidative potential for ambient particles: evidence for the importance of soluble transition metals. *Atmospheric Chemistry and Physics* **12**, 11317-11350.

Cho AK, Sioutas C, Miguel AH, Kumagai Y, Schmitz DA, Singh M, Eiguren-Fernandez A, Froines JR. 2005. Redox activity of airborne particlate matter at different sites in the Los Angeles Basin. *Environmental Research* **99**, 40-47.

Dietz KJ. 1985. A possible rate limiting function of chloroplast hexosemonophosphate isomerase in starch synthesis of leaves. *Biochimica et Biophysica Acta* **839**, 240-248.

Dyson BC, Allwood JW, Feil R, Xu YUN, Miller M, Bowsher CG, Goodacre R, Lunn JE, Johnson GN. 2015. Acclimation of metabolism to light in *Arabidopsis thaliana*: the glucose 6-phosphate/phosphate translocator GPT2 directs metabolic acclimation. *Plant, Cell & Environment* **38**, 1404-1417.

Gerhardt R, Stitt M, Heldt HW. 1987. Subcellular metabolite levels in spinach leaves. Regulation of sucrose synthesis during diurnal alterations in photosynthetic partitioning. *Plant Physiology* **83**, 399-407.

Gray DW, Breneman SR, Topper LA, Sharkey TD. 2011. Biochemical characterization and homology modeling of methyl butenol synthase and implications for understanding hemiterpene synthase evolution in plants. *Journal of Biological Chemistry* **286**, 20582-20590.

Hanson KR, McHale NA. 1988. A starchless mutant of *Nicotiana sylvestris* containing a modified plastid phosphoglucomutase. *Plant Physiology* **88**, 838-844.

Heldt H-W, Piechulla B. 2005. *Plant Biochemistry*. Burlington MA: Elsevier Academic Press.

Hirasawa M, Brandes HK, Hartman FC, Knaff DB. 1998. Oxidation-reduction properties of the regulatory site of spinach phosphoribulokinase. *Archives of Biochemistry and Biophysics* **350**, 127-131.

Hirasawa M, Ruelland E, Schepens I, Issakidis-Bourguet E, Miginiac-Maslow M, Knaff DB. 2000. Oxidation-reduction properties of the regulatory disulfieds of sorghum chloroplast nicotinamide adenine dinucleotide phosphate-malate dehydrogenase. *Biochemistry* **39**, 3344-3350.

Hirasawa M, Schürmann P, Jacquot JP, Manieri W, Jacquot P, Keryer E, Hartman FC, Knaff DB. 1999. Oxidation-reduction properties of chlorplast thioredoxins, ferredoxin:thioredoxin reductase, and thioredoxin f-regulated enzymes. *Biochemistry* **38**, 5200-5205.

Hutchison RS, Ort DR. 1995. Measurment of equilibrium midpoint potentials of thiol/disulfide regulatory groups on thioredoxin activated chloroplast enzymes. *Methods in Enzymology* **252**, 220-228.

Kammerer B, Fischer K, Hilpert B, Schubert S, Gutensohn M, Weber A, Flügge UI. 1998. Molecular characterization of a carbon transporter in plastids from heterotrophic tissues: The glucose 6-phosphate phosphate antiporter. *The Plant Cell* **10**, 105-117.

Knaff DB. 2000. Oxidation-reduction properties of thioredoxins and thioredoxin-regulated enzymes. *Physiologia Plantarum* **110**, 309-313.

Kofler H, Häusler RE, Schulz B, Grȍner F, Flügge UI, Weber A. 2000. Molecular characterisation of a new mutant allele of the plastid phosphoglucomutase in *Arabidopsis* , and complementation of the mutant with the wild-type cDNA. *Molecular and General Genetics* **263**, 978-986.

Kruckeberg AL, Neuhaus HE, Feil R, Gottlieb LD, Stitt M. 1989. Decreased-activity mutants of phosphoglucose isomerase in the cytosol and chloroplast of *Clarkia xantiana*. Impact on mass-action ratios and fluxes to sucrose and starch, and estimation of flux control coefficients and elasticity coefficients. *Biochemical Journal* **261**, 457-467.

Kunz HH, Häusler RE, Fettke J, Herbst K, Niewiadomski P, Gierth M, Bell K, Steup M, Flügge UI, Schneider A. 2010. The role of plastidial glucose-6-phosphate/phosphate translocators in vegetative tissues of *Arabidopsis thaliana* mutants impaired in starch biosynthesis. *Plant Biology* **12**, 115-128.

Kunz HH, Zamani-Nour S, Hausler RE, Ludewig K, Schroeder JI, Malinova I, Fettke J, Flugge UI, Gierth M. 2014. Loss of cytosolic phosphoglucose isomerase affects carbohydrate metabolism in leaves and is essential for fertility of Arabidopsis. *Plant Physiology* **166**, 753-765.

Leakey ADB, Xu F, Gillespie KM, McGrath JM, Ainsworth EA, Ort DR. 2009. Genomic basis for stimulated respiration by plants growing under elevated carbon dioxide. *Proceedings of the National Academy of Sciences of the United States of America* **106**, 3597-3602.

Leegood RC, Kobayashi Y, Neimanis S, Walker DA, Heber U. 1982. Co-operative activation of chloroplast fructose-1,6-bisphosphatase by reductant, pH, and substrate. *Biochimica et Biophysica Acta* **682**, 168-178.

Lendzian KJ. 1980. Modulation of glucose-6-phosphate dehydrogenase by NADPH, NADP+ and dithiothreitol at variable NADPH/NADP+ ratios in an illuminated reconstituted spinach (Spinacia oleracea L.) chloroplast system *Planta* **148**, 1-6.

Lendzian KJ, Ziegler H. 1970. Regulation of glucose-6-phosphate dehydrogenase in spinach chloroplasts by light. *Planta* **94**, 27-36.

LiCata VJ, Allewell NM. 1997. Is substrate inhibition a consequence of allostery in aspartate transcarbamylase? *Biophysical Chemistry* **64**, 225-234.

Lowry OH, Passonneau JV. 1969. Phosphoglucomutase kinetics with the phosphates of fructose, glucose, mannose, ribose, and galactose. *Journal of Biological Chemistry* **244**.

Meyer T, Hölscher C, Schwöppe C, von Schaewen A. 2011. Alternative tageting of Arabidopsis plastidic glucose-6-phosphate dehydrogenase G6PD1 involves cysteine-dependent interaction with G6PD4 in the cytosol. *The Plant Journal* **66**, 745-758.

Nakamoto H, Edwards G. 1983a. Dark activation of maize leaf NADP-malate dehydrogenase and pyruvate, orthophosphate dikinase in vivo under anaerobic conditions. *Plant Science* **32**, 139-146.

Nakamoto H, Edwards G. 1983b. Influence of environmental factors on the light activation of pyruvate, PI dikinase and NADP-malate dehydrogenase in maize. *Functional Plant Biology* **10**, 279-289.

Née G, Aumont-Nicaise M, Zaffagnini M, Nessler S, Valerio-Lepiniec M, Bourguet-Issakidis E. 2014. Redox regulation of chloroplastic G6PDH activity by thioredoxin occurs through structural changes modifying substrate accessibility and cofactor binding. *Biochem J* **457**, 117-125.

Née G, Zaffagnini M, Trost P, Issakidis-Bourguet E. 2009. Redox regulation of chloroplastic glucose-6-phosphate dehydrogenase: A new role for f-type thioredoxin. *FEBS Letters* **583**, 2827-2832.

Olavarría K, Valdés D, Cabrera R. 2012. The cofactor preference of glucose-6-phosphate dehydrogenase from *Escherichia coli* - modelling the physiological production of reduced cofactors. *FEBS Journal* **279**, 2296-2309.

Ray WJ, Roscelli GA. 1964. A kinetic study of the phosphoglucomutase pathway. *Journal of Biological Chemistry* **239**, 1228-1236.

Scheibe R, Geissler A, Fickenscher K. 1989. Chloroplast glucose-6-phosphate dehydrogenase: K_m shift upon light modulation and reduction. *Archives of Biochemistry and Biophysics* **274**, 290-297.

Schnarrenberger C, Oeser A. 1974. Two isoenzymes of glucosephosphate isomerase from spinach leaves and their intracellular compartmentation. *European Journal of Biochemistry* **45**, 77-82.

Schnarrenberger C, Oeser A, Tolbert NE. 1973. Two enzymes each of glucose-6-phosphate dehydrogenase and 6-phosphogluconate dehydrogenase in spinach leaves. *Archives of Biochemistry and Biophysics* **154**, 438-448.

Semenikhina AV, Popova A, Matasova LV. 1999. Catalytic properties of glucose-6-phosphate dehydrogenase from pea leaves. *Biochemistry* **64**, 863-866.

Sharkey TD, Vassey TL. 1989. Low oxygen inhibition of photosynthesis is caused by inhibition of starch synthesis. *Plant Physiology* **90**, 385-387.

Sharkey TD, Weise SE. 2016. The glucose 6-phosphate shunt around the Calvin-Benson Cycle. *Journal of Experimental Botany* **67**, 4067-4077.

Shreve DS, Levy HR. 1980. Kinetic mechanism of glucose-6-phosphate dehydrogenase from the lactating rat mammary gland. *Journal of Biological Chemistry* **255**, 2670-2677.

Smirnoff N, Arnaud D. 2019. Hydrogen peroxide metabolism and functions in plants. *New Phytologist* **221**.

Strand DD, Fisher N, Davis GA, Kramer D. 2016. Redox regulation of the antimycin A sensitive pathway of cyclic electron flow around photosystem I in higher plant thylakoids. *Biochimica et Biophysica Acta Bioenergetics* **1857**, 1-6.

Strand DD, Livingston AK, Satoh-Cruz M, Froehlich JE, Maurino VG, Kramer DM. 2015. Activation of cyclic electron flow by hydrogen peroxide in vivo. *Proceedings of the National Academy of Sciences* **112**, 5539-5544.

Szecowka M, Heise R, Tohge T, Nunes-Nesi A, Vosloh D, Huege J, Feil R, Lunn J, Nikoloski Z, Stitt M, Fernie AR, Arrivault S. 2013. Metabolic fluxes in an illuminated Arabidopsis rosette. *The Plant Cell Online* **25**, 694-714.

Wakao S, Benning C. 2005. Genome-wide analysis of glucose-6-phosphate dehydrogenases in Arabidopsis. *The Plant Journal* **41**, 243-256.

Weise SE, Weber A, Sharkey TD. 2004. Maltose is the major form of carbon exported from the chloroplast at night. *Planta* **218**, 474-482.

Wenderoth I, Scheibe R, von Schaewen A. 1997. Identification of the cysteine residues involved in redox modification of plant plastidic glucose-6-phosphate dehydrogenase. *Journal of Biological Chemistry* **272**, 26985-26990

Wendt UK, Wenderoth I, Tegeler A, von Schaewen A. 2000. Molecular characterization of a novel glucose-6-phosphate dehydrogenase from potato (*Solanum tuberosum L.*). *The Plant Journal* **23**, 723-733.

Wintermans JGFM, DeMots A. 1965. Spectrophotometric characteristics of chlorophylls a and b and their pheophytins in ethanol. *Biochimica et Biophysica Acta* **109**, 448-453.

Woodrow IE, Walker DA. 1983. Regulation of stromal sedoheptulose-1,7-bisphosphatase activity and its role in controlling the reductive pentose phosphate pathway of photosynthesis. *Biochimica et Biophysica Acta* **722**, 508-516.

Wright DP, Huppe HC, Turpin DH. 1997. In vivo and in vitro studies of glucose-6-phosphate dehydrogenase from barley root plastids in relaiton to reductant supply for NO_2^- assimilation. *Plant Physiology* **114**, 1413-1419.

Yu TS, Lue WL, Wang SM, Chen J. 2000. Mutation of Arabidopsis plastid phosphoglucose isomerase affects leaf starch synthesis and floral initiation. *Plant Physiology* **123**, 319-326.

CHAPTER 4

The cytosolic glucose-6-phosphate shunt is a major source of respiration in the light during photosynthesis

This research was done in collaboration with Dr. Nerea Ubierna Lopez, Dr. Berkley Walker, and Alan McClain. N.U.L. and B.W. collected and analyzed g_m data. A.M. helped collect and analyze fluorescence data.

4.1 ABSTRACT

During the day, plants both assimilate and respire CO_2. The processes contributing to respiration in the light (R_L, also often called day respiration or R_D) are unknown, although mitochondrial respiration, glycolysis, and non-stoichiometric photorespiration and have been proposed (Cousins *et al.*, 2011; Tcherkez *et al.*, 2017). Here, we propose that the glucose-6-phosphate shunt is responsible for the majority of R_L. In $^{13}CO_2$ labelling studies, R_L is conventionally defined as a slow-to-label efflux of carbon from leaves. Therefore, we use efflux of $^{12}CO_2$ in a $^{13}CO_2$ environment as a measurement for R_L (Loreto et al., 2001).

Our goal is to understand the source of carbon and the enzymatic reactions responsible for R_L. We found that glucose-6-phosphate (G6P) shunts in both the plastid and cytosol are the major source of R_L and that understanding the biochemical characteristics of G6PDH can help predict changes in the source of R_L.

4.2 INTRODUCTION

In the light, leaves both assimilate and respire CO_2. Respiration encompasses two distinct processes: photorespiration and light respiration (R_L, sometimes called day respiration or R_D). R_L has been defined in several ways: 1) a non-photorespiratory efflux of CO_2, 2) an efflux of non-recently fixed carbon as CO_2 (Gauthier *et al.*, 2010; Schnyder *et al.*, 2003; Tcherkez *et al.*, 2012; Tcherkez *et al.*, 2011; Wingate *et al.*, 2007) or 3) non-photorespiratory oxygen consumption. Based on the definition of R_L as non-recently fixed carbon, methods have been developed to measure respiration as an efflux of $^{12}CO_2$ in a $^{13}CO_2$ environment (Busch, 2013; Loreto *et al.*, 2001). Here we primarily use the definition of R_L as an efflux of non-recently fixed carbon as CO_2. This definition of respiration is still very broad and can encompass many metabolic pathways with decarboxylation steps. It is often assumed that respiration in the light comes from the tricarboxylic acid (TCA) cycle in the mitochondria (see Tcherkez *et al.* (2017) for a review).

Previous assumptions about sources of respiration cannot fully explain the magnitude of the measured flux. R_L has been measured to be 0.2-2.2 μmol m^{-2} s^{-1} (Gong *et al.*, 2018; Loreto *et al.*, 2001). Isotopic labelling studies and metabolic flux analysis show that flux to and through the TCA pathway is very small (Calvin and Massini, 1952; Holm-Hansen *et al.*, 1959; Ma *et al.*, 2014; Moses *et al.*, 1959; Tcherkez *et al.*, 2005) and CO_2 efflux from the TCA cycle has been measured to be 0.02-0.05 μmol m^{-2} s^{-1} (Abadie *et al.*, 2017; Tcherkez *et al.*, 2009). Several key TCA cycle enzymes, such as isocitrate dehydrogenase (Igamberdiev and Gardeström, 2003) and pyruvate dehydrogenase (Tovar-Mendez *et al.*, 2003), are inactive in the light. While some carbon can be redirected to non-cyclic pathways around the TCA cycle, based on flux map predictions there is still not enough flux through the decarboxylation steps to account for the magnitude of day respiration (Sweetlove *et al.*, 2010).

Glycolysis, another possible source of R_L, also cannot account for the measured magnitude, as downstream products of glucose breakdown do not label when fed ^{14}C glucose. Key enzymes are also metabolically down-regulated (Lin *et al.*, 1989; Plaxton and Podestá, 2006; Scheible *et al.*, 2000; Stitt, 1990; Vittorio *et al.*, 1954). Non-stoichiometric photorespiration has also been proposed as a source of R_L (Cousins *et al.*, 2011). However, it has been shown that labeling effects from photorespiration last less than three minutes (Atkin *et al.*, 1998; Karl *et al.*, 2002). Here we propose that the glucose 6-phosphate (G6P) shunt as described by Sharkey and Weise (2016) is the source of R_L. The G6P shunt results in the decarboxylation of 6-phosphogluconate (6PG) to ribulose 5-phosphate (Ru5P), releasing a CO_2.

Understanding the source and location of light respiration has significant consequences for our understanding of both leaf level gas-exchange and global modeling of photosynthesis. On a leaf scale, accurate measurement of light respiration can affect photosynthetic calculations. For example, equations for modelling photosynthesis and electron transport both include R_L (Harley *et al.*, 1992; Sharkey *et al.*, 2007). The location of respiration can change calculations for refixation and conductance (Berghuijs *et al.*, 2019). R_L also impacts larger scales of gas-exchange. On an ecosystem scale, respiratory losses can account for 40% or more of total production (Gifford, 2003), and accurate estimations of respiration are necessary for understanding carbon-use efficiency and global modeling of photosynthesis (Heskel *et al.*, 2013; Heskel and Tang, 2018; Smith and Dukes, 2012; Tcherkez *et al.*, 2017). Insight into the underlying processes of respiration can help analyze and predict changes in response to changes in temperature, CO_2 concentrations, light, and other environmental factors.

In this paper, our goal is to explore the hypothesis that the G6P shunt is responsible for light respiration. We found that all loss-of-function mutants of glucose-6-phosphate dehydrogenase (G6PDH), the first committed step of the G6P shunt, decreased R_L. We also determined total

respiration based on fluorescence measurements and were able to divide respiration into four different sources: unlabeled G6P shunt, labeled G6P shunt, unlabeled other sources, and labeled other sources. Overall, we conclude that the G6P shunt can account for approximately 80% of light respiration and possibly nearly 100%.

4.3 MATERIALS AND METHODS

4.3.1 Plant material

Arabidopsis were germinated on rockwool plugs (Grodan, https://www.grodan.com) in 2 mL microcentrifuge tubes. After germination, plants were transferred to a hydroponic system in a growth chamber at a 12 h light at 120 μmol m^{-2} s^{-1}, 23˚C and 12 h dark at 21˚C. Plants were grown in Hoagland's solution. Plants grown on soil were planted in SureMix soil (Michigan Grower Products, Inc., Galesburg, MI, U.S.A.). They were grown in the same light and temperature conditions as the hydroponically grown plants.

Several lines of Arabidopsis mutants were ordered from the Arabidopsis Biological Resource Center (https://www.abrc.osu.edu) and homozygous knockouts were confirmed by PCR. Lines for analysis of G6PDH loss-of-function mutants were SAIL_1252, SALK_139479, SALK_045083, and SALK_124797 for G6PDH1, 3, 5, and 6, respectively. We also used starch-compromised mutants: *pgm*, *adg*, and *phs1-1* knockouts (TC75, SALK_133788C, and SALK_055562) (Ajjawi *et al.*, 2009; Caspar *et al.*, 1985; Wang *et al.*, 2002; Zeeman *et al.*, 2004). Plastidic membrane transporter mutants were loss-of-function for the xylulose-5-phosphate/phosphate translocator (XPT) and the triose phosphate translocator (TPT) (SAIL_378_C01 and SALK_028503). The *hpr1* plants (SALK_067724 and SALK_143584) were characterized by Timm *et al.* (2008). The *hcef1* and *hcef4* plants, characterized by loss-of-function FBPase or PRK were obtained from David Kramer (Livingston *et al.*, 2010). Arabidopsis Col-0 grown alongside the mutants was used for wild type controls.

For fluorescence and mesophyll conductance measurements, *Nicotiana tabacum* seeds were planted in SureMix soil (Michigan Grower Products, Inc., Galesburg, MI, U.S.A.). The plants were grown in the greenhouse starting in August 2019 with an average daytime temperature of 27˚C and nighttime temperature of 20˚C. Plants were fertilized twice per week with commercially available Peters 20-20-20 fertilizer (ICL Specialty Fertilizers, https://www.icl-sf.com) at 100 ppm. Experiments were done when plants were 5-12 weeks old on the fifth through seventh fully expanded leaves. For experiments measuring the effect of assimilation on R_L, *Nicotiana benthamiana* were grown as described above for *N. tabacum*.

4.3.2 Measurement of $^{12}CO_2$ efflux

Efflux of $^{12}CO_2$ was measured similar to Loreto *et al.* (2001). Hydroponically grown Arabidopsis were placed in an Arabidopsis chamber attached to a LI-COR 6800 (LI-COR Biosciences, Lincoln, NE, USA). To assess the effect of assimilation on R_L, greenhouse-grown *N. benthamiana* was used. The light was set to 150 µmol m^{-2} s^{-1}. 1200, 400, 100, and 50 µmol m^{-2} s^{-1} of light was used in experiments analyzing the effect of assimilation rate on R_L. Air was supplied at a rate of 0.8 L min^{-1}. CO_2 was supplied by an external tank controlled by a flow controller (50 mL min^{-1} max range, Alicat Scientific, https://www.alicat.com) at approximately 400 ppm CO_2 as measured by the sample IRGA. Fifty ppm CO_2 was also used in experiments analyzing the effect of assimilation rate on R_L. Nitrogen and oxygen were also supplied by external tanks via a custom gas mixer. Oxygen was kept at 21% or 2% of total gas provided, depending on the experiment. Nitrogen provided the rest of the gas and some portion of the N_2 was bubbled through deionized water to keep the air at 21 mmol mol^{-1} of water. Leaf temperature was 21˚C. Output from the LI-COR gas exchange system was fed from the sample output into a LI-800 GasHound (LI-COR Biosciences, Lincoln, NE, USA) at a rate of ~160 µmol s^{-1}. The GasHound was only 3% sensitive to $^{13}CO_2$, allowing us to accurately measure the $^{12}CO_2$

efflux (this is the same instrument used by Loreto *et al.* (1999) and Loreto *et al.* (2001)). The GasHound was connected to a voltmeter in order to read output. Plants were acclimated until photosynthesis was steady, approximately 20 min. After acclimation, CO_2 was rapidly switched to $^{13}CO_2$ (Sigma-Aldrich, https://www.sigmaaldrich.com) at the same concentration. The entire chamber was switched over from $^{12}CO_2$ to $^{13}CO_2$ within 1.5 min. Output from the voltmeter was read at 20 min, once steady state labelling had been reached (Figure S4.1) and used to calculate the rate of $^{12}CO_2$ efflux.

4.3.3 $^{13}CO_2$ labelling of Arabidopsis at steady state

Plants were treated and acclimated as described above in "Measurement of $^{12}CO_2$ efflux". After acclimation, CO_2 was rapidly switched to $^{13}CO_2$ at the same concentration. The entire chamber was switched over from $^{12}CO_2$ to $^{13}CO_2$ within 1.5 min. After 20 min, the chamber was opened and, without disrupting the light source, two leaves were rapidly harvested by plunging into liquid nitrogen. Frozen leaves were collected in 2 mL microcentrifuge tubes and stored at -80˚C for further analysis by mass spectrometry.

4.3.4 Metabolite extraction and mass spectrometry

Metabolites were analyzed using methods modified from Lunn *et al.* (2006). Frozen plant material was ground using a ball mill (Retsch, https://www.retsch.com) and suspended in 1.8 mL ice cold 30:70 chloroform: methanol. The mixture was incubated at -20˚C for 2 h, vortexing every 0.5 h. 1.5 mL deionized water was added, samples were vortexed, and centrifuged at 22000 g for 10 min at 4˚C. The aqueous fraction was collected and kept on ice. The non-aqueous fraction was re-extracted with an additional 1.5 mL deionized water and the second collected aqueous fraction was added to the first. Samples were frozen and freeze dried using a FreeZone Triad Freeze Dryer (Labconco, https://labconco.com). Dried samples were resuspended in 200

μL of 0.5 mM KOH and relative labelling of carbon in metabolites was measured using mass spectrometry.

Parameters for detection of metabolites were optimized using 10 μM standards purchased from Sigma-Aldrich (https://www.sigmaaldrich.com) (Table 4.1). LC/MS-MS was carried out on an Acquity TQD Tandem Quadrupole UPLC/MS/MS (Waters, https://www.waters.com) operated in electrospray negative ion mode with multiple reaction monitoring. The capillary voltage was 2.5 kV; the cone voltage, 2 V; the extractor voltage, 3 V. The source temperature was 130˚C and the desolvation temperature was 350˚C. Gas flow for the desolvation and cone was set to 700 and 40 L h^{-1}, respectively. MassLynx software and the Acquity UPLC Console were used to control the instrument. Samples were passed through a 4x35 mm Dionex IonPac ATC-3 Trap Column, a 2x50 mm Dionex IonPac AG11-HC Guard Column, and a 2x250 mm Dionex IonPac AS11-HC Analytical Column (ThermoFisher Scientific, www.thermofisher.com) with a multi-step gradient which was modified from Cocuron and Alonso (2014). Eluent A (0.5 mM KOH) and eluent B (75 mM KOH): 0-0.5 min, 100% A; 0.5-4 min, 100-95.2% A; 4-8 min, 95.2-87.3% A; 8-10 min, 87.3-73.8% A; 10-28 min, 73.8-33.5% A; 28-31 min, 33.6-0% A; 31-36 min, 0% A; 36-36.01 min, 0-100% A; 36.01-40 min, 100% A. The flow rate was 0.35 mL min^{-1}. Peaks were integrated using MassLynx software.

4.3.5 Mesophyll conductance measurements

Online $^{13}CO_2$ isotope discrimination was measured to estimate mesophyll conductance. This was done by measuring infrared absorptance of CO_2 isotopologues to calculate photosynthetic discrimination. Specifically, a LI-6800 system was assembled with a 3x3 cm^2 chamber and fitted with a LI-6800–02 light source (LI-COR Biosciences, Lincoln, NE, USA). This was coupled with a dual quantum cascade laser (QCL, QC-TILDAS, Aerodyne Research, Billerica, MA, USA) absorption spectroscope. The entire gas exchange system was placed in a growth cabinet

(Percival Scientific, Perry Iowa, USA), where the temperature was held at 25 ºC to match leaf temperature settings. The air flow to the chamber was set to 400 μmol s^{-1}, sample CO_2 was 39 Pa, light intensity was 600 μmol m^{-2} s^{-1}, and the vapor pressure difference was maintained at 1 kPa. Leaves were acclimated for 1 h before simultaneous measurements of gas and isotope exchange started. To accomplish this, part of the flow of the reference and sample LI-6800 lines was diverted and delivered to the QCL after being dried by a combination of Nafion tubing (Perma Pure LLC, Lakewood, NJ, USA) and an ethanol/dry-ice trap. Prior to data collection, the laser was checked for CO_2 concentration dependency and different schemes for data calibration were compared. These tests demonstrated that the instrument was linear in the measured range of concentrations and that results from the applied calibration schemes (offset vs. concentration series, (Holloway-Phillips *et al.*, 2019; Tazoe *et al.*, 2011)) were not different (data not show). Therefore, experimental data were corrected using the simplest approach, the offset method (Holloway-Phillips *et al.*, 2019). This method requires two working standards of known isotope composition and concentrations bracketing those measured in the LI-6800 reference and sample lines.

The working standards were generated with a system of three mass flow-controllers (Alicat MC series, Alicat Scientific, Tucson, AZ, USA) arranged within an in-house mixing system (GUS – Gas Utility System) allowing precise control of programmable CO_2 concentrations in a programmable N_2/O_2 background (Built and designed by H. Stuart-Williams, Farquhar Laboratory, RSB, ANU, ACT, Australia). To accomplish this, N_2 and O_2 and were first mixed using two mass flow controllers and a portion of this flow was diverted into a continuously flowing CO_2 doping loop. Within the CO_2 doping loop, the pressure-regulated pure CO_2 working standard was introduced through a capillary into the gas stream which then passed through a third mass flow controller before rejoining the synthetic N_2/O_2 gas mix. CO_2 concentration

control was accomplished by modulating the flow through the third mass flow controller into the CO_2-free synthetic air using a predictive feedback algorithm, with CO_2 concentration reported by the laser system, until the desired setpoint was reached. Excess flow through the loop is dumped through a pressure regulator so that the concentration was not flow dependent. Gas delivery into the QCL sample cell was accomplished via an 8-position outlet selection valve (EUTA-2VLSC8MWE2, Valco Instruments, Houston, TX, USA) which allowed programmable sampling from the LI-COR sample line, LI-COR reference line, or the isotopic standard. Gas sampling regime, working standard CO_2 mixing and data collection were controlled via a custom software and hardware package (GUS + software Vinland, built and designed by H. Stuart-Williams, Farquhar Laboratory, RSB, ANU, ACT, Australia) with the user-interface running on a personal computer and communicating with an Arduino Mega (Arduino.org) to sense and control the hardware.

To correct for QCL signal drift and precise calibration of raw $\delta^{13}C$ values, we sequentially sampled gas supplied by the LI-COR lines and working standards with a CO_2 partial pressure of 39 Pa (low working standard, LWS) or 46.5 Pa (high working standard, HWS). The working standards were generated to order from various mixes of CO_2 source gas and isotopically characterized via isotope-ratio mass spectrometry using CO_2 released from phosphoric acid dissolved carbonate standards ((Bowen, 1966)Air Liquide, Newark, DE, USA).The measurement sequence consisted of LWS, HWS, five consecutive alternating pairs of reference/sample lines, LWS, HWS. Raw molar fractions for the different isotopologues were used to calculate raw $\delta^{13}C$ values expressed in parts per thousand (‰) as $\delta^{13}C = R_{sample}/R_{VPDB} - 1$, where R_{sample} and R_{VPDB} are the $^{13}C/^{12}C$ ratios in the sample and the Vienna Pee Dee Belemnite standard, respectively. Subsequently, the differences between known and raw $\delta^{13}C$ values for the LWS and HWS were linearly regressed against their CO_2 concentrations. The intercept and slope of this regression

line was used to correct samples raw $\delta^{13}C$ values as: $\delta\,^{13}C_{corrected} = \delta^{13}C_{raw}$ + intercept + slope*[CO_2]. The averages for the five measurements of each reference and sample corrected $\delta\,^{13}C$ values were used to calculate observed photosynthetic discrimination ($\Delta\,^{13}C$) as described by Evans *et al.* (1986). Subsequently, g_m was calculated using Eq. 44 in Ubierna *et al.* (2018).

4.3.6 Total respiration from fluorescence measurements

N. tabacum leaves were placed in a LI-COR 6800 with the multiphase flash fluorometer (LI-COR Biosciences, Lincoln, NE, USA) with 2% oxygen, controlled by a custom gas mixer, 500 µmol m^{-2} s^{-1} of light, 80 Pa CO_2 and 2.1 kPa of water vapor in the air entering the chamber. Leaf temperature was 25˚C. Plants were acclimated until photosynthesis and stomatal conductance were steady, ~30 min to 1 h. Fluorescence was measured at 5 light intensities (400, 100, 75, 50, and 25 µmol m^{-2} s^{-1}), each with 5 different light colors (50:50 red: blue, 10:90 red: blue, 90:10 red: blue, 25:75 red: blue, and 75:25 red: blue). We used this data to correct for the efficiency of transfer of absorbed light energy for red (f_{red}) and blue light (f_{blue}) (McClain and Sharkey, 2020; McCree, 1970). We also measured absorptance of the leaf using a SpectroClip Jaz TR integrating sphere (Ocean Optics, Inc., https://www.oceaninsight.com) in order to correct red and blue absorptance for each leaf. Finally, we generated a light response curve at 400 ppm CO_2 at 200, 400, 600, 800, 1000, and 1200 µmol m^{-2} s^{-1} of light. Using data from the McCree correction (McCree, 1970), absorptance measurements, and mesophyll conductance measurements, we calculated total non-photorespiratory respiration (R_T) based on electron transport using the equation 4.1.

$$R_T = \frac{J_f * \frac{1-\Gamma*}{C_c}}{\left(4+8*\frac{\Gamma*}{J_f}\right)} - A \quad \text{Eq. 4.1}$$

We determined J_f using equation 4.2

$$J_f = \phi II * I * \alpha * \beta * \gamma \quad \text{Eq. 4.2}$$

where α is the measured absorptivity, β is partitioning of light energy between PS I and PS II and assumed to be 0.5, and γ is the McCree corrected value for (f_{red} + f_{blue}).

The value for C_c in Eq. 4.1 was calculated using Eq. 4.3

$$C_c = C_i - \frac{A}{g_m} \qquad \text{Eq. 4.3}$$

4.3.7 Calculations of total respiration sources

We averaged mesophyll conductance values from six plants to use as a constant value of g_m for greenhouse-grown *N. tabacum* for our calculations. In addition to determining a value of g_m, we also calculated percent refixation by comparing C_i to C_c calculated by Eq. 4.3.

Total respiration (R_T), as calculated by fluorescence, was compared to efflux of $^{12}CO_2$ (R_L), measured on the same leaf to calculate the percentage of total respiration that can be accounted for by $^{12}CO_2$ efflux.

$$^{12}R = {R_T}/{R_L} \qquad \text{Eq. 4.4}$$

Percentage of respiration from the efflux of unlabeled CO_2 (^{12}R) was averaged across six leaves. $^{12}CO_2$ efflux was corrected for refixation as determined by measurements of mesophyll conductance ($^{12}_{T}R$).

$$^{12}_{T}R = {^{12}R}\Big/{1 - g_m} \qquad \text{Eq. 4.5}$$

Eighty % of R_L was attributed to the cytosolic G6P shunt, as determined from measurements of R_L in G6PDH5 loss-of function mutants ($^{12}_{S}R$) (s for shunt). The other 20% of $^{12}CO_2$ efflux was attributed to other sources ($^{12}_{O}R$) (o for other).

$$^{12}_{S}R = (0.8 * {}^{12}_{T}R) \qquad \text{Eq. 4.6}$$

$$^{12}_{O}R = {}^{12}_{T}R - {}^{12}_{S}R \qquad \text{Eq. 4.7}$$

The difference between the respiration measured by fluorescence and R_L signifies an efflux of $^{13}CO_2$ that our detection method was blind to.

$$^{13}_{T}R = R_T - {}^{12}_{T}R \quad \text{Eq. 4.8}$$

We also accounted for the source carbon being partially labeled ($^{13}_{S}R$). If the shunt is primarily cytosolic and if the glucose of UDPG has the same degree of label as cytosolic G6P, we can estimate the proportion of label in the source of the G6P shunt by LC/MS/MS measurements of steady state labelling in UDP-glucose (0.60).

$$^{13}_{S}R = \frac{^{12}_{S}R}{0.4} * 0.6 \quad \text{Eq. 4.9}$$

The rest of the labeled portion of respiration was attributed to respiration from other labeled sources ($^{13}_{O}R$).

$$^{13}_{O}R = {}^{13}_{T}R - {}^{13}_{S}R \quad \text{Eq. 4.10}$$

Overall, we could determine four distinct sources of CO_2 efflux from our experiments: $^{12}CO_2$ from the cytosolic shunt, $^{13}CO_2$ from the cytosolic shunt, $^{12}CO_2$ from other sources, and $^{13}CO_2$ from other sources.

4.3.8 Growth analysis

Arabidopsis seeds for G6PDH1, 3, 5, 6, and Col-0 were germinated on soil. Pictures of leaf area were collected every three days from germination until flowering. Total leaf area was analyzed using Adobe Photoshop (Adobe, https://adobe.com).

4.4 RESULTS

4.4.1 Effect of photorespiration on $\mathbf{R_L}$

We measured R_L by efflux of $^{12}CO_2$ into a $^{13}CO_2$ atmosphere in 2% and 21% oxygen to test if non-stoichiometric photorespiration contributed to the efflux of CO_2. In 21% oxygen, R_L was 1.51± 0.05 µmol m^{-2} s^{-1} and in 2% oxygen, R_L was 1.25 ± 0.21 µmol m^{-2} s^{-1} (Figure 4.1). However, we found that there was no statistical difference between the treatments. Labelling in Calvin-Benson cycle metabolites also did not change (Figure S4.2). Therefore, we conclude that non-stoichiometric photorespiration does not contribute to R_L under the conditions used here.

4.4.2 Effect of loss-of function G6PDH isoforms on $\mathbf{R_L}$

We measured R_L in loss-of-function mutants of G6PDH1, 3, 5, and 6 (Figure 4.2). We could not find a homozygous mutant of G6PDH2 and G6PDH4 is considered to be a non-functional isoform, therefore these mutants were not included in the characterization. All G6PDH mutants resulted in a significant decrease of R_L. G6PDH1 reduced R_L by 32%; G6PDH3 by 40%; G6PDH5 by 79%; and G6PDH6 by 37%. When categorized by compartment, the cytosolic isoforms (G6PDH5 and 6) had a larger impact on R_L, indicating that the majority of the contribution of the G6P shunt comes from the cytosolic pathway, especially from G6PDH5. Additionally, though to a lesser extent, the plastidic G6P shunt (G6PDH1 and 3) contributes to R_L.

4.4.3 Steady-state ^{13}C labelling in UDP-glucose and ADP-glucose

In order to understand the labelling composition of the plastidic and cytosolic G6P pools, we measured labelling in UDP-glucose and ADP-glucose, which are compartmentally separated (Table 4.2). These metabolites are directly downstream of G6P in sucrose and starch metabolism, respectively. At steady-state, we assumed that the labelling of UDP-glucose and ADP-glucose closely reflect the labelling of their precursor G6P pools. ADP-glucose has been previously used in metabolic flux analysis to reflect the labeling of plastidic G6P pools (Szecowka *et al.*, 2013). G6P pool turnover is < 20 s and UDP-glucose pool turnover is < 10 s , therefore we assumed using UDP-glucose to reflect labeling of cytosolic G6P to be a reasonable assumption as well (Hasunuma *et al.*, 2010). We found that in *N. tabacum*, at steady-state after 20 min of labelling with $^{13}CO_2$, ADP-glucose was 82 ± 9% labeled and UDP-glucose was 60 ± 11% labeled. We use these measurements as a proxy of the percentage of labelling for G6P pools in the plastid and cytosol.

4.4.4 g_m *in* N. tabacum

Averaged across six greenhouse-grown *N. tabacum* plants, we determined g_m to be 8.5 ± 1.9 μmol m^{-2} s^{-1} Pa^{-1}. We used this value as a fixed value for all *N. tabacum* plants in our experiments.

4.4.5 Estimation of total respiration and contribution of the G6P shunt

We used data from fluorescence measurements, mesophyll conductance, R_L measurements in G6PDH loss-of-function mutants, and steady-state labeling in UDP-glucose to calculate contributions to respiration from four different sources: unlabeled cytosolic G6P shunt, labeled cytosolic G6P shunt, unlabeled other sources, and labeled other sources. Measurement of total respiration, as calculated by fluorescence, varied from 1.17 to 3.45 μmol m^{-2} s^{-1} across six leaves. This accounted for 14 ± 8% of assimilation. Unlabeled efflux of CO_2 accounted for 28 ± 15% of total respiration (Figure 4.3a). 30% of respired carbon was re-fixed, as determined from our measurement of g_m. After adjusting the contribution of the unlabeled efflux of CO_2 for refixation, the contribution to total respiration increased to 41% (Figure 4.3b). We assumed that 79% of this came from the cytosolic G6P shunt, as determined by measurements of R_L in G6PDH mutants. We did not sum the decrease in respiration from all G6PDH loss-of-function mutants as some G6PDH isoforms are known to be co-regulated (Averill *et al.*, 1998; Meyer *et al.*, 2011; Wakao and Benning, 2005). Therefore, we used the value from the G6PDH5 loss-of-function mutant. From this, we attributed 33% of total respiration to unlabeled CO_2 from the cytosolic G6P shunt (Figure 4.3c). Based on measurement of UDP-glucose, we assumed that cytosolic G6P pool was 60% labeled and the cytosolic G6P shunt accounted for 82% of respiration (Figure 4.3d). From this, we calculated that 33% of total respiration came from unlabeled cytosolic G6P shunt, 50% from labeled cytosolic G6P shunt, 8% from other unlabeled sources, and 9% came from other labeled sources (Figure 4.3e).

4.4.6 Growth analysis of G6PDH loss-of-function mutants

To determine if the decrease in R_L in G6PDH loss-of-function mutants resulted in a physiologically significant retention of carbon, we analyzed the leaf area of G6PDH mutants and Col-0 wild type plants from germination until flowering. We found that most of the G6PDH mutants had larger leaf area (Figure 4.4, Figure S4.3). At 25 days post-germination, G6PDH3 was 1.2-fold larger than wild type ($p = 0.096$), G6PDH5 was 1.5-fold larger ($p = 0.006$), and G6PDH6 was 1.3-fold larger ($p = 0.032$). G6PDH1 was not significantly larger than wild type.

4.4.7 Effect of mutations in central carbon metabolism on $\mathbf{R_L}$ *and PGA labeling*

We measured R_L in several lines that had mutations in Calvin-Benson cycle enzymes. R_L data from *hpr1-1* and *hrp1-2* has been previous been published by Li *et al.* (2019) (Figure 4.5a). We additionally measured R_L in *hcef1* and *hcef4* which are loss-of-function FBPase and PRK, respectively. We found that *hcef1* had a four-fold increase in R_L, while *hcef4* did not have an increase in R_L (Figure 4.5b). We also measured R_L in XPT and TPT knockouts and found that neither line had changes in R_L (Figure 4.5c).

In order to test the hypothesis from Sharkey and Weise (2016) that starch provided the source of unlabeled carbon for R_L, we measured R_L in several mutants unable to synthesize or degrade starch (Figure 4.6). In *pgm* and *adg* mutants, we found that R_L increased. R_L did not change in *phs1* mutants which are unable to re-mobilize starch after it has been synthesized. We also measured percent label in PGA in the starch compromised mutants. Labeling in PGA decreased in all mutants (Figure 4.7).

4.4.8 Effect of assimilation rate on $\mathbf{R_L}$

We measured R_L at four different light intensities and two different CO_2 concentrations in *N. benthamiana* and plotted R_L as a function of assimilation rate. We found that at both ambient and low CO_2, unlabeled R_L decreased as assimilation increased (Figure 4.8).

4.5 DISCUSSION

4.5.1 Proposed sources of respiration in the light

In this paper we have sought to understand the source of respiration in the light. It has been previously shown that the TCA cycle flux is vanishingly small (Calvin and Massini, 1952; Holm-Hansen *et al.*, 1959; Ma *et al.*, 2014; Moses *et al.*, 1959; Tcherkez *et al.*, 2005). The CO_2 efflux from the TCA cycle is about 1-10% of what has been measured for R_L, both in our studies and previously published measurements (Abadie *et al.*, 2017; Busch *et al.*, 2012; Gong *et al.*, 2018; Loreto *et al.*, 2001; Tcherkez *et al.*, 2009). We have also shown that non-stoichiometric photorespiration cannot explain respiration in the light: the absence of photorespiration in 2% oxygen does not affect R_L. Our analysis of G6PDH loss-of-function mutants show that loss of the G6P shunt in both the cytosol and plastid can substantially decrease R_L.

4.5.2 The cytosolic and plastidic G6P shunt

The largest change in R_L is seen in the cytosolic mutants, G6PDH5 and 6. In the cytosol, the pentose phosphate products may be used for nucleotide synthesis or could be transported into the plastid on the xylulose phosphate-phosphate transporter (Eicks *et al.*, 2002). Within the plastid, pentose phosphates can reenter the Calvin-Benson cycle or be used for plastidic nucleotide synthesis.

Cytosolic G6PDH5 has a K_m for $NADP^+$ of 19 µM, a K_i for NADPH of 28 µM, and a V_{max} of 1.5 µmol mg^{-1} min^{-1}. For G6PDH6, the K_m for $NADP^+$ is 6500 µM, and a V_{max} of 100 µmol mg^{-1} min^{-1} (Wakao and Benning, 2005). The K_i for NADPH for G6PDH6 or the K_m for G6P for either isoform has not been determined. Unlike plastidic isoforms of G6PDH, cytosolic isoforms are not inactivated in a reducing environment and can remain fully active during the day. G6PDH5 and 6 transcripts have been found in whole leaves and are constitutively expressed (von

Schaewen *et al.*, 1995; Wakao and Benning, 2005). Previous studies have also shown physiologically relevant activity of cytosolic G6PDH (Hauschild and von Schaewen, 2003).

The large contribution to respiration by the cytosolic G6P shunt does not, however, eliminate the contribution of the plastidic pathway. Sharkey and Weise (2016) proposed a functional plastidic pathway during the day and this was further supported by Preiser *et al.* (2019). Plastidic G6PDH isoforms are redox regulated and have decreased activity in the light due to an increase in K_m (Née *et al.*, 2014; Preiser *et al.*, 2019; Scheibe *et al.*, 1989). This will limit futile cycling around the Calvin-Benson cycle. On the other hand, our work here shows that the kinetics and regulation of plastidic G6PDH play a physiological role to allow flux through this pathway under specific conditions. H_2O_2 can also significantly increase the activity of the plastidic G6PDH1 independent of the redox potential in the stroma (Preiser *et al.*, 2019).

4.5.3 $\mathbf{R_L}$ *from the G6P shunt can explain mutant phenotypes*

In addition to identifying the source of R_L, we also sought to understand R_L phenotypes in several mutant lines. Li *et al.* (2019) showed in *hpr1* plants, the glucose-6-phosphate transporter (GPT2) is induced which would allow G6P import into the plastid from the cytosol. This increases the unlabeled pool of G6P in the plastid and overcomes the regulatory kinetics of plastidic G6PDH to increase R_L. Similarly, *hcef1* plants have increased GPT2 which bypasses the deletion of plastidic FBPase (Sharkey and Weise, 2016). This will increase unlabeled plastidic G6P and overcome G6PDH regulation and increase R_L, requiring additional ATP. This can explain the high cyclic electron flow phenotype for which the plant was identified (Livingston *et al.*, 2010). The G6P shunt consumes and produces two NADPH so does not require additional linear electron flow. However, it also consumes three ATP for every G6P that enters the shunt. Increased cyclic electron flow is necessary to make up the extra ATP. *hcef4*, another high cyclic phenotype, is a knockdown of PRK. In this mutant, pentose phosphates and hexose phosphates

most likely accumulate. Accumulation of plastidic G6P can overcome the K_m regulation of reduced plastidic G6PDH and enter the G6P shunt. However, in this case, the substrate for the G6P shunt could come from plastidic G6P which is mostly labeled. This is why a high cyclic electron flow phenotype is seen, but not a respiration phenotype. In both of these mutants, hydrogen peroxide may also accumulate (Livingston, 2010). This has been shown to G6PDH activity (Preiser *et al.*, 2019).

We also measured R_L in starch mutants. Not all starch-compromised mutants have increased R_L: it is only mutants where GPT2 is induced (Kunz *et al.*, 2010; Weise *et al.*, 2019). Similar to *hcef1* and *hpr* plants, this increases unlabeled plastidic G6P and overcomes regulation of G6PDH to increase flux through the plastidic G6P pathway. Therefore, increases in unlabeled plastidic respiration are closely linked to GPT2 and changes in plastidic G6P concentrations and steady-state labeling.

Surprisingly, XPT and TPT loss-of-function mutants do not change R_L. We predicted that inability for carbon to leave the plastid to enter the cytosolic G6P shunt or the inability to transport products of the G6P shunt would affect the rates or labelling of R_L. However, plastidic carbon transporters are notoriously promiscuous and when one is lost, carbon would still be able to cross the plastidic membrane using a different transporter (Eicks *et al.*, 2002; Kammerer *et al.*, 1998).

Finally, we have also shown that R_L inversely correlates with assimilation caused by changes in light intensity. It is possible that cytosolic $NADP^+$ and NADPH concentrations may change, reducing substrate availability and increasing inhibitor concentrations. Another possibility is that increases in assimilation may decrease pool turnover time leading to increased labeling of substrate pools resulting in an apparent decrease in respiration.

4.5.4 $\mathbf{R_L}$ *and the slow to label pool of carbon*

Our analysis of starch-compromised mutants also addressed the hypothesis of Sharkey and Weise (2016) that starch is the source of the slow-to-label pool of carbon that enters the Calvin-Benson cycle. Since R_L has also been defined as an unlabeled flux of carbon, we investigated if these had a common source. Surprisingly, unlabeled CO_2 efflux increased and percent labeling decreased in plants compromised in starch metabolism. Therefore, we conclude that starch is not the source of the slow-to-label pool.

We have shown that when carbon is imported into the plastid from the cytosol, the unlabeled efflux of CO_2 increases. Additionally, the cytosolic shunt is a larger component of the unlabeled efflux (based on G6PDH loss-of-function mutants). Based on these findings, the source of unlabeled carbon may come from pools of metabolites from the cytosol, vacuole, or peroxisome that enter the Calvin-Benson cycle as re-assimilated carbon or pentoses from the cytosolic G6P shunt. The starch-compromised mutants partition more carbon to sucrose synthesis and so intermediates of sucrose synthesis, including cytosolic G6P, are likely to be increased, which could explain the increased R_L of these plants.

4.5.5 Limitations of measuring $\mathbf{R_L}$ *as an unlabeled efflux of* CO_2

Several methods have been developed to measure R_L, however, all methods have limitations. Both the Kok and Laisk methods use estimations from other parameters at low light or CO_2 (for a summary of the advantages and disadvantages of these methods and others, see Tcherkez *et al.* (2017)). Both of these methods assume that R_L will not change under these conditions. However, changes in activity of the enzymes due different redox status of the cell or other signaling mechanisms is likely.

Measuring respiration as an unlabeled efflux of CO_2, while it has been historically defined as such, is also limiting. Substrate pools of G6P in both the plastid and cytosol are partially labelled when $^{13}CO_2$ is used as a carbon source. The G6P pool is ~80% labeled in the plastid and ~60%

labeled in the cytosol. $^{12}CO_2$ efflux measurements would not detect the majority of the CO_2 release. Therefore, while these measurements are correct values for unlabeled efflux of CO_2, if respiration is defined more generally as a non-photorespiratory efflux of CO_2 in the light, it underestimates total respiration. Our approach, using fluorescence and $^{12}CO_2$ evolution, allow us to examine how total respiration comprises labeled and unlabeled components from both the shunt and other sources. At least 80% of total respiration can be attributed to the shunt, but less than half of this is from unlabeled sources.

Overall, this calls for a reevaluation of our definitions of respiration and our measurement techniques. Light respiration is characterized by more than unlabeled efflux of CO_2, while it may be a unique feature of some of the substrate carbon. Additionally, biochemistry of key enzymes and regulation needs to be taken into consideration when selecting and evaluating conditions traditionally used to measure respiration in the light.

4.6 CONCLUSION

Overall, we have shown that the G6P shunt in both the plastid and cytosol is the main source of respiration in the light. Other pathways, such as the TCA cycle or glycolysis may contribute, but to a smaller extent. Contrary to previous thought, changes respiration in the light compared to dark respiration is not a reorganization or down-regulation of the same metabolic pathways that occur in the dark but occupies a metabolically distinct pathway. Additionally, we believe that due to limitations in methodology, the efflux of CO_2 in the light is greater than previously assumed, up to 20% of assimilation.

4.7 ACKNOWLEDGEMENTS

This research was funded by U.S. Department of Energy Grant DE-FG02-91ER2002 (T.D.S., A.L.P., A.M.M., B.J.W., N.U.L.). A.L.P is also supported by a Barnett Rosenburg Endowed Research Assistantship from the College of Natural Science at Michigan State University.

A.M.M is also supported by a fellowship from Michigan State University under the Training Program in Plant Biotechnology for Health and Sustainability (T32-GM110523). T.D.S received partial salary support from Michigan AgBioResearch.

APPENDIX

TABLE 4.1- Parameters used for detection of several Calvin-Benson cycle metabolites with LC/MS/MS.

Parameters were optimized using 10 μM standards before analyzing samples. Heavier isotopes for each metabolite were also measured with the same cone and collision voltage and daughter m/z as each +0 isotopologue.

Metabolite	Cone (V)	Collision (V)	+0 Parent (m/z)	Daughter (m/z)
PGA	26	10	185	97
G6P/F6P	26	18	259	97
Ru5P/R5P/Xu5P	26	18	229	97
RuBP	26	18	309	97
6PG	34	18	275	97
ADP	42	25	588	346
UDP	42	25	565	323

TABLE 4.2- Labelling of ADP-glucose and UDP-glucose mole fraction in *Nicotiana tabacum* after 20 minutes at steady state.

ADP-glucose	82 ± 9%
UDP-glucose	60 ± 11%

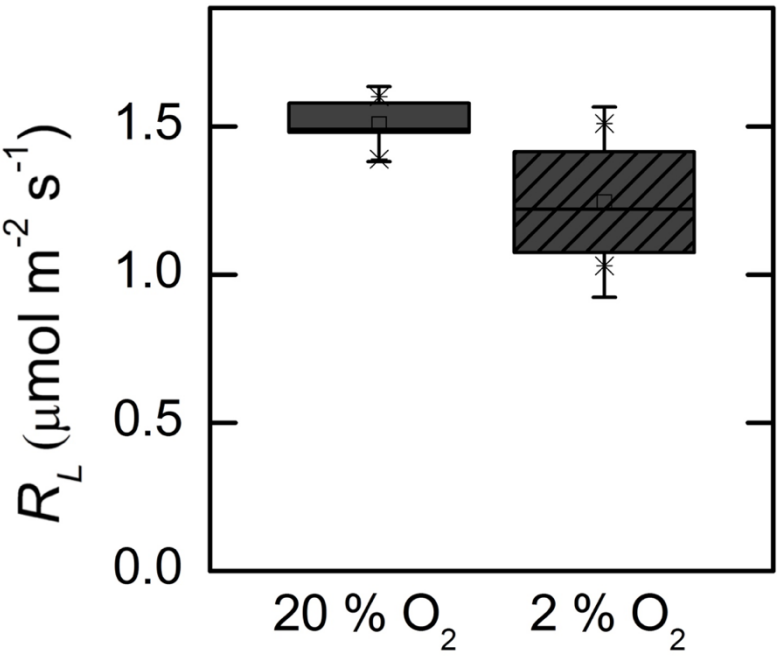

FIGURE 4.1- Effect of Photorespiration on R_L.

R_L was measured as the efflux of $^{12}CO_2$ when a leaf was in a $^{13}CO_2$ environment. The box encompasses the middle two quartiles, mean is represented as an open square, and media is represented as a horizontal line inside the box. Whiskers show the standard deviation. N=5 for both treatments. There was no statistically significant difference between the two treatments.

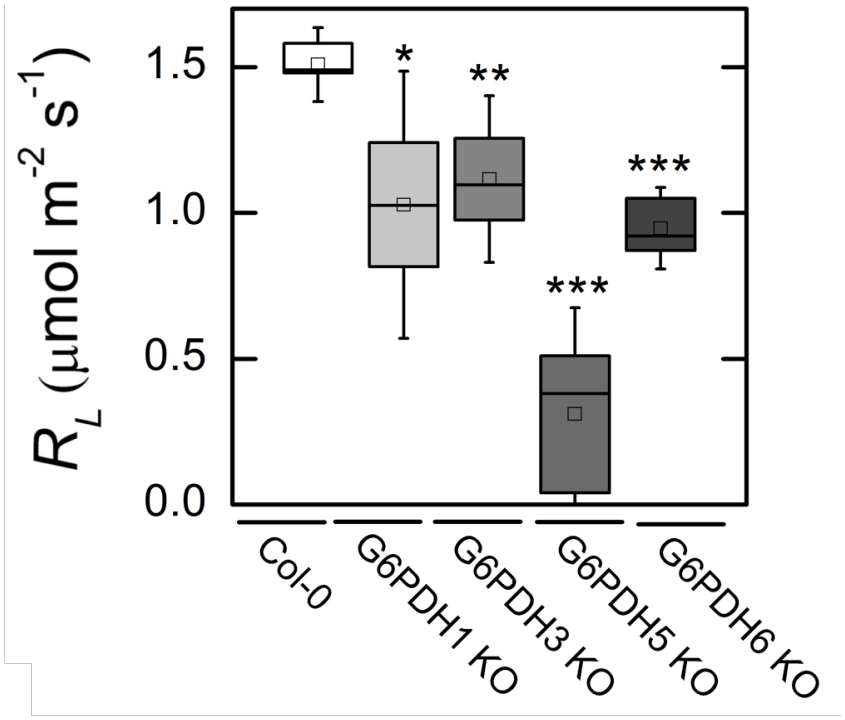

FIGURE 4.2- Effect of Loss-of-Function G6PDH Isoforms on R_L.

R_L was measured as the efflux of $^{12}CO_2$ when a leaf was in a $^{13}CO_2$ environment. The box encompasses the middle two quartiles, mean is represented as an open square, and media is represented as a horizontal line inside the box. Whiskers show the standard deviation. For wild type, n=5; for G6PDH1 and 3, n=4; for G6PDH 5 and 6, n=4. Bars with an asterisk (*) are significantly different from control samples as determined by Student's t-test ($P < 0.05$); bars with a double asterisk (**) are significantly different from control samples as determined by Student's t-test ($P < 0.005$); bars with a triple asterisk (***) are significantly different from control samples as determined by Student's t-test ($P < 0.0001$).

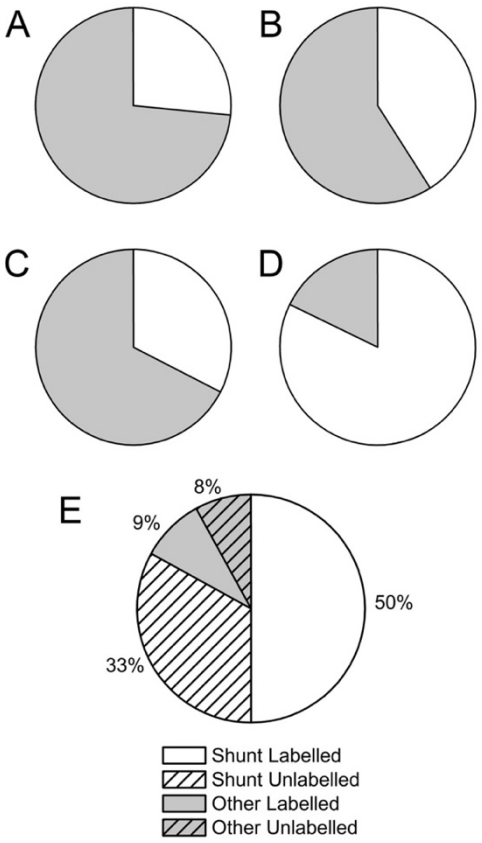

FIGURE 4.3- Estimation of total respiration and contribution of the cytosolic G6P shunt.

Total respiration (gray) was compared to contribution of R_L from the cytosolic G6P shunt (white). Measured R_L accounts for 29% of total respiration (a), but when adjusted for refixation, accounts for 41% (b). The cytosolic shunt could account for approximately 80% of unlabeled R_L, or 33% of total respiration (c). However, the substrate pool for the cytosolic G6P is not completely unlabeled. When partial labeling of the cytosolic G6P pool is taken into consideration, the cytosolic G6P shunt can account for 82% of total respiration (d). Based on this, total respiration can be subdivided into four categories: unlabeled respiration from the cytosolic G6P shunt, labeled respiration from the cytosolic G6P shunt, unlabeled respiration from other sources, and labeled respiration from other sources (e).

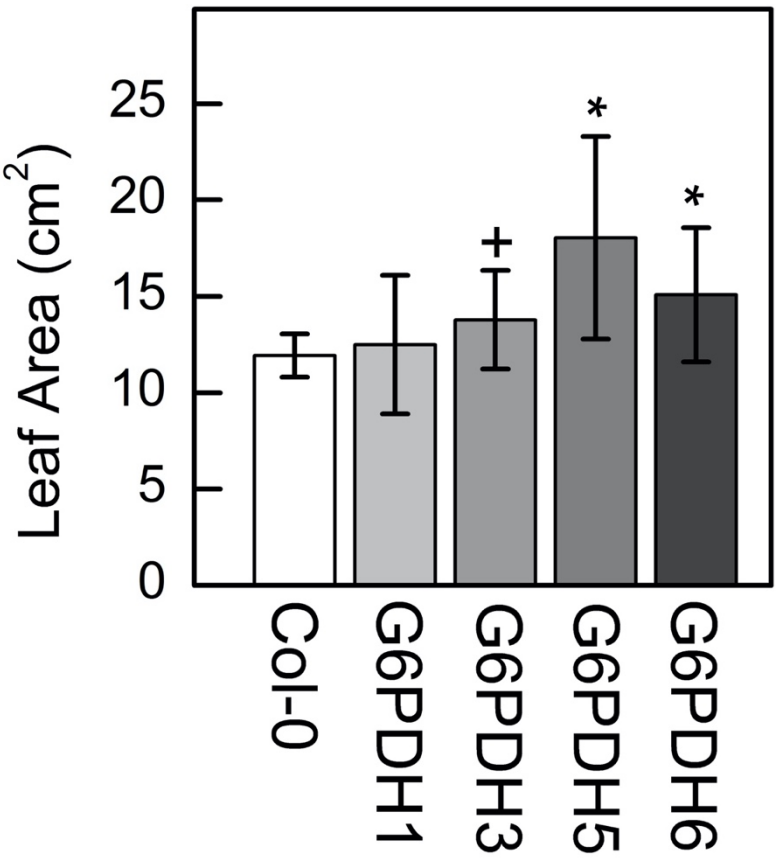

FIGURE 4.4- Growth analysis of G6PDH loss-of-function mutants.

Leaf area of G6PDH mutants and wild type Col-0 were measured from germination to flowering. At 25 days, G6PDH3, 5, and 6 were all larger than wild type plants. Each bar represents mean and error bars represent S.D. N-5 for G6PDH1 and 3, n=6 for G6PDH6, and n=8 for G6PDH5 and wild type. Bars with a cross (+) are significantly different from corresponding empty vector samples as determined by Student's t-test ($P < 0.1$). Bars with an asterisk (*) are significantly different from corresponding empty vector samples as determined by Student's t-test ($P < 0.05$).

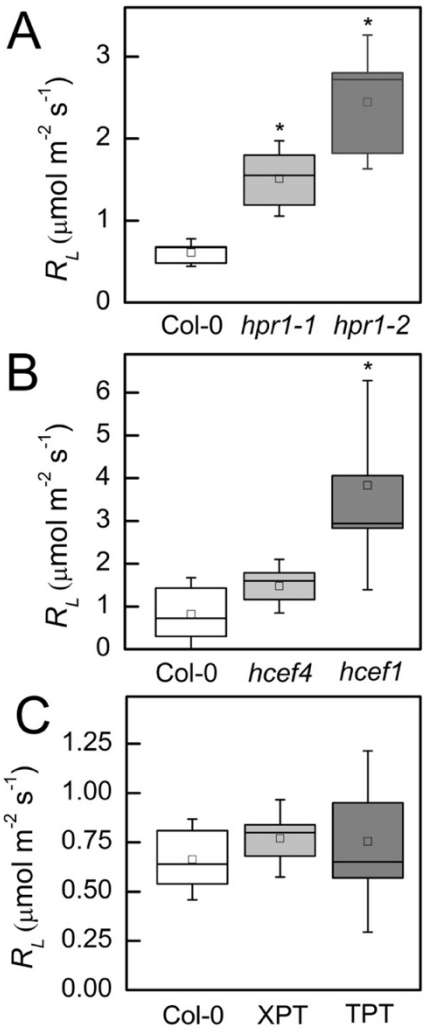

FIGURE 4.5- Effect of *hpr* (a) *hcef1 and hcef4* (b) and XPT and TPT loss-of-function (c) on R_L.

R_L was measured as the efflux of $^{12}CO_2$ when a leaf was in a $^{13}CO_2$ environment. The box encompasses the middle two quartiles, mean is represented as an open square, and media is represented as a horizontal line inside the box. Whiskers show the standard deviation. N=5 for wild type, *hcef1*, *hcef4*, XPT, TPT. N=3 for *hpr1* mutants. Bars with an asterisk (*) are significantly different from control samples as determined by Student's t-test ($P < 0.05$).

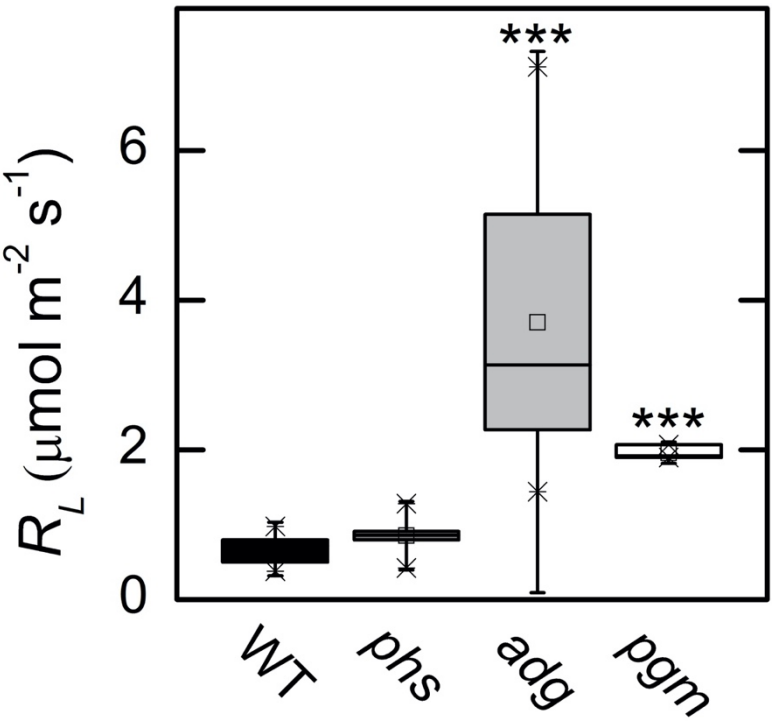

FIGURE 4.6- Effect of starch-compromised on R_L. R_L was measured as the efflux of $^{12}CO_2$ when a leaf was in a $^{13}CO_2$ environment.

The box encompasses the middle two quartiles, mean is represented as an open square, and media is represented as a horizontal line inside the box. Whiskers show the standard deviation. N=5 for wild type and *phs1-1*, n=4 for *adg*, and n=3 for *pgm*. Bars with a triple asterisk (***) are significantly different from control samples as determined by Student's t-test ($P < 0.0001$).

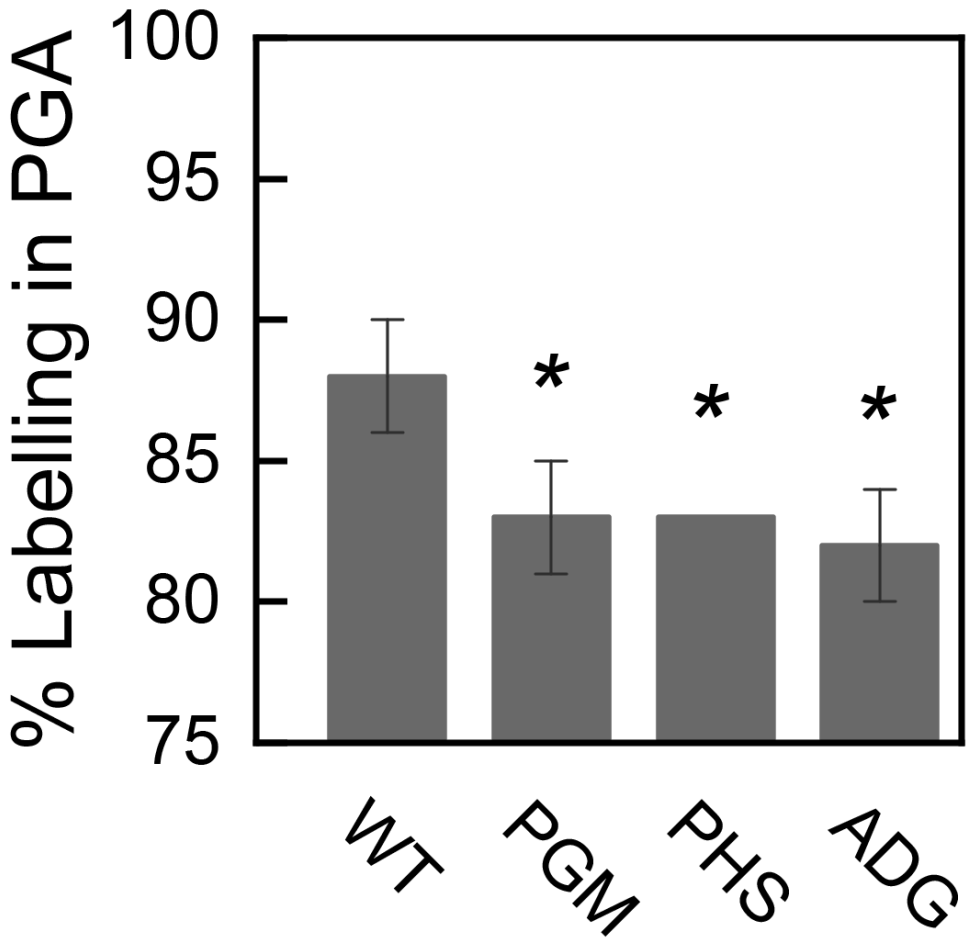

FIGURE 4.7- Labelling of PGA in starch-compromised mutants.

Starch-compromised mutants were labelled for 20 min with $^{13}CO_2$ and quantified with LC-MS/MS. All mutants had small decreases in percent labelling of PGA (n=5). An asterisk signifies statistical difference as determined by Student's t-test (* = $p < 0.05$).

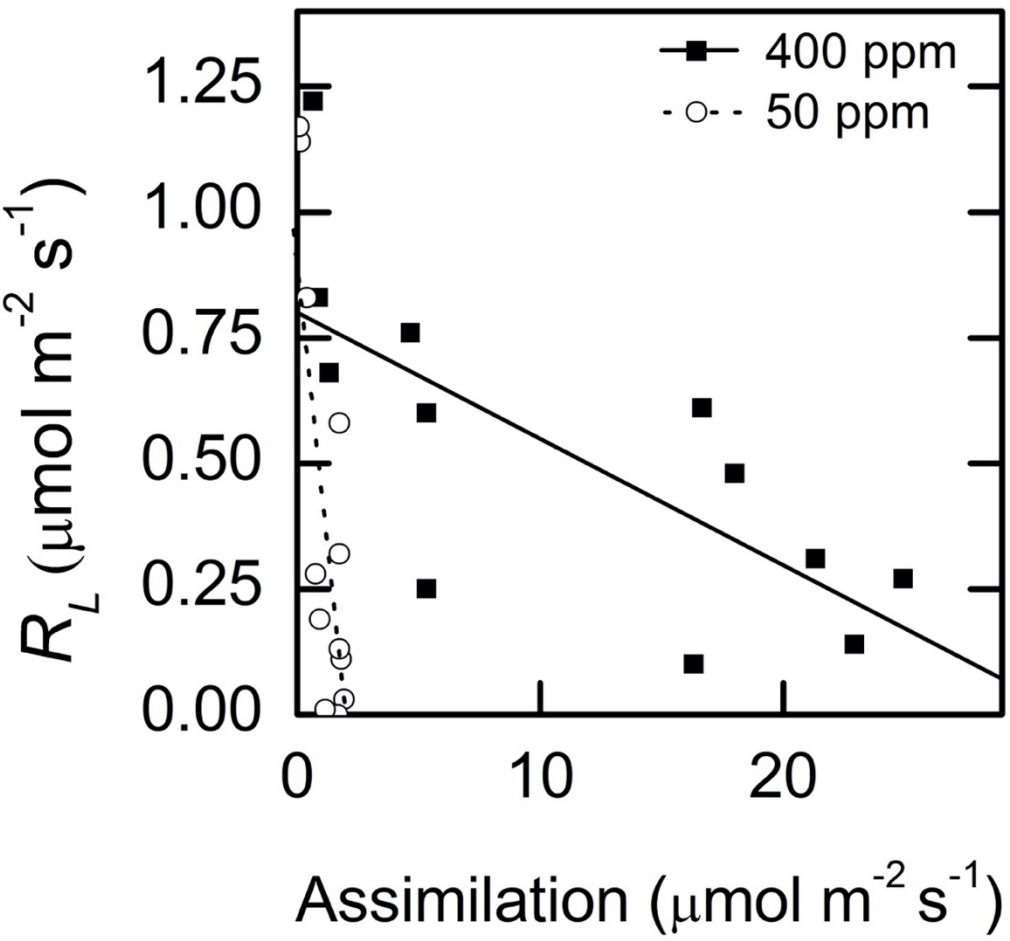

FIGURE 4.8- Effect of assimilation on R_L. R_L was at four different light intensities (1200, 400, 100, and 50 μmol m^{-2} s^{-1}) on the same leaf at two different CO_2 concentrations.

Each measurement had three biological replicates.

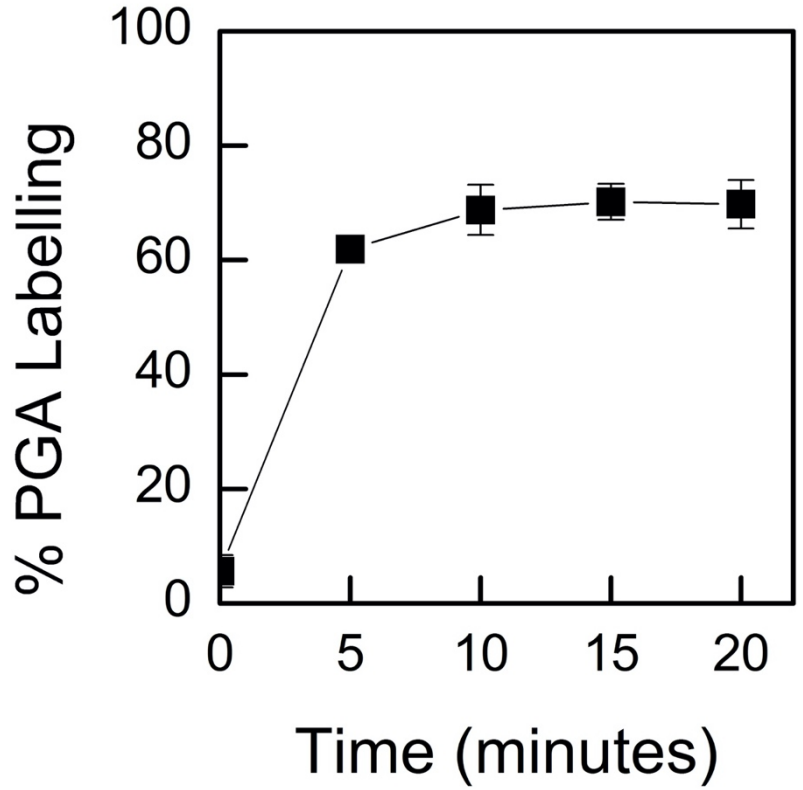

FIGURE S4.1- Labelling of PGA after 5, 10, 15, and 20 min of 400 ppm $^{13}CO_2$ as determined by LC-MS/MS.

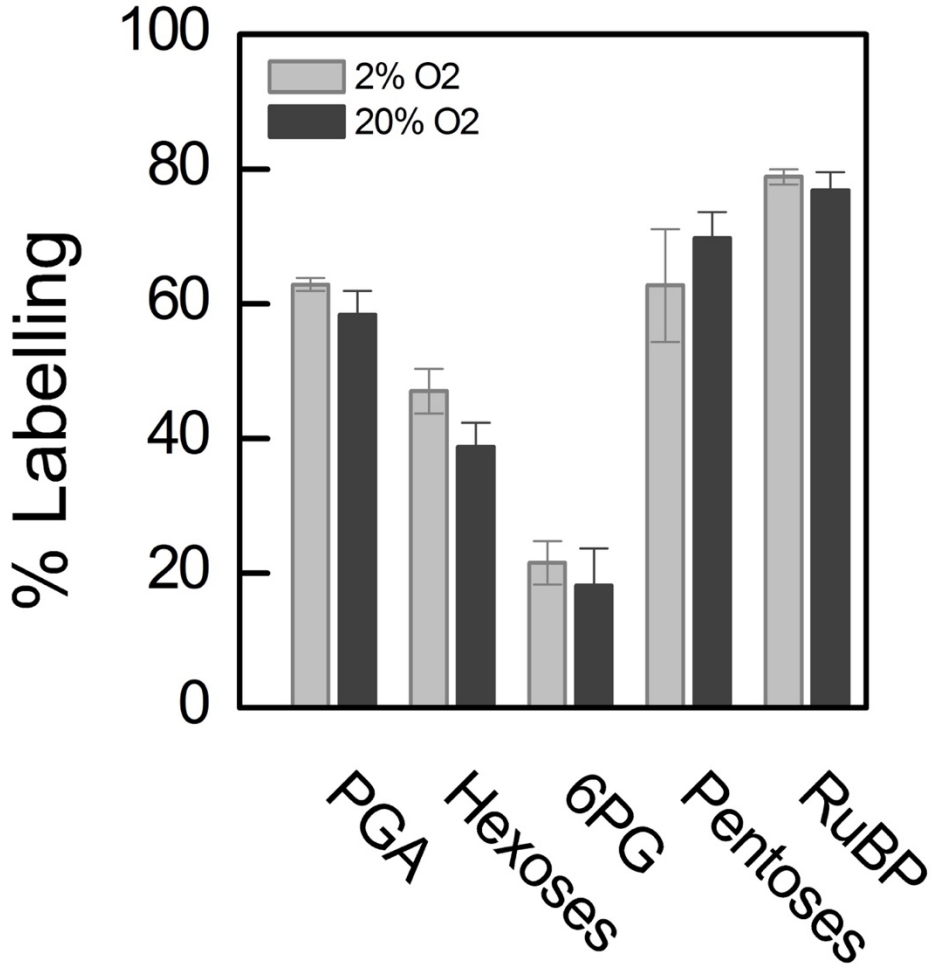

FIGURE S4.2- Labelling of Calvin-Benson cycle metabolites after 20 min of 400 ppm $^{13}CO_2$ with 21% and 2% oxygen as determined by LC-MS/MS.

FIGURE S4.3- Comparison of area of G6PDH loss-of-function mutant and wild type Col-0 at 25 days post-germination.

LITERATURE CITED

LITERATURE CITED

Abadie C, Blanchet S, Carroll A, Tcherkez G. 2017. Metabolomics analysis of postphotosynthetic effects of gaseous O_2 on primary metabolism in illuminated leaves. *Functional Plant Biology* **44**, 929-940.

Ajjawi I, Lu Y, Savage LJ, Bell SM, Last RL. 2009. Large-scale reverse genetics in Arabidopsis: case studies from the Chloroplast 2010 Project. *Plant Physiol* **152**, 529-540.

Atkin OK, Evans JR, Siebke K. 1998. Relationship between the inhibition of leaf respiration by light and enhancement of leaf dark respiration following light treatment. *Australian Journal of Biological Science* **25**, 437-443.

Averill RH, Bailey-Serres J, Kruger NJ. 1998. Co-operation between cytosolic and plastidic oxidative pentose phosphate pathways revealed by 6-phosphogluconate dehydrogenase-deficient genotypes of maize. *The Plant Journal* **14**, 449-457.

Berghuijs HNC, Yin X, Tri Ho Q, Retta MA, Nicolai BM, Struik PC. 2019. Using a reaction-diffusion model to estimate day respiration and reassimilation of (photo)respired CO_2 in leaves. *New Phytologist* **223**, 619-631.

Bowen R. 1966. *Paleotemperature Analysis, Volume 2*: Elsevier.

Busch FA. 2013. Current methods for estimating the rate of photorespiration in leaves. *Plant Biology* **15**, 648-655.

Busch FA, Sage TL, Cousins AB, Sage RF. 2012. C_3 plants enhance rates of photosynthesis by reassimilating photorespired and respired CO2. *Plant, Cell & Environment*, doi: 10.1111/j.1365-3040.2012.02567.x.

Calvin M, Massini P. 1952. The path of carbon in photosynthesis. XX. The steady-state. *Experimenta* **8**, 445-457.

Caspar T, Huber SC, Somerville C. 1985. Alterations in growth, photosynthesis, and respiration in a starchless mutant of *Arabidopsis thaliana* (L.) deficient in chloroplast phosphoglucomutase activity. *Plant Physiology* **79**, 11-17.

Cocuron J-C, Alonso AP. 2014 *Liquid chromatography tandem mass spectrometry for measuring ^{13}C-labeling in intermediates of the glycolysis and pentose phosphate pathway.* Totwa, NJ: Humana Press.

Cousins A, Walker B, Pracharoenwattana I, Smith S, Badger M. 2011. Peroxisomal hydroxypyruvate reductase is not essential for photorespiration in Arabidopsis but its absence causes an increase in the stoichiometry of photorespiratory CO2 release. *Photosynthesis Research* **108**, 91-100.

Eicks M, Maurino V, Knappe S, Flügge U-I, Fischer K. 2002. The plastidic pentose phosphate translocator represents a link between the cytosolic and the plastidic pentose phosphate pathways in plants. *Plant Physiology* **128**, 512-522.

Evans JR, Sharkey TD, Berry JA, Farquhar GD. 1986. Carbon isotope discrimination measured concurrently with gas exchange to investigate CO2 diffusion in leaves of higher plants. *Australian Journal of Plant Physiology* **13**, 281-292.

Gauthier PP, Bligny R, Gout E, Mahé A, Nogués S, Hodges M, Tcherkez G. 2010. In folio isotopic tracing demonstrates that nitrogen assimilation into glutamate is mostly independent from current CO_2 assimilation in illuminated leaves of Brassica napus. *New Phytologist* **185**, 988-999.

Gifford RM. 2003. Plant respiration in productivity models: conceptualisation, representation and issues for global terrestrial carbon-cycle research. *Functional Plant Biology* **30**, 171.

Gong XY, Tcherkez G, Wenig J, Schäufele R, Schnyder H. 2018. Determination of leaf respiration in the light: comparison between an isotopic disequilibrium method and the Laisk method. *New Phytologist* **218**, 1371-1382.

Harley PC, Loreto F, Di Marco G, Sharkey TD. 1992. Theoretical considerations when estimating the mesophyll conductance to CO_2 flux by analysis of the response of photosynthesis to CO2. *Plant Physiology* **98**, 1429-1436.

Hasunuma T, Harada K, Miyazawa S-I, Kondo A, Fukusaki E, Miyake C. 2010. Metabolic turnover analysis by a combination of in vivo ^{13}C-labelling from $^{13}CO_2$ and metabolic profiling with CE-MS/MS reveals rate-limiting steps of the C_3 photosynthetic pathway in Nicotiana tabacum leaves. *Journal of Experimental Botany* **61**, 1041-1051.

Hauschild R, von Schaewen A. 2003. Differential regulation of glucose-6-phosphate dehydrogenase isoenzyme activities in potato. *Plant Physiology* **133**, 47-62.

Heskel MA, Atkin OK, Turnbull MH, Griffin KL. 2013. Bringing the Kok effect to light: a review on the integration of daytime respiration and net ecosystem exchange. *Ecosphere* **4**, art98.

Heskel MA, Tang J. 2018. Environmental controls on light inhibition of respiration and leaf and canopy daytime carbon exchange in a temperate deciduous forest. *Tree Physiology* **38**, 1886-1902.

Holloway-Phillips M, Cernusak LA, Stuart-Williams H, Ubierna N, Farquhar G. 2019. Two-source d^{18}O method to validate the CO^{18}O-photosynthetic discrimination model: implications for mesophyll conductance. *Plant Physiology* **181**, 1175-1190.

Holm-Hansen O, Nishida K, Moses V, Calvin M. 1959. Effects of mineral salts on short-term incorporation of carbon dioxide in *Chlorella*. *Journal of Experimental Botany* **10**, 109-124.

Igamberdiev A, Gardeström P. 2003. Regulation of NAD- and NADP- dependent isocitrate dehydrogenases by reduction levels of pyridine nucleotides in mitochondria and cytosol of pea leaves. *Biochemica et Biophysica Acta- Bioenergetics* **1606**, 117-125.

Kammerer B, Fischer K, Hilpert B, Schubert S, Gutensohn M, Weber A, Flügge UI. 1998. Molecular characterization of a carbon transporter in plastids from heterotrophic tissues: The glucose 6-phosphate phosphate antiporter. *The Plant Cell* **10**, 105-117.

Karl T, Fall R, Rosenstiel TN, Prazeller P, Larsen B, Seufert G, Lindinger W. 2002. On-line analysis of the $^{13}CO_2$ labeling of leaf isoprene suggests multiple subcellular origins of isoprene precursors. *Planta* **215**, 894-905.

Kunz HH, Häusler RE, Fettke J, Herbst K, Niewiadomski P, Gierth M, Bell K, Steup M, Flügge UI, Schneider A. 2010. The role of plastidial glucose-6-phosphate/phosphate translocators in vegetative tissues of *Arabidopsis thaliana* mutants impaired in starch biosynthesis. *Plant Biology* **12**, 115-128.

Li J, Weraduwage SM, Preiser AL, Weise SE, Strand DD, Froehlich JE, Kramer D, Hu J, Sharkey TD. 2019. A Cytosolic bypass and G6P shunt in plants lacking peroxisomal hydroxypyruvate reductase. *Plant Physiology* **180**, 783-792.

Lin M, Turnpin DH, Plaxton WC. 1989. Pyruvate kinase isozymes from the green alga *Selenastrum minutum. Archives of Biochemistry and Biophysics* **269**, 228-238.

Livingston AK. 2010. Redefining cyclic electron flow around photosystem I (CEF1): The induction, pathway, and rol of CEF1 in C3 plants, Washington State University, 159.

Livingston AK, Cruz JA, Kohzuma K, Dhingra A, Kramer DM. 2010. An *Arabidopsis* mutant with high cyclic electron flow around photosystem I (*hcef*) involving the NADPH dehydrogenase complex. *The Plant Cell* **22**, 221-233.

Loreto F, Delfine S, Di Marco G. 1999. Estimation of photorespiratory carbon dioxide recycling during photosynthesis. *Australian Journal of Plant Physiology* **26**, 733-736.

Loreto F, Velikova V, Di Marco G. 2001. Respiration in the light measured by $^{12}CO_2$ emission in $^{13}CO_2$ atmosphere in maize leaves. *Australian Journal of Plant Physiology* **28**, 1103-1108.

Lunn JE, Feil R, Hendriks JH, Gibon Y, Morcuende R, Osuna D, Scheible WR, Hajirezaei M, Stitt M. 2006. Sugar-induced increases in trehalose 6-phosphate are correlated with redox activation of ADP-glucose pyrophosphorylase and higher rates of starch synthesis in Arabidopsis thaliana. *Biochemical Journal* **397**, 139-148.

Ma F, Jazmin LJ, Young JD, Allen DK. 2014. Isotopically nonstationary ^{13}C flux analysis of changes in Arabidopsis thaliana leaf metabolism due to high light acclimation. *Proceedings of the National Academy of Sciences* **111**, 16967-16972.

McClain AM, Sharkey TD. 2020. Building a better equation for electron transport estimated from Chl fluorescence: accounting for nonphotosynthetic light absorption. *New Phytologist* **225**, 604-608.

McCree KJ. 1970. The action spectrum, absorptance and quantum yield of photosynthesis in crop plants. *Agricultural Meteorology* **9**, 191-216.

Meyer T, Hölscher C, Schwöppe C, von Schaewen A. 2011. Alternative tageting of Arabidopsis plastidic glucose-6-phosphate dehydrogenase G6PD1 involves cysteine-dependent interaction with G6PD4 in the cytosol. *The Plant Journal* **66**, 745-758.

Moses V, Holm-Hansen O, Bassham JA, Calvin M. 1959. The relationship between the metabolic pools of photosynthetic and respiratory intermediates. *Journal of Molecular Biology* **1**, 21-29.

Née G, Aumont-Nicaise M, Zaffagnini M, Nessler S, Valerio-Lepiniec M, Bourguet-Issakidis E. 2014. Redox regulation of chloroplastic G6PDH activity by thioredoxin occurs through structural changes modifying substrate accessibility and cofactor binding. *Biochemistry Journal* **457**, 117-125.

Plaxton WC, Podestá FE. 2006. The functional organization and control of plant respiration. *Critical Reviews in Plant Sciences* **25**, 159-198.

Preiser AL, Fischer N, Banerjee A, Sharkey T. 2019. Plastidic glucose-6-phosphate dehydrogenase is regulated to maintain activity in the light. *Biochemical Journal* **476**, 1539-1551.

Scheibe R, Geissler A, Fickenscher K. 1989. Chloroplast glucose-6-phosphate dehydrogenase: K_m shift upon light modulation and reduction. *Archives of Biochemistry and Biophysics* **274**, 290-297.

Scheible WR, Krapp A, Stitt M. 2000. Reciprocal diurnal changes of phosphoenolpyruvate carboxylase expression and cytosolic pyruvate kinase, citrate synthase and NADP-isocitrate dehydrogenase expression regulate organic acid metabolism during nitrate assimilation in tobacco leaves. *Plant, Cell & Environment* **23**, 1155-1167.

Schnyder H, Schaüfele R, Lötscher M, Gebbing T. 2003. Disentangling CO_2 fluxes: direct measurements of mesocosm-scale natural abundance $^{13}CO_2/^{12}CO_2$ gas exchagne, ^{13}C discrimination, and labelling of CO_2 exchange flux components in controlled environments. *Plant, Cell & Environment* **26**, 1863-1874.

Sharkey TD, Bernacchi CJ, Farquhar GD, Singsaas EL. 2007. Fitting photosynthetic carbon dioxide response curves for C_3 leaves. *Plant, Cell & Environment* **30**, 1035-1040.

Sharkey TD, Weise SE. 2016. The glucose 6-phosphate shunt around the Calvin-Benson Cycle. *Journal of Experimental Botany* **67**, 4067-4077.

Smith NG, Dukes JS. 2012. Plant respiration and photosynthesis in global-scale models: incorporating acclimation to temperature and CO2. *Global Change Biology* **19**, 45-63.

Stitt M. 1990. Fructose-2,6-bisphosphate as a regulatory molecule in plants. *Annual Review of Plant Physiology and Plant Molecular Biology* **41**, 153-185.

Sweetlove LJ, Beard KFM, Nunes-Nesi A, Fernie AR, Ratcliffe RG. 2010. Not just a circle: flux modes in the plant TCA cycle. *Trends in Plant Science* **15**, 462-470.

Szecowka M, Heise R, Tohge T, Nunes-Nesi A, Vosloh D, Huege J, Feil R, Lunn J, Nikoloski Z, Stitt M, Fernie AR, Arrivault S. 2013. Metabolic fluxes in an illuminated Arabidopsis rosette. *The Plant Cell Online* **25**, 694-714.

Tazoe Y, von Caemmerer S, Estavillo GM, Evans JR. 2011. Using tunable diode laser spectroscopy to measure carbon isotope discrimination and mesophyll conductance to CO_2 diffusion dynamically at different CO_2 concentrations. *Plant, Cell & Environment* **34**, 580-591.

Tcherkez G, Cornic G, Bligny R, Gout E, Ghashghaie J. 2005. *In vivo* respiratory metabolism of illuminated leaves. *Plant Physiology* **138**, 1596-1606.

Tcherkez G, Gauthier P, Buckley TN, Busch FA, Barbour MM, Bruhn D, Heskel MA, Gong XY, Crous KY, Griffin K, Way DA, Turnbull MH, Adams MA, Atkin OK, Farquhar G, Cornic G. 2017. Leaf day respiration: low CO_2 flux but high significance for metabolism and carbon balance. *New Phytologist* **216**, 986-1001.

Tcherkez G, Mahé A, Gauthier P, Mauve C, Gout E, Bligny R, Cornic G, Hodges M. 2009. *In folio* respiratory fluxomics revealed by ^{13}C isotopic labeling and H/D isotope effects highlight the noncyclic nature of the tricarboxylic acid 'cycle' in illuminated leaves. *Plant Physiology* **151**, 620-630.

Tcherkez G, Mahé A, Guérard F, Boex-Fontvieille ERA, Gout E, Lamothe M, Barbour MM, Bligny R. 2012. Short-term effects of CO_2 and O_2 on citrate metabolism in illuminated leaves. *Plant, Cell & Environment* **35**, 2208-2220.

Tcherkez G, Mauve C, Lamothe M, Le Bras C, Grapin A. 2011. The $^{13}C/^{12}C$ isotopic signal of day-respired CO_2 in varigated leaves of *Pelargonium x horotum*. *Plant, Cell & Environment* **34**, 270-283.

Timm S, Nunes-Nesi A, Pärnik T, Morgenthal K, Wienkoop S, Keerberg O, Weckwerth W, Kleczkowski LA, Fernie AR, Bauwe H. 2008. A cytosolic pathway for the conversion of hydroxypyruvate to glycerate during photorespiration in Arabidopsis. *Plant Cell* **20**, 2848-2859.

Tovar-Mendez A, Miernyk JA, Randall DD. 2003. Regulation of pyruvate dehydrogenase complex activity in plant cells. *European Journal of Biochemistry* **270**, 1043-1049.

Ubierna N, Holloway-Phillips MM, Farquhar G. 2018. Using stable carbon isotopes to study C_3 and C_4 photosynthesis: models and calculations. In: Covshoff S, ed. *Photosynthesis. Methods in Molecular Biology*, Vol. 1170. New York, NY: Humana Press.

Vittorio PV, Krotkov G, Reed GB. 1954. Synthesis of radioactive sucrose by tobacco leaves from ^{14}C uniformly labelled glucose and glucose-1-phosphate. *Canadian Journal of Botany* **32**, 369-377.

von Schaewen A, Langenkämper G, Graeve K, Wenderoth I, Scheibe R. 1995. Molecular characterization of the plastidic glucose-6-phosphate dehydrogenase from potato in comparison to its cytosolic counterpart. *Plant Physiology* **109**, 1327-1335.

Wakao S, Benning C. 2005. Genome-wide analysis of glucose-6-phosphate dehydrogenases in Arabidopsis. *The Plant Journal* **41**, 243-256.

Wang SM, Lue WI, Yu TS, Long JH, Wang CN, Eimert K, Chen J. 2002. Characterization of *ADG1*, an *Arabidopsis* locus encoding for ADPG pyrophosphorylase small subunit, demonstrates that the presence of the small subunit is required for large subunit stability. *The Plant Journal* **13**, 63-70.

Weise SE, Liu T, Childs KL, Preiser AL, Katulski HM, Perrin-Porzondek C, Sharkey TD. 2019. Transcriptional regulation of the glucose-6-phosphate/phosphate translocator 2 is related to carbon exchange across the chloroplast envelope. *Frontiers in Plant Science* **10**, 827.

Wingate L, Seibt U, Moncrieff JB, Jarvis PG, Lloyd J. 2007. Variations in 13C discrimination during CO_2 exchange by *Picea sitchensis* branches in the field. *Plant, Cell & Environment* **30**, 600-616.

Zeeman SC, Smith SM, Smith AM. 2004. The breakdown of starch in leaves. *New Phytologist* **163**, 247-261.

CHAPTER 5

Concluding remarks

5.1 INTRODUCTION

In this dissertation, my goal was to investigate the proposed presence of the glucose-6-phosphate shunt (Sharkey and Weise, 2016). This alternative pathway oxidizes glucose 6-phosphate (G6P) to ribulose 5-phosphate (Ru5P) and releases a CO_2. This results in a futile cycle around the Calvin-Benson cycle that fixes no carbon, consumes ATP, and remains redox neutral. Previously there was little experimental evidence for flux through this pathway and it was not thought to happen concurrently with the Calvin-Benson cycle. Presence of the G6P shunt could provide insight into remaining questions in central carbon metabolism such as the persistence of unlabeling in Calvin-Benson cycle intermediates in a $^{13}CO_2$ or $^{14}CO_2$ environment (Canvin *et al.*, 1979; Delwiche and Sharkey, 1993; Hasunuma *et al.*, 2010; Ma *et al.*, 2014; Mahon *et al.*, 1974; Szecowka *et al.*, 2013), the source of respiration in the light (R_L), and explanations for several mutant phenotypes (Li *et al.*, 2019; Livingston *et al.*, 2010).

Previous work had characterized kinetics for PGI (Backhausen *et al.*, 1997; Dietz, 1985; Mathur *et al.*, 2005; Schnarrenberger and Oeser, 1974) and G6PDH (Anderson *et al.*, 1974; Buchanan, 1980; Née *et al.*, 2014; Née *et al.*, 2009; Scheibe *et al.*, 1989; Wakao and Benning, 2005). However, these findings had not been applied to understand the presence and physiological implications of the G6P shunt. Therefore, I wanted to confirm and expand on these previous findings, as well as reexamine them in light of this hypothesis.

5.2 REVIEW OF WORK

5.2.1 PGI is a key regulatory enzyme in partitioning carbon out of the Calvin-Benson cycle

In this work, I examined the kinetics and inhibition of plastidic and cytosolic PGI. I assayed recombinant PGI isoforms using coupled spectrophotometry or novel mass spectrometry assays. I confirmed previous findings that the K_m of G6P is higher than that of F6P in the plastidic isoform, but not the cytosolic isoform (Dyson and Noltmann, 1968; Schnarrenberger and Oeser,

1974). Additionally, the magnitude of the difference in K_m can be modulated in the dark and light, indicating that this kinetic limitation is dynamic and most likely important for regulation. The difference in K_m's, in combination with the observation that plastidic PGI is at disequilibrium so that G6P is lower than expected (Backhausen *et al.*, 1997; Gerhardt *et al.*, 1987; Schnarrenberger and Oeser, 1974; Sharkey and Vassey, 1989; Szecowka *et al.*, 2013), allows PGI to act as a one-way valve. Carbon is allowed out of the Calvin-Benson cycle, but is not easily allowed back in. Additionally, I showed that PGI is not inhibited by PGA as previously assumed (Backhausen *et al.*, 1997; Dietz, 1985; Mathur *et al.*, 2005; Sharkey and Weise, 2016), but is instead inhibited by E4P and 6PG. This likely stabilizes the Calvin-Benson cycle by preventing too much carbon from being portioned out of the cycle as photosynthetic rates increase. Finally, I showed the physiological relevance of regulation of plastidic PGI by expressing the unregulated cytosolic PGI in the plastid. I found that this disrupts both starch synthesis and degradation.

Overall, I have demonstrated that PGI is an important regulatory enzyme in partitioning carbon out of the Calvin-Benson cycle and in starch degradation.

5.2.2 Plastidic G6PDH can maintain activity in the light

The goal of this study was to reexamine the assumption that plastidic G6PDH is not active during the day due to redox regulation (Anderson *et al.*, 1974; Buchanan, 1980; Buchanan *et al.*, 2015; Heldt and Piechulla, 2005; Née *et al.*, 2014; Scheibe *et al.*, 1989). G6PDH1 is highly sensitive to the redox status of the plastid and loses ~80% of its activity when reduced. However, while G6PDH2 and 3 are sensitive to the redox status, they still maintain majority of their activity when reduced. Additionally, G6PDH1's midpoint potential is close to that of other redox-regulated Calvin-Benson cycle enzymes and is in a range where it can easily be dynamically regulated. Oxidation of G6PDH1 can occur by thioredoxin or by hydrogen

peroxide. I also showed that G6PDH is highly sensitive to its substrate concentrations in several ways, apart from classic Michalis-Menten kinetics. First, I found that all three isoforms were substrate-inhibited by G6P. Second, I showed that presence of G6P can protect G6PDH1 from redox deactivation.

This work has demonstrated that plastidic G6PDH is not fully inactive during the day and can be dynamically regulated by substrate concentration and redox status of the plastid to allow significant flux through the plastidic G6P shunt

5.2.3 The G6P shunt is responsible for $\mathbf{R_L}$

Here I built upon the previous work that showed plastidic G6PDH can be active during the day to investigate the source of respiration in the light. I used methods developed by Loreto *et al.* (2001) to measure R_L as an efflux of $^{12}CO_2$ in a $^{13}CO_2$ environment. I used loss-of-function plastidic and cytosolic G6PDH to test our hypothesis that the G6P shunt is the source of respiration. All G6PDH loss-of-function plants had decreased R_L. In particular, G6PDH5 showed a loss of ~80% of unlabeled respiration. I used this, along with measurements of fluorescence and g_m, to attribute respiration to four sources: unlabeled shunt, labeled shunt, unlabeled other sources, and labeled other sources. I found that the shunt could account for ~80% of total respiration. Additionally, G6PDH5 loss-of-function plants grow significantly larger than wild type, most likely due to less CO_2 lost through respiration. Finally, the G6P shunt as the source of respiration can explain several mutant phenotypes such as increase in R_L in starch-compromised mutants, *hpr1*, and *hcef1*.

Overall, I have provided evidence that the cytosolic and plastidic G6P shunts are the main source of respiration in the light.

5.3 FUTURE DIRECTIONS

5.3.1 PGI regulation

This work has demonstrated that PGI plays an important regulatory role in partioning carbon out of the Calvin Benson cycle. However, how PGI is regulated is still not well-understood. It is unknown how plastidic PGI maintains a disequilibrium and how the K_m of G6P is dynamically regulated. It has been shown that PGI has several post-translationally modified amino acids. The plastidic PGI has a phosphorylated serine at position 595 and the cytosolic PGI has an acetylated alanine at position 2 (de la Fuentes et al 2008, Bienvenut et al 2012). However, it is unknown if these modifications affect enzymatic kinetics. Mass spectra of recombinant proteins from *E. coli* can demonstrate if this modification is present. If not, other systems of recombinant expression may be employed to investigate this further.

Additional experiments using our transgenic PGI system should be done to better understand the regulation of the plastidic PGI. Our systems severely disrupted PGI in the plastid by overexpressing the unregulated cytosolic PGI. Constructs should be made with the cytosolic PGI behind the native plastidic PGI promoter and the plastidic PGI with a 35S promoter to explore two aspects of PGI regulation. Plastidic PGI has been shown to have limiting activity in the light (Backhausen *et al.*, 1997). Overexpression of plastidic PGI may overcome this limitation. On the other hand, expressing cytosolic PGI in the plastid addresses the difference in K_m's for G6P and F6P and the maintenance of disequilibrium.

5.3.2 Variation of $\mathbf{R_L}$

The cytosolic and plastidic G6P shunts are responsible for majority of $R_{L.}$ However, it is still unknown how this may vary between plant species or in different environmental conditions. It has been shown that respiration in the light can be affected by temperature, nutrient availability, water availability and position in a canopy (Heskel *et al.*, 2014; Jassal *et al.*, 2007; Sperlich *et*

al., 2016; Way and Yamori, 2013; Weerasinghe *et al.*, 2014). Investigation of the regulation and expression of G6PDH in different environmental conditions can lead to new predictions and a more robust understanding of how the G6P shunt and R_L may respond in non-standard laboratory conditions. This can inform not only cellular models of photosynthesis, but whole plant and ecosystem models.

5.3.3 Source of the slow-to-label pool

We have identified part of the pathway that allows the slow-to-label pool of carbon into the Calvin-Benson cycle. The initial source of this carbon is still unknown. Our work has shown that the starch hypothesis proposed by Sharkey and Weise (2016) is not supported. Starch-compromised mutants do not have decreased unlabeled R_L and ADP-glucose is labeled at the same percentage as Calvin-Benson cycle intermediates. The data presented here indicates that the slow-to-label pool is cytosolic or vacuolar. Cytosolic isoforms, G6PDH5 and 6, loss-of-function plants have the greatest impact on R_L. Additionally, R_L increases when GPT2 allows import of unlabeled cytosolic G6P into the plastid. We propose two possible sources of slow-to-label carbon:

Glucose in the vacuole could be exported to the cytosol and phosphorylated by hexokinase. This becomes part of the cytosolic G6P pool and can enter the cytosolic G6P shunt.

Sucrose may be broken down into fructose and glucose which can be phosphorylated to F6P and G6P.

Both of these proposed sources can explain the lower percentage of labeling in UDP-glucose compared to that of triose phosphates and ADP-glucose. These hypotheses may be investigated using Arabidopsis engineered to emit isoprene crossed with loss-of-function mutants that disrupt these sources. Methods developed in chapter 6 allow fast and non-invasive analysis of Calvin-Benson cycle labeling.

LITERATURE CITED

LITERATURE CITED

Anderson LE, Ng T-CL, Kyung-Eun Yoon P. 1974. Inactivation of pea leaf chloroplastic and cytoplasmic glucose 6-phosphate dehydrogenases by light and dithiothreitol. *Plant Physiology* **53**, 835-839.

Backhausen JE, Jöstingmeyer P, Scheibe R. 1997. Competitive inhibition of spinach leaf phosphoglucose isomerase isoenzymes by erythrose 4-phosphate. *Plant Science* **130**, 121-131.

Buchanan BB. 1980. Role of light in the regulation of chloroplast enzymes. *Annual Review of Plant Physiology* **31**, 341-374.

Buchanan BB, Gruissem W, Jones RL. 2015. *Biochemistry & Molecular Biology of Plants*. Rockville: American Society of Plant Physiologists.

Canvin DT, Gibbs M, Latzko E. 1979. Photorespiration: Comparison between C_3 and C_4 plants. *Encyclopedia of Plant Physiology NS Vol 6 Photosynthesis II*. Berlin: Springer, 368-396.

Delwiche CF, Sharkey TD. 1993. Rapid appearance of ^{13}C in biogenic isoprene when $^{13}CO_2$ is fed to intact leaves. *Plant, Cell & Environment* **16**, 587-591.

Dietz KJ. 1985. A possible rate limiting function of chloroplast hexosemonophosphate isomerase in starch synthesis of leaves. *Biochimica et Biophysica Acta* **839**, 240-248.

Dyson JED, Noltmann EA. 1968. The effect of pH and temperature on the kinetic parameters of phosphoglucose isomerase. *The Journal of Biological Chemistry* **243**, 1401-1414.

Gerhardt R, Stitt M, Heldt HW. 1987. Subcellular metabolite levels in spinach leaves. Regulation of sucrose synthesis during diurnal alterations in photosynthetic partitioning. *Plant Physiology* **83**, 399-407.

Hasunuma T, Harada K, Miyazawa S-I, Kondo A, Fukusaki E, Miyake C. 2010. Metabolic turnover analysis by a combination of in vivo ^{13}C-labelling from $^{13}CO_2$ and metabolic profiling with CE-MS/MS reveals rate-limiting steps of the C_3 photosynthetic pathway in Nicotiana tabacum leaves. *Journal of Experimental Botany* **61**, 1041-1051.

Heldt H-W, Piechulla B. 2005. *Plant Biochemistry*. Burlington MA: Elsevier Academic Press.

Heskel MA, Bitterman D, Atkin OK, Turnbull MH, Griffin K. 2014. Seasonality of foliar respiration in two dominant plant species from the Arctic tundra: response to long-term warming and short-term temperature variability. *Functional Plant Biology* **41**, 287-300.

Jassal RS, Black TA, Cai T, Morgenstern K, Li Z, Gaumont-Guay D, Nesic Z. 2007. Components of ecosystem respiration and an estimate of net primary productivity of an intermediate-aged Douglas-fir stand. *Agricultural and Forest Meteorology* **144**, 44-57.

Li J, Weraduwage SM, Preiser AL, Weise SE, Strand DD, Froehlich JE, Kramer D, Hu J, Sharkey TD. 2019. A cytosolic bypass and G6P shunt in plants lacking peroxisomal hydroxypyruvate reductase. *Plant Physiology* **180**, 783-792.

Livingston AK, Cruz JA, Kohzuma K, Dhingra A, Kramer DM. 2010. An *Arabidopsis* mutant with high cyclic electron flow around photosystem I (*hcef*) involving the NADPH dehydrogenase complex. *The Plant Cell* **22**, 221-233.

Loreto F, Velikova V, Di Marco G. 2001. Respiration in the light measured by $^{12}CO_2$ emission in $^{13}CO_2$ atmosphere in maize leaves. *Australian Journal of Plant Physiology* **28**, 1103-1108.

Ma F, Jazmin LJ, Young JD, Allen DK. 2014. Isotopically nonstationary 13C flux analysis of changes in Arabidopsis thaliana leaf metabolism due to high light acclimation. *Proceedings of the National Academy of Sciences* **111**, 16967-16972.

Mahon JD, Fock H, Canvin DT. 1974. Changes in specific radioactivities of sunflower leaf metabolites during photosynthesis in $^{14}CO_2$ and $^{12}CO_2$ at normal and low oxygen. *Planta* **120**, 125-134.

Mathur D, Ahsan Z, Tiwari M, Garg LC. 2005. Biochemical characterization of recombinant phosphoglucose isomerase of *Mycobacterium tuberculosis*. *Biochemical and Biophysical Research Communications* **337**, 626-632.

Née G, Aumont-Nicaise M, Zaffagnini M, Nessler S, Valerio-Lepiniec M, Bourguet-Issakidis E. 2014. Redox regulation of chloroplastic G6PDH activity by thioredoxin occurs through structural changes modifying substrate accessibility and cofactor binding. *Biochemistry Journal* **457**, 117-125.

Née G, Zaffagnini M, Trost P, Issakidis-Bourguet E. 2009. Redox regulation of chloroplastic glucose-6-phosphate dehydrogenase: A new role for f-type thioredoxin. *FEBS Letters* **583**, 2827-2832.

Scheibe R, Geissler A, Fickenscher K. 1989. Chloroplast glucose-6-phosphate dehydrogenase: K_m shift upon light modulation and reduction. *Archives of Biochemistry and Biophysics* **274**, 290-297.

Schnarrenberger C, Oeser A. 1974. Two isoenzymes of glucosephosphate isomerase from spinach leaves and their intracellular compartmentation. *European Journal of Biochemistry* **45**, 77-82.

Sharkey TD, Vassey TL. 1989. Low oxygen inhibition of photosynthesis is caused by inhibition of starch synthesis. *Plant Physiology* **90**, 385-387.

Sharkey TD, Weise SE. 2016. The glucose 6-phosphate shunt around the Calvin-Benson Cycle. *Journal of Experimental Botany* **67**, 4067-4077.

Sperlich D, Barbeta A, Ogaya R, Sabaté S, Peñuelas J. 2016. Balance between carbon gain and loss under long-term drought: impacts on foliar respiration and photosynthesis in *Quercus ilex* L. *Journal of Experimental Botany* **41**, 153-185.

Szecowka M, Heise R, Tohge T, Nunes-Nesi A, Vosloh D, Huege J, Feil R, Lunn J, Nikoloski Z, Stitt M, Fernie AR, Arrivault S. 2013. Metabolic fluxes in an illuminated Arabidopsis rosette. *The Plant Cell Online* **25**, 694-714.

Wakao S, Benning C. 2005. Genome-wide analysis of glucose-6-phosphate dehydrogenases in Arabidopsis. *The Plant Journal* **41**, 243-256.

Way DA, Yamori W. 2013. Thermal acclimation of photosynthesis: on the importance of adjusting our definitions and accounting for thermal acclimation of respiration. *Photosynthesis Research* **119**, 89-100.

Weerasinghe LK, Creek D, Crous KY, Xiang S, Liddell MJ, Turnbull MH, Atkin OK. 2014. Canopy position affects the relationships between leaf respiration and associated traits in a tropical rainforest in Far North Queensland. *Tree Physiology* **34**, 564-584.

CHAPTER 6

Additional studies: the source of carbon for the methyl-D-erythritol 4-phosphate pathway

---

This research was done in collaboration with Dr. Sarathi Weraduwage and Dr. Thomas D. Sharkey. S.W. provided the plant material and collected the isoprene data. T.D.S. analyzed the isoprene mass spectrometry data.

6.1 INTRODUCTION

The methyl-D-erythritol 4-phosphate (MEP) pathway in plants is found in the plastid and is the source of building blocks for many specialized terpenoid metabolites (Figure 6.1) (Arigoni *et al.*, 1997; Lichtenthaler *et al.*, 1997a; Lichtenthaler *et al.*, 1997b; Schwender *et al.*, 1997; Zeidler *et al.*, 1997). In the first step of the pathway, 1-deoxy-D-xylulose 5-phosphate (DXP) is synthesized from pyruvate and glyceraldehyde 3-phosphate (GAP) (Rohmer *et al.*, 1996). In later steps of the pathway, 4-hydroxy-3- methylbut-2-enyl diphosphate (HMBDP) is reduced to isopentenyl diphosphate (IDP) and dimethylallyl diphosphate (DMADP) (Eisenreich *et al.*, 1998; Rohmer *et al.*, 1993). IDP and DMADP are used as a 5-carbon building blocks for terpenoids.

Terpenoids made from the MEP pathway are found in algae and higher plants (Arigoni *et al.*, 1997; Lichtenthaler *et al.*, 1997a; Lichtenthaler *et al.*, 1997b; Schwender *et al.*, 1997). They are used in many biological processes and play roles in regulation, transport, defense, and signaling (for a review, see Tholl (2015)). They are also used commercially for rubber, drugs, biofuels, flavor and fragrance, pigments, and many other applications (Ajikumar *et al.*, 2008; Ajikumar *et al.*, 2010; Caputi and Aprea, 2011; Klein-Marcuschamer *et al.*, 2007; Misawa, 2011; Roberts, 2007; Rude and Schirmer, 2009). In addition to synthesis of more complex terpenoids, DMADP can be converted to isoprene, a single isoprenoid unit, by isoprene synthase (Figure 6.1). Isoprene is emitted by some plants (Hanson *et al.*, 1999; Harley *et al.*, 2004; Harley *et al.*, 1999; Loreto *et al.*, 2002; Loreto *et al.*, 1998; Sharkey *et al.*, 2008) and may help plants respond to ozone and increases in temperature (Sharkey *et al.*, 2008). Isoprene also plays an important role in atmosphere chemistry (Guenther *et al.*, 2006; Sharkey *et al.*, 2008).

One remaining question in our understanding of the MEP pathway is the lack of complete labeling in isoprene when fed $^{13}CO_2$ or $^{14}CO_2$. Isoprene will only label to ~80% within 20 min (Delwiche and Sharkey, 1993; Karl *et al.*, 2002; Loreto *et al.*, 1996; Schnitzler *et al.*, 2004). This

led to the proposal of two souces of carbon (GAP and pyruvate): the Calvin-Benson cycle and a non-recently fixed source. However, this pattern of labeling is also seen in Calvin-Benson cycle intermediates (Hasunuma *et al.*, 2010; Ma *et al.*, 2014; Mahon *et al.*, 1974; Szecowka *et al.*, 2013). It has been shown that labeling patterns in isoprene can vary. When eucalypts are heated from 30˚C to 45˚C, the proportion of unlabeled isoprene increases (Guidoletti *et al.*, 2019). Similar results were shown with drought stress in poplar (Brilli *et al.*, 2007). It is unknown if Calvin-Benson cycle metabolites follow the same pattern under these conditions. Here we examine labeling patterns of the Calvin-Benson cycle and isoprene in transgenic poplar that has been engineered to emit isoprene (Vickers *et al.*, 2010) to determine if the Calvin-Benson cycle is the sole source of carbon for the MEP pathway.

6.2 MATERIALS AND METHODS

6.2.1 Plant material

Populus nigra x *maximowiczii* 'NM6' (a hybrid poplar) cuttings provided by Professor Kyung-Hwan Han of the Great Lakes Bioenergy Research Center (GLBRC) were planted in Suremix growing medium in 1 L pots. These pots were kept in the greenhouse and fertilized with 1/2-strength Hoagland's solution (Hoagland and Arnon, 1938) three days of each week; plants were watered with deionized water the remaining four days of the week. The conditions in the greenhouse were recorded with the aid of HOBO data loggers (Onset Computer Corporation, MA). During the growth season the plants grew under a 16-hour photoperiod, an average light intensity of 160 μmol m^{-2} s^{-1} during the day, and average day/night temperatures of 25°C/ 18°C.

6.2.2 $^{13}CO_2$ labeling of poplar at steady state

Two-month-old poplar trees were used for the experiment. Two leaves, one for each temperature from five trees were used. The 13th and 14th fully expanded leaf of each plants, counted from the top of the canopy, were used to obtain measurements. Pots with trees were

brought to the lab and a leaf was inserted into the 11.46 cm^2 leaf chamber of the fast-kill instrument.

The setup of the fast-kill instrument was used as described in Schrader *et al.* (2007). A KL1500 quartz halogen lamp (Schott Glas, Mainz, Germany) was used to illuminate the top of the leaf chamber, and the light intensity was set to 1000 µmol m^{-2} s^{-1}, measured with a LI-COR quantum sensor (LI-250A, LI-COR Biosciences, NE). The temperature inside the leaf chamber was controlled by a water bath circulating water in the aluminum block of the gas exchange chamber. A thermocouple inserted in the leaf chamber with the sensor touching the abaxial surface of the leaf was connected to a LI-6800 portable gas exchange system (LI-COR Biosciences, Lincoln, NE) that read and recorded the temperature in the leaf chamber. The average temperature for the two temperature treatments of the experiment were 30°C and 40°C. A custom chamber adapter (LI-6800-19) was used to connect the head of the LI-6800 to the leaf chamber of the fast kill to allow air flow between the LI-6800 and the leaf chamber. Air containing 79% N_2 and 21% O_2, controlled by mass-flow controllers (Alicat Scientific, https://www.alicat.com), was humidified and then supplied to the LI-6800. Average water vapor content in the leaf chamber as read and recorded by the LI-6800 was 2 kPa. The Bev-A-Line tubing supplying gasses from the console to the head of the LI-6800 was interrupted close to the back of the LI-6800 head with a Swagelok T-joint to allow the supply of either unlabeled ($^{12}CO_2$) or labeled ($^{13}CO_2$, supplier - Sigma-Aldrich, MO) CO_2. The CO_2 was diluted with air to about (10%). A four-way ball valve before the point of injection of CO_2 to the T-joint allowed for a rapid switch between the addition of either isotope of CO_2 to the gas stream. CO_2 was supplied by an external tank controlled by a 5 mL min^{-1} flow controller (Alicat Scientific, https://www.alicat.com) to bring the partial pressure of CO_2 in the air entering the leaf chamber

to 40 Pa as measured by the sample IRGA. The entire chamber was switched over from $^{12}CO_2$ to $^{13}CO_2$ within 1.5 min.

First, the leaf was left to equilibrate for 90 min in the leaf chamber supplied with unlabeled CO_2 and at either 30°C or 40°C. During this period, photosynthesis and isoprene emission was measured simultaneously using the LI-6800 and a Fast Isoprene Sensor (FIS, Hills Scientific, CO), respectively. To measure isoprene, the exhaust air of the LI-6800 was directed to the FIS. Isoprene emission was averaged over 5 s intervals by the FIS. The operational basics of the FIS are described in Guenther and Hills (1998). The flow rates in the LI-6800 (500 μmol s^{-1}) and the FIS (280 μmol s^{-1}) allowed for 60% of the air stream from the leaf chamber to enter the FIS. After incubation for 90 min, the CO_2 supply was switched to $^{13}CO_2$ and held for 20 min. After 15 min of labeling, the exhaust port of the LI-6800 was immediately connected to the screw cap valve of a Tedlar gas sampling bag with Thermogreen LB-2 Septa (Supelco, PA); by opening the screw cap valve, the gas efflux from the leaf chamber collected in the Tedlar bag for 2 min being careful not to induce a backpressure on the LI-COR. After 2 min the valve was closed and the Tedlar bag was labeled and stored. A 3.011 ppm isoprene standard was also collected in a Tedlar gas sampling bag.

At 20 min, the fast kill mechanism was released causing liquid-nitrogen-cooled copper blocks to smash and freeze a leaf piece without interruption of the light source. Frozen leaves were collected in 2 mL microcentrifuge tubes and stored at -80˚C for further analysis by mass spectrometry.

6.2.3 Metabolite extraction and mass spectrometry for metabolites

Phosphoglycerate (PGA), 6-phosphogluconate (6PG), ADP-glucose, and UDP-glucose were analyzed using methods modified from Lunn *et al.* (2006) (we measured labeling in PGA instead of GAP, the immediate substrate for the MEP pathway. Levels of PGA are much higher than

those of GAP and provide a more reliable signal). Frozen plant material was ground using a ball mill (Retsch, https://www.retsch.com) and suspended in 1.8 mL ice cold 30:70 chloroform: methanol. The mixture was incubated at -20˚C for 2 h, vortexing every 0.5 h. 1.5 mL deionized water was added, samples were vortexed, and centrifuged at 22,000 g for 10 min at 4˚C. The aqueous fraction was collected and kept on ice. The non-aqueous fraction was re-extracted with an additional 1.5 mL deionized water and the second collected aqueous fraction was added to the first. Samples were frozen and freeze dried using a FreeZone Triad Freeze Dryer (Labconco, https://labconco.com). Dried samples were resuspended in 200 µL of 0.5 mM KOH and relative labeling of carbon in metabolites was measured using a coupled mass spectrometry.

Parameters for detection of metabolites were optimized using 10 µM standards purchased from Sigma-Aldrich (https://www.sigmaaldrich.com) (Table 6.1). LC/MS-MS was carried out at the of Mass Spectrometry and Metabolomics Core of Michigan State University (https://rtsf.natsci.msu.edu/mass-spectrometry/) on an Acquity TQD Tandem Quadrupole UPLC/MS/MS (Waters, https://www.waters.com) and was operated in electrospray negative ion mode with multiple reaction monitoring. The capillary voltage was 2.5 kV; the cone voltage, 2 V; the extractor voltage, 3 V. The source temperature was 130˚C and the desolvation temperature was 350˚C. Gas flow for the desolvation and cone was set to 700 and 40 L h^{-1}, respectively. MassLynx software and the Acquity UPLC Console were used to control the instrument. Samples were passed through a Dionex IonPac ATC-3 Trap Column, a Dionex IonPac AG11-HC Guard Column, and a Dionex IonPac AS11-HC Analytical Column (ThermoFisher Scientific, www.thermofisher.com) with a multi-step gradient which was modified from Cocuron and Alonso (2014). Eluent A (0.5 mM KOH) and eluent B (75 mM KOH): 0-0.5 min, 100% A; 0.5-4 min, 100-95.2% A; 4-8 min, 95.2-87.3% A; 8-10 min, 87.3-73.8% A; 10-28 min, 73.8-

33.5% A; 28-31 min, 33.6-0% A; 31-36 min, 0% A; 36-36.01 min, 0-100% A; 36.01-40 min, 100% A. The flow rate was 0.35 mL min^{-1}.

6.2.3 Mass spectrometry for isoprene

The mass fragments analysis of isoprene samples was carried out using gas chromatography–mass spectrometry (GC/MS) at the of Mass Spectrometry and Metabolomics Core of Michigan State University (https://rtsf.natsci.msu.edu/mass-spectrometry/). An Agilent 7010B Triple Quadrupole GC/MS system (Agilent, CA) was used. An EZ-Guard GC column was used (VF5 CP9013, Agilent, 30 m length, 10 m guard length, EZ Guard, 7 in cage, 0.25 mm inner diameter). Prior to taking measurements, the oven housing the GC column was allowed 1 h to reach 230^{o}C.

Isoprene collected in the Tedlar bag was sampled using a solid phase microextraction (SPME) fused-silica fiber. After the oven had reached 230^{o}C, and before being used for sampling, the needle end of the SPME fiber holder (577330-U) was placed in the heated zone of the GC injection port. The SPME fiber was carefully protruded into the GC injection port and locked into place in the exposed position by pushing down the plunger of the holder and then rotating the plunger clockwise to lock in the retaining screw. After conditioning the SPME fiber in the GC injection port for 20 min the fiber was retracted into the holder and removed from the GC injection port.

To facilitate the insertion of the SPME fiber into the Tedlar bag, a bag containing a gas sample was placed on benchtop (with the screw cap facing upward) and the SPME fiber holder was positioned directly above it and held vertically and straight with the aid of a ring stand. Next, the Thermogreen LB-2 Septa of the Tedlar bag was pierced by the septum-piercing needle located at the end of the SPEME holder and the plunger was pushed in to extend the SPME fiber into the gas sample. The SPME fiber was allowed to adsorb analytes for 10 min. At the end of 10

min, the SPME fiber was carefully retracted from the Tedlar bag and immediately inserted into the injector port of the GC (as described previously) and was allowed to desorb for 2 min at 230ºC. During desorption, isoprene was collected in a cryotrap cooled to -10ºC with CO_2. Immediately after the 2 min desorption period, the AgilentQQQ/MassHunter program was started and run for 6.75 min. Isoprene was released from the cryotrap by rapid heating a process so that it entered the column as a very sharp band. At the end of the program, the SPME fiber was retracted and the process was repeated with the rest of the gas samples. Seventy eV electron ionization was used.

Mass fragments of unlabeled isoprene (mass-to-charge ratio [m/z] 67, 68), and its isotopologues containing one to five ^{13}C carbons (up to m/z = 73) were measured by the mass spectrometer of the Agilent 7010B Triple Quadrupole GC/MS system. Scan mode was used, scanning from m/z 30 to 300 with a scan time of 150 ms.Quality analysis and the mass spectra were generated by the AgilentQQQ/MassHunter program.

6.2.4 Data analysis

The mass spectra obtained from the ^{13}C labeled metabolites were analyzed using TargetLynx Application Manager, an option with Waters MassLynx™ Software, (Waters Corporation, MA). Files were converted from the MassHunter file format to NetCDF format using MassHunter software and then converted from to a Waters .raw files using Waters DataBridge software. The ion ratios and peak integration automatically generated by TargetLynx were manually reviewed to optimize peak integration. The final outputs included the retention time, peak area, peak quality as indicated by the signal to noise ratio. The peak areas represent abundance of the isotopologues of interest.

During chemical ionization, some isoprene loses a hydrogen such that the most abundant ion in the mass spectrum is the M-1 ion but there also is a significant amount of the M+0 ion.

Therefore, the mass spectrometer data was deconvoluted to separate the contribution of the two ions of each isotopologue. The isoprene isotopologues (^{i}I, where i is the molecular mass, e.g. with no ^{13}C, i = 68) were computed from the ion counts at different mass-to-charge readings (^{j}M, where j is the m/z for the i^{th} ion). Therefore, the total amount of a particular isotopologue would be:

$$^{68}I = \alpha \cdot {}^{67}M + (1 - \alpha) \cdot {}^{68}M \quad \text{Eq. 6.1}$$

where α is the proportion of ions at M-1 and can be estimated as follows using the mass spectrum of isoprene from an unlabeled leaf.

$$\alpha = \frac{^{67}M}{(^{67}M + {}^{68}M - 0.055 \cdot {}^{67}M/_{\alpha})} \quad \text{Eq. 6.2}$$

The presumed natural abundance of ^{13}C in isoprene (1.1% of carbons) is accounted for by the term ^{68}M-0.055•$^{67}M/\alpha$. Data obtained in this study yielded α = 0.62. Once α is known, each isotopologue can be computed as

$$^{i}I = (^{j}M - {}^{i-1}I \cdot (1 - \alpha))/\alpha \quad \text{Eq. 6.3}$$

In the case of ^{68}I, there is no i – 1 isotopologue so the equation simplifies to

$$^{68}I = {}^{67}M/\alpha \quad \text{Eq. 6.4}$$

Most of the M+0 isotopologue in isoprene after 15 min of labeling comes from a small exchange of MEcDP from the cytosol (González-Cabanelas *et al.*, 2015; Wright *et al.*, 2014; Xiao *et al.*, 2012). We corrected for this when calculating the average labeling.

6.3 RESULTS

6.3.1 Steady-state ^{13}C labeling in central carbon metabolism and isoprene

At 30˚C, we found that 93 ± 2% of the carbon in PGA labelled with ^{13}C. In the isoprene sample, 88 ± 1% of the carbon was labelled with ^{13}C. While this was statistically different from the total degree of label by a two tailed Student's t-test, the difference is not likely

physiologically significant (Figure 6.2). The distribution among the isotopologues for PGA and isoprene are given in Table 6.2. 6PG was 51 ± 10% labeled, ADP-glucose was 93 ± 1%, and UDP-glucose was 62 ± 10% (Figure 6.2)

At 40˚C, we found that 74 ± 3% of the carbon in PGA labelled with ^{13}C (Figure 6.2). In the isoprene sample, 72 ± 4% of the carbon was labelled with ^{13}C and this was not statistically different from PGA labeling (Figure 6.2). The proportion of each isotopologue is given in Table 6.3. 6PG was 64 ± 6% labeled, ADP-glucose was 73 ± 3%, and UDP-glucose was 41 ± 3% (Figure 6.2).

6.4 DISCUSSION

6.4.1 Source of PGA for the MEP pathway

In this experiment, we sought to understand the source of carbon for the MEP pathway and isoprene sythesis. It has been shown that PGA and isoprene remain partially unlabeled when fed $^{13}CO_2$ or $^{14}CO_2$ (Delwiche and Sharkey, 1993; Hasunuma *et al.*, 2010; Karl *et al.*, 2002; Loreto *et al.*, 1996; Ma *et al.*, 2014; Mahon *et al.*, 1974; Schnitzler *et al.*, 2004; Szecowka *et al.*, 2013); however this is the first report that has concurrently measured PGA and isoprene labeling. In isoprene, except for the first report by Delwiche and Sharkey (1993), the lack of complete labeling has been attributed to two sources of carbon, for example, one source for GAP and a different source for pyruvate. However, both PGA and isoprene label at a similar rate and to the same level (Figure 6.2, 6.3) (Canvin *et al.*, 1979; Delwiche and Sharkey, 1993). We used heat to manipulate labeling in isoprene, as shown by Guidoletti *et al.* (2019), and measured labeling in PGA and isoprene to determine if the Calvin-Benson cycle is the source of carbon for isoprene. As previous studies have shown, we found that PGA and isoprene are partially unlabeled. In the MEP pathway, unlabeled MEcDP can be imported into the plastid (González-Cabanelas *et al.*, 2015; Wright *et al.*, 2014; Xiao *et al.*, 2012) and can account for M+0 isotopologue of isoprene

as the M+0 isotopologue of PGA is negligibly small. However, even when corrected for this, isoprene still remains more unlabeled than predicted. In fact, after correction, labeling in isoprene is more similar to that of PGA. This indicates that the Calvin-Benson cycle is the only source of carbon for MEP pathway substrates.

Additionally, ^{13}C enrichments of UDP-glucose and 6PG do not correlate at both temperatures. We have used UDP-glucose as a proxy of cytosolic G6P labeling (Chapter 4) which enters the G6P shunt. 6PG is produced as an intermediate of the G6P shunt, therefore we would expect their labeling to be similar. While labeling in these metabolites were not statistically different at 30˚C, they were at 40˚C. Surprisingly 6PG had a higher percentage of labeling than UDP-glucose. This indicates an increase of the plastidic shunt, which begins with plastidial G6P and so should have an isotopic composition similar to ADPG. Temperature may increase the rates of both the cytosolic shunt, reducing the label in UDPG, and the plastidial shunt, increasing the label in 6PG.

6.4.2 Isoprene as a window on labeling of the Calvin-Benson cycle

An understanding of the carbon source for the MEP pathway also provides a unique tool to examine the source of the slow-to-label carbon pool in the Calvin-Benson cycle. The amount of label in isoprene is a direct reflection of the amount of label in the Calvin-Benson cycle and can be used as a non-invasive measurement of the labeling status of PGA.

Model plants engineered to emit isoprene, like *Arabidopsis thaliana,* can be manipulated to test hypotheses for the source of the slow-to-label pool. Samples can easily be collected non-destructively and analyzed with isoprene capture and subsequent mass spectrometry. Samples collected this way do not have complications with sample collection and degradation like Calvin-Benson cycle metabolites.

6.5 CONCLUSION

Contrary to previous thought, we have shown that the Calvin-Benson cycle is the only source of carbon for the MEP pathway and isoprene synthesis. Additionally, we have provided a novel tool for analyzing labeling patterns of the Calvin-Benson cycle.

6.6 ACKNOWLEDGEMENTS

This research was funded by U.S. Department of Energy Grant DE-FG02-91ER2002 (T.D.S., A.L.P.). S.W. was funded by the Great Lakes Bioenergy Research Center, U.S. Department of Energy, Office of Science, Office of Biological and Environmental Research under award number DE-SC0018409. A.L.P was also supported by a Barnett Rosenburg Endowed Research Assistantship from the College of Natural Science at Michigan State University. T.D.S. received partial salary support from Michigan AgBioResearch

APPENDIX

TABLE 6.1- Parameters used for detection of several Calvin-Benson cycle metabolites with LC/MS/MS.

Parameters were optimized using 10 μM standards before analyzing samples. Heavier isotopes for each metabolite were also measured with the same cone and collision voltage and daughter m/z as each +0 isotopologue.

Metabolite	Cone (V)	Collision (V)	+0 Parent (m/z)	Daughter (m/z)
PGA	26	10	185	97
6PG	34	18	275	97
ADP	42	25	588	346
UDP	42	25	565	323

TABLE 6.2- Mass isotopologues of PGA and isoprene at 30˚C.

Samples were collected at 15-17 min for isoprene at 20 min for the other metabolites. Isoprene data were deconvoluted to correct for the presence of the m-1 isotopologue and corrected for dilution by import of unlabeled MEcDP. Total label percentage shows the proportion of carbons that are ^{13}C in the whole sample. Errors shown are S.D. (n=5).

Isotopologue	PGA	Isoprene
m+0	2.1 ± 0.6%	6.6 ± 0.1%
m+1	1.9 ± 0.5%	2.7 ± 1.2%
m+2	10.5 ± 2.2%	3.6 ± 1.2%
m+3	85.6 ± 3.3%	11.1 ± 0.8%
m+4		12.1 ± 2.5 %
m+5		64.0 ± 3.6%
Total % Label	93.2 ± 1.7%	88.4 ± 1.4%

TABLE 6.3- Mass isotopologues of PGA and isoprene at 40˚C.

Samples were collected at 15-17 min for isoprene at 20 min for the other metabolites. Isoprene data were deconvoluted to correct for the presence of the m-1 isotopologue and corrected for dilution by import of unlabeled MEcDP. Total label percentage shows the proportion of carbons that are ^{13}C in the whole sample. Errors shown are standard deviation with N=5.

Isotopologue	PGA	Isoprene
m+0	9.5 ± 1.1%	7.4 ± 1.2%
m+1	11.3 ± 2.4%	7.0 ± 2.2%
m+2	27.9 ± 3.4%	14.5 ± 2.9%
m+3	51.2 ± 5.6%	19.8 ± 1.3%
m+4		20.7 ± 1.3%
m+5		30.6 ± 5.9%
Total % Label	73.6 ± 3.1%	71.8 ± 3.7%

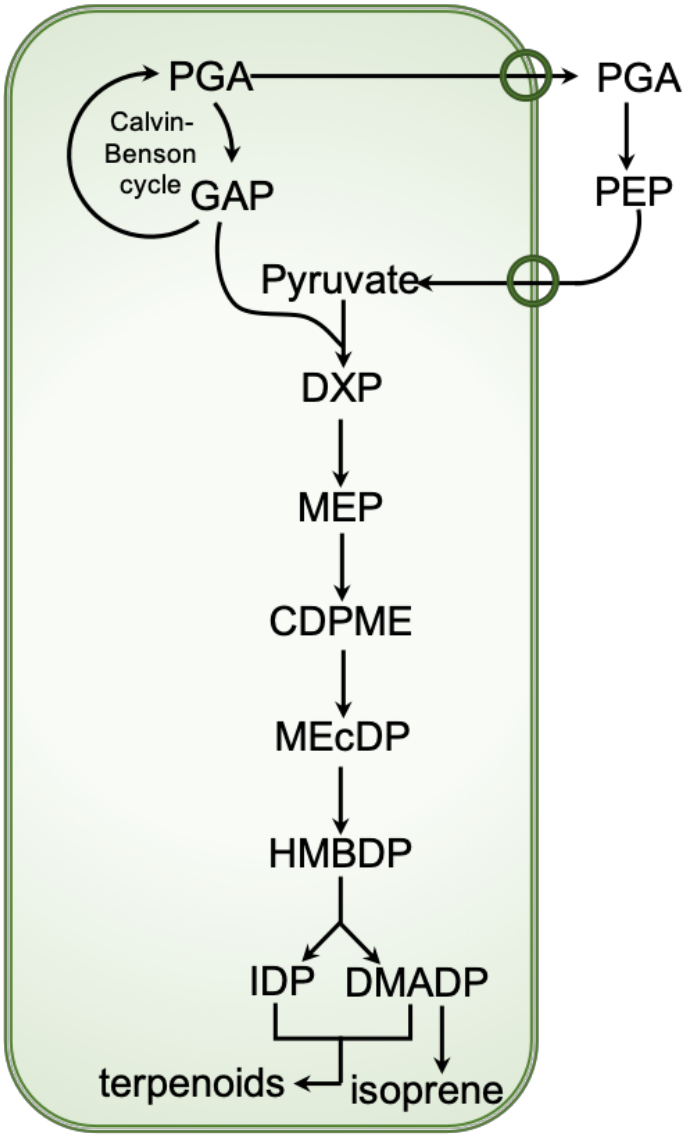

FIGURE 6.1- The methyl-D-erythritol 4-phosphate (MEP) pathway.

PGA= 3-phosphoglyceric acid, GAP = glyceraldehyde 3-phosphate, PEP = phosphoenolpyruvate, DXP = 1-deoxy-D-xylulose 5-phosphate, MEP = 2-C-methylerythritol 4-phosphate, CDPME = 4-diphosphocytidyl-2-C-methylerythritol, MEcDP = 2-C-methyl-D-erythritol 2,4-cyclodiphosphate, HBDP = (E)-4-hydroxy-3-methyl-but-2-enyl pyrophosphate, IDP = isopentenyl pyrophosphate, DMADP = dimethylallyl pyrophosphate.

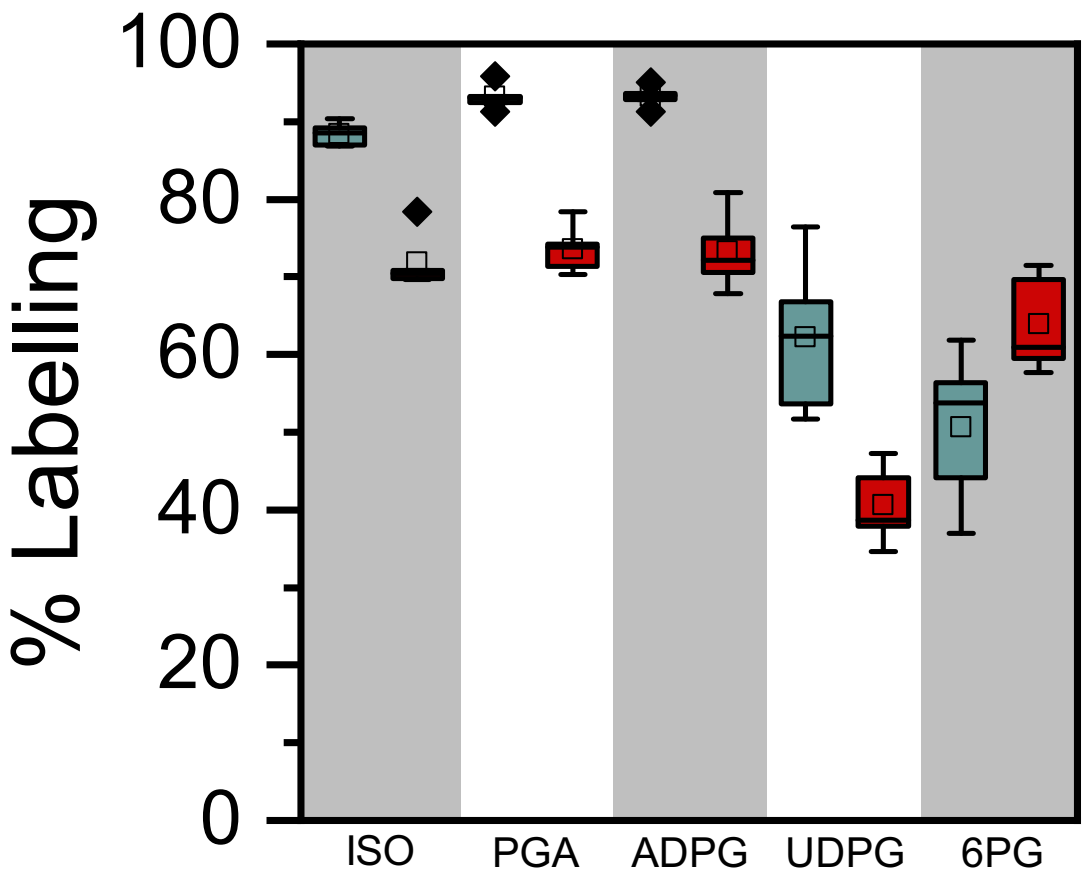

FIGURE 6.2- Degree of label in isoprene, PGA, ADP-glucose, UDP-glucose, and 6PG at 30˚C and 40˚C.

Samples were collected at 15-17 min for isoprene at 20 min for PGA. Total label percentage shows the proportion of carbons that are ^{13}C in the whole sample. Blue indicates samples taken at 30˚C and red indicated samples taken at 40˚C. The box encompasses the middle two quartiles, mean is represented as an open square, and median is represented as a horizontal line inside the box. Whiskers show the standard deviation with N=5 for both treatments.

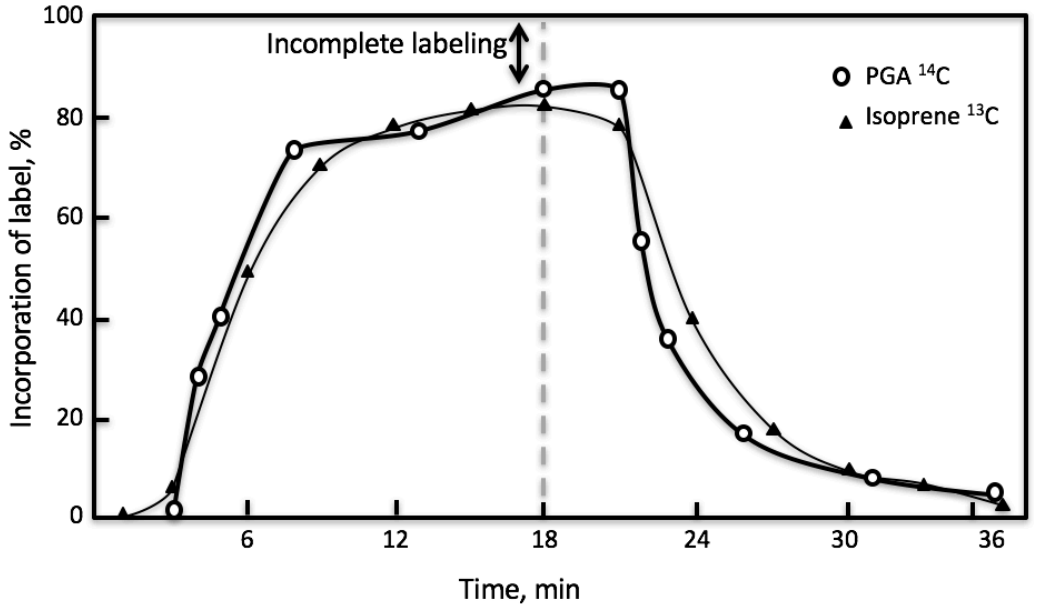

FIGURE 6.3- Incomplete labeling of 3-phosphoglyceric acid (PGA) and isoprene.

PGA and isoprene show similar labeling kinetics when fed $^{13}CO_2$ or $^{14}CO_2$. Data from Delwiche and Sharkey (1993) and Canvin *et al.* (1979).

LITERATURE CITED

LITERATURE CITED

Ajikumar PK, Tyo K, Carlsen S, Mucha O, Phon TH, Stephanopoulos G. 2008. Terpenoids: opportunities for biosynthesis of natural product drugs using engineered microorganisms. *Molecular Pharmaceutics* **5**, 167-190.

Ajikumar PK, Xiao W-H, Tyo KEJ, Wang Y, Simeon F, Leonard E, Mucha O, Phon TH, Pfeifer B, Stephanopoulos G. 2010. Isoprenoid pathway optimization for taxol precursor overproduction in *Escherichia coli*. *Science* **330**, 70-74.

Arigoni D, Sagner S, Latzel C, Eisenreich W, Bacher A, Zenk MH. 1997. Terpenoid biosynthesis from 1-deoxy-D-xylulose in higher plants by intramolecular skeletal rearrangement. *Proceedings of the National Academy of Sciences of the United States of America* **94**, 10600-10605.

Brilli F, Barta C, Fortunati A, Lerdau M, Loreto F, Centritto M. 2007. Response of isoprene emission and carbon metabolism to drought in white poplar (*Populus alba*) saplings. *New Phytologist* **175**, 244-254.

Canvin DT, Gibbs M, Latzko E. 1979. Photorespiration: Comparison between C_3 and C_4 plants. *Encyclopedia of Plant Physiology NS Vol 6 Photosynthesis II*. Berlin: Springer, 368-396.

Caputi L, Aprea E. 2011. Use of terpenoids as natural flavouring compounds in food industry. *Recent Patents on Food, Nutrition & Agriculture* **3**, 9-16.

Cocuron J-C, Alonso AP. 2014 *Liquid chromatography tandem mass spectrometry for measuring ^{13}C-labeling in intermediates of the glycolysis and pentose phosphate pathway.* Totwa, NJ: Humana Press.

Delwiche CF, Sharkey TD. 1993. Rapid appearance of ^{13}C in biogenic isoprene when $^{13}CO_2$ is fed to intact leaves. *Plant, Cell & Environment* **16**, 587-591.

Eisenreich W, Schwarz M, Cartayrade A, Arigoni D, Zenk MH, Bacher A. 1998. The deoxyxylulose phosphate pathway of terpenoid biosynthesis in plants and microorganisms. *Chemistry & Biology* **5**, R221-R233.

González-Cabanelas D, Wright LP, Paetz C, Onkokesung N, Gershenzon J, Rodríguez-Concepción M, Phillips MA. 2015. The diversion of 2-C-methyl-D-erythritol-2,4-cyclodiphosphate from the 2-C-methyl-d-erythritol 4-phosphate pathway to hemiterpene glycosides mediates stress responses in Arabidopsis thaliana. *The Plant Journal* **82**, 122-137.

Guenther A, Karl T, Harley P, Wiedinmyer C, Palmer PI, Geron C. 2006. Estimates of global terrestrial isoprene emissions using MEGAN (Model of Emissions of Gases and Aerosols from Nature). *Atmospheric Chemistry and Physics* **6**, 3181-3210.

Guenther AB, Hills AJ. 1998. Eddy covariance measurement of isoprene fluxes. *Journal of Geophysical Research* **103**, 13,145-113,152.

Guidoletti G, Pallozzi E, Gavrichkova O, Scartazza A, Mattioni M, Loreto F, Calfapietra C. 2019. Emission of constitutive isoprene, induced monoterpenes, and other volatiles under high temperatures in Eucalyptus camaldulensis: A ^{13}C labelling study. *Plant, Cell & Environment* **42**, 1929-1938.

Hanson DT, Swanson S, Graham LE, Sharkey TD. 1999. Evolutionary significance of isoprene emission from mosses. *American Journal of Botany* **86**, 634-639.

Harley P, Vasconcellos P, Vierling L, Cleomir de S. Pinhiero C, Greenberg J, Guenther A, Klinger L, Soares de Almeida S, Neill D, Baker T, Phillips O, Malhi Y. 2004. Variation in potential for isoprene emissions among Neotropical forest sites. *Global Change Biology* **10**, 630-650.

Harley PC, Monson RK, Lerdau MT. 1999. Ecological and evolutionary aspects of isoprene emission from plants. *Oecologia* **118**, 109-123.

Hasunuma T, Harada K, Miyazawa S-I, Kondo A, Fukusaki E, Miyake C. 2010. Metabolic turnover analysis by a combination of in vivo ^{13}C-labelling from $^{13}CO_2$ and metabolic profiling with CE-MS/MS reveals rate-limiting steps of the C3 photosynthetic pathway in Nicotiana tabacum leaves. *Journal of Experimental Botany* **61**, 1041-1051.

Hoagland DR, Arnon DI. 1938. The water culture method for growing plants without soil. Berkley: UC Agric. Exp. Sta. Circular 347, 1-39.

Karl T, Fall R, Rosenstiel TN, Prazeller P, Larsen B, Seufert G, Lindinger W. 2002. On-line analysis of the $^{13}CO_2$ labeling of leaf isoprene suggests multiple subcellular origins of isoprene precursors. *Planta* **215**, 894-905.

Klein-Marcuschamer D, Ajikumar PK, Stephanopoulos G. 2007. Engineering microbial cell factories for biosynthesis of isoprenoid molecules: beyond lycopene. *Trends in Biotechnology* **25**, 417-424.

Lichtenthaler HK, Rohmer M, Schwender J. 1997a. Two independent biochemical pathways for isopentenyl diphosphate and isoprenoid biosynthesis in higher plants. *Physiologia Plantarum* **101**, 643-652.

Lichtenthaler HK, Schwender J, Disch A, Rohmer M. 1997b. Biosynthesis of isoprenoids in higher plant chloroplasts proceeds via a mevalonate-independent pathway. *FEBS Letters* **400**, 271-274.

Loreto F, Centritto M, Baraldi R, Rapparini F, Liu S. 2002. Emission of isoprenoids from natural vegetation in the Beijing region (Northern China). *Plant Biosystems* **136**, 251-255.

Loreto F, Ciccioli P, Brancaleoni E, Cecinato A. 1998. Measurement of isoprenoid content in leaves of Mediterranean *Quercus spp*. by a novel and sensitive method and estimation of the isoprenoid partition between liquid and gas phase inside the leaves. *Plant Science* **136**, 25-30.

Loreto F, Ciccioli P, Cecinato A, Brancaleoni E, Frattoni M, Fabozzi C, Tricoli D. 1996. Evidence of the photosynthetic origin of monoterpenes emitted by *Quercus ilex* L leaves by ^{13}C labeling. *Plant Physiology* **110**, 1317-1322.

Lunn JE, Feil R, Hendriks JH, Gibon Y, Morcuende R, Osuna D, Scheible WR, Hajirezaei M, Stitt M. 2006. Sugar-induced increases in trehalose 6-phosphate are correlated with redox activation of ADP-glucose pyrophosphorylase and higher rates of starch synthesis in Arabidopsis thaliana. *Biochemical Journal* **397**, 139-148.

Ma F, Jazmin LJ, Young JD, Allen DK. 2014. Isotopically nonstationary ^{13}C flux analysis of changes in Arabidopsis thaliana leaf metabolism due to high light acclimation. *Proceedings of the National Academy of Sciences* **111**, 16967-16972.

Mahon JD, Fock H, Canvin DT. 1974. Changes in specific radioactivities of sunflower leaf metabolites during photosynthesis in $^{14}CO_2$ and $^{12}CO_2$ at normal and low oxygen. *Planta* **120**, 125-134.

Misawa N. 2011. Pathway engineering for functional isoprenoids. *Current Opinion in Biotechnology* **22**, 627-633.

Roberts SC. 2007. Production and engineering of terpenoids in plant cell culture. *Nature Chemical Biology* **3**, 387-395.

Rohmer M, Knani M, Simonin P, Sahm H. 1993. Isoprenoid biosynthesis in bacteria: A novel pathway for the early steps leading to isopentenyl diphosphate. *Biochemical Journal* **295**, 517-524.

Rohmer M, Seemann M, Horbach S, Bringer-Meyer S, Sahm H. 1996. Glyceraldehyde 3-phosphate and pyruvate as precursors of isoprenic units in an alternative non-mevalonate pathway for terpenoid biosynthesis. *Journal of the American Chemical Society* **118**, 2564-2566.

Rude MA, Schirmer A. 2009. New microbial fuels: a biotech perspective. *Current Opinion in Microbiology* **12**, 274-281.

Schnitzler JP, Graus M, Kreuzwieser J, Heizmann U, Rennenberg H, Wisthaler A, Hansel A. 2004. Contribution of different carbon sources to isoprene biosynthesis in poplar leaves. *Plant Physiology* **135**, 152-160.

Schrader SM, Kleinbeck KR, Sharkey TD. 2007. Rapid heating of intact leaves reveals initial effects of stromal oxidation on photosynthesis. *Plant, Cell & Environment* **30**, 671-678.

Schwender J, Zeidler J, Gröner R, Müller C, Focke M, Braun S, Lichtenthaler FW, Lichtenthaler HK. 1997. Incorporation of 1-deoxy-D-xylulose into isoprene and phytol by higher plants and algae. *FEBS Letters* **414**, 129-134.

Sharkey TD, Wiberley AE, Donohue AR. 2008. Isoprene emission from plants: Why and how. *Annals of Botany* **101**, 5-18.

Szecowka M, Heise R, Tohge T, Nunes-Nesi A, Vosloh D, Huege J, Feil R, Lunn J, Nikoloski Z, Stitt M, Fernie AR, Arrivault S. 2013. Metabolic fluxes in an illuminated Arabidopsis rosette. *The Plant Cell Online* **25**, 694-714.

Tholl D. 2015. Biosynthesis and biological functions of terpenoids in plants. In: Schrader J, Bohlmann J, eds. *Biotechnology of Isoprenoids*, Vol. 148: Springer, Cham.

Vickers C, Possell M, Hewitt CN, Mullineaux P. 2010. Genetic structure and regulation of isoprene synthase in Poplar (*Populus spp*.). *Plant Molecular Biology* **73**, 547-558.

Wright LP, Rohwer JM, Ghirardo A, Hammerbacher A, Ortiz-Alcaide M, Raguschke B, Schnitzler J-P, Gershenzon J, Phillips MA. 2014. Deoxyxylulose 5-phosphate synthase controls flux through the methylerythritol 4-phosphate pathway in Arabidopsis. *Plant Physiology* **165**, 1488-1504.

Xiao Y, Savchenko T, Baidoo EE, Chehab WE, Hayden DM, Tolstikov V, Corwin JA, Kliebenstein DJ, Keasling JD, Dehesh K. 2012. Retrograde signaling by the plastidial metabolite MEcPP regulates expression of nuclear stress-response genes. *Cell* **149**, 1525-1535.

Zeidler JG, Lichtenthaler HK, May HU, Lichtenthaler FW. 1997. Is isoprene emitted by plants synthesized via the novel isopentenyl pyrophosphate pathway? *Zeitschrift fur Naturforschung* **52**, 15-23.